공학박사 학위논문

플라즈마 전기화학법을 응용한 형광 금속 산화막의 개발 및 특성연구

Plasma enhanced electrochemical preparation for photo-luminescent metal oxide films

2015년 8월

서울대학교 대학원

재료공학부

강 은 희

플라즈마 전기화학법을 응용한 형광 금속 산화막의 개발 및 특성연구

Plasma enhanced electrochemical preparation for photo-luminescent metal oxide films

지도 교수 홍 성 현

이 논문을 공학박사 학위논문으로 제출함
2015 년 8 월

서울대학교 대학원
재료공학부
강 은 희

강 은 희의 박사 학위논문을 인준함
2015 년 5 월

위 원 장 _____ 강 신 후 _____ (인)

부위원장 _____ 홍 성 현 _____ (인)

위   원 _____ 박 병 우 _____ (인)

위   원 _____ 윤 철 수 _____ (인)

위   원 _____ 손 기 선 _____ (인)

Abstract

Plasma enhanced electrochemical preparation for photo-luminescent metal oxide films

Eun-Hee Kang

Department of Materials Science and Engineering

The Graduate School

Seoul National University

Electrochemical coating technologies of metal surface have been widely used for decades in various industries, because it provides the thick and anti-corrosive films with a simple and inexpensive process. Especially, plasma electrolytic oxidation (PEO), which is a high electrical power-induced technology, has much attention in recent years due to their excellent film property. The PEO produces adherent ceramic-like coatings, which are beneficial to enhance the corrosion, heat and wear resistance, so the oxidized film can be applied in many industrial fields such as aerospace, automobile and portable electric devices. During PEO process, a high–voltage discharge zone is generated as spark or arc, and the thick ceramic coating is directly formed on the surface of metals together with elements in the electrolyte. At the discharge zone, the oxide films are locally changed with high temperature and pressure atmosphere, and estimated

temperature at this region is around 8000 K at a hot core and 1800 K at a cold circumferential area. Using this extraordinary phenomenon, we applied the plasma discharge in PEO process to generate the photo-luminescent oxide film by adding the rare-earth ions in the electrolytes, and the rare-earth doped phosphor film was successfully formed on the metal substrate. So far, the luminescent film was fabricated by screen printing technique, combustion CVD, spin coating, sol-gel soft lithography, and radio-frequency magnetron sputtering, but those kinds of phosphor films showed many problems such as poor uniformity of film thickness and low adhesion to the substrate. In case of PEO process, the rare-earth ions are directly incorporated during oxidation process, so well adhesive luminescent films can be obtained.

In this thesis, we firstly studied the new approaches of plasma enhanced electrochemical process to develop a luminescent metal oxide film by doping rare-earth ions at the moment of plasma generation with one-step process. At the first section, white luminescent europium doped aluminum oxide film will be investigated in detail. The white luminescent oxidized film was mainly composed of γ-Al_2O_3, and the photoluminescence spectrum consisted of two emission peaks centered at 405 nm and 488 nm with a broad FWHM (~197.6 nm). In order to figure out the origin of these emission peaks, the results of cathodoluminescence, elemental analysis, rietveld refinement, decay time of photoluminescence, TEM analysis and electronic structure calculation will be discussed in this thesis. In

addition, blue light emitting cerium doped magnesium silicate films also will be introduced by comparing Mg_2SiO_4:Ce phosphor in the second chapter.

Keywords: white phosphor, plasma electrolytic oxidation, photoluminescence, aluminum oxide, rare-earths
Student Number: 2009-20580

Contents

List of Tables

List of Figures

xiii

Chapter 1. General backgrounds

1.1. Luminescent materials

1.1.1. Inorganic phosphor materials

Photoluminescence property in inorganic phosphor materials are based on the interaction of ceramic host lattice and homogeneously distributed activator in the crystal system [1-3]. Concentration of activator ions are varied from few ppm to 20~30 at% depending on the activator and host lattice type. Luminescence mechanism in energy band is shown in the schematic Figure 1.1. When external light comes in phosphor materials, the host lattice absorbs the light energy and transfer to activator ion. In solid system, after electrons are promoted into excited states by absorbing photons, they return to the ground state by spontaneous emission of photons. When electrons in ground states absorb enough excitation energies, they will be lifted up to the excited state by forming valence electrons in the excited state and leaving behind holes in the ground state. The photon is emitted when an electron in an excited state drops down to recombine holes in the ground state, so electron energy state of activator is crucial factors for determining emission intensity and wavelength of emission light. Furthermore, the host materials around activator ions play a decisive role in photoluminescence property such as intensity, wavelength, decay time and thermal stability, so the selection of

host and activator materials is very important for designing appropriate phosphors.

In general, oxide[4, 5], nitride [6, 7], oxy-nitride[8, 9] and sulfides[10, 11] systems are used as host materials, and rare earths (Eu^{2+}, Eu^{3+}, Ce^{3+}, Yb^{2+}, Tb^{3+}, Sm^{3+}, Gd^{3+}, Pr^{3+}, Dy^{3+}) and transition metals are commonly used as an activator in phosphors [12-14]. According to the selection of host and activator materials, the phosphors can be applied to various industrial fields. The phosphor materials are widely used in emergency sign area due to its phosphorescence property, and they also applied to money as a florescence security. The major application of luminescent inorganic material is lightening device such as fluorescence lamp and white LEDs[15]. Fluorescent lamp phosphors (red, green, blue) convert the ultraviolet emission of a rare-gas/mercury discharge plasma into visible (white) light, and yellow phosphors ($YAG:Ce^{3+}$) have been used to convert blue LED light to white light in commercial white LEDs [16, 17]. Furthermore, RGB phosphor materials were the most important materials in history of display device from cathode ray tube monitor to LED back lighting monitor. In recent years, new-type display device called as laser phosphor display (LPD) [18] were developed which is large-format display technology similar to cathode ray tube (CRT) [19] technology but uses lasers instead of an electron gun to activate the phosphors that create the images.

1.1.2 White light phosphors

Generally, in lightening area, white luminescence which covers full range of visible light region is obtained by combining two or three phosphor materials like fluorescent lamp or using yellow phosphors pumped with blue light LEDs (Figure 1.2). However, these kind of white luminescence are not fully covered visible light range, so many researchers are trying to make white luminescence like sun light. A color rendering index (CRI) is a quantitative measure of the ability of a light source to reveal the colors of various objects faithfully in comparison with an ideal or natural light source. A reference source, such as blackbody radiation, is defined as having a CRI of 100. The best possible faithfulness to a reference is specified by a CRI of one hundred, while the very poorest is specified by a CRI below zero.

In phosphor materials, many researchers have been focused for several decades on white luminescent phosphors. Because it is quiet hard to generate white luminescence from one luminescence center, mixing various luminescence center method is commonly used. First, combining two different host crystal is the most favorable way to fabricate white luminescence[20]. According to the selection of cations in host matrix, emission spectrum wavelengths can be adjusted, so white luminescence can be obtained by controlling the ratio of cations. When there are variable vacancy sites or cation sites for substitution, emission spectrum can be broadened due to their various luminescence centers, and white

emission can be obtained in this way[21]. Using various activators in a single host matrix can be the other options for producing intense white luminescence [22]. When the two different dopants were added in crystal system, the luminescence energy from one activator can be transferred to the other, and two different emissions can be combined.

1.1.3 Phosphor film

These days, fabricating luminescent film has been much interest due to its wide applications. So far, the luminescent film was fabricated by screen printing technique, combustion CVD, spin coating, sol-gel soft lithography, and radio-frequency magnetron sputtering [23-25]. The screen printing and spin coating techniques are the most simple fabrication process to form a phosphor film, so these processes are widely used in variety applications. However, the fabricated phosphor film by those processes has critical problems in adhesion. Therefore, it has laminations to apply in the high-end technology. In the case of CVD and sputtering process, the adhesion of phosphor film on substrate is quite good, and those processes can be applied to small scale of device with high uniformity. However, those process is quiet expensive to maintain the equipment, and the process of fabricating phosphor target is too complicate. Therefore, new process which is simple and inexpensive method and which produces highly uniformed phosphor film is needed. In case of PEO process, the equipment is quietly simple

and it is appropriate for mass production. In addition, the ceramic like oxide layer is directly formed during oxidation process, so well adhesive luminescent films with high uniformity can be obtained.
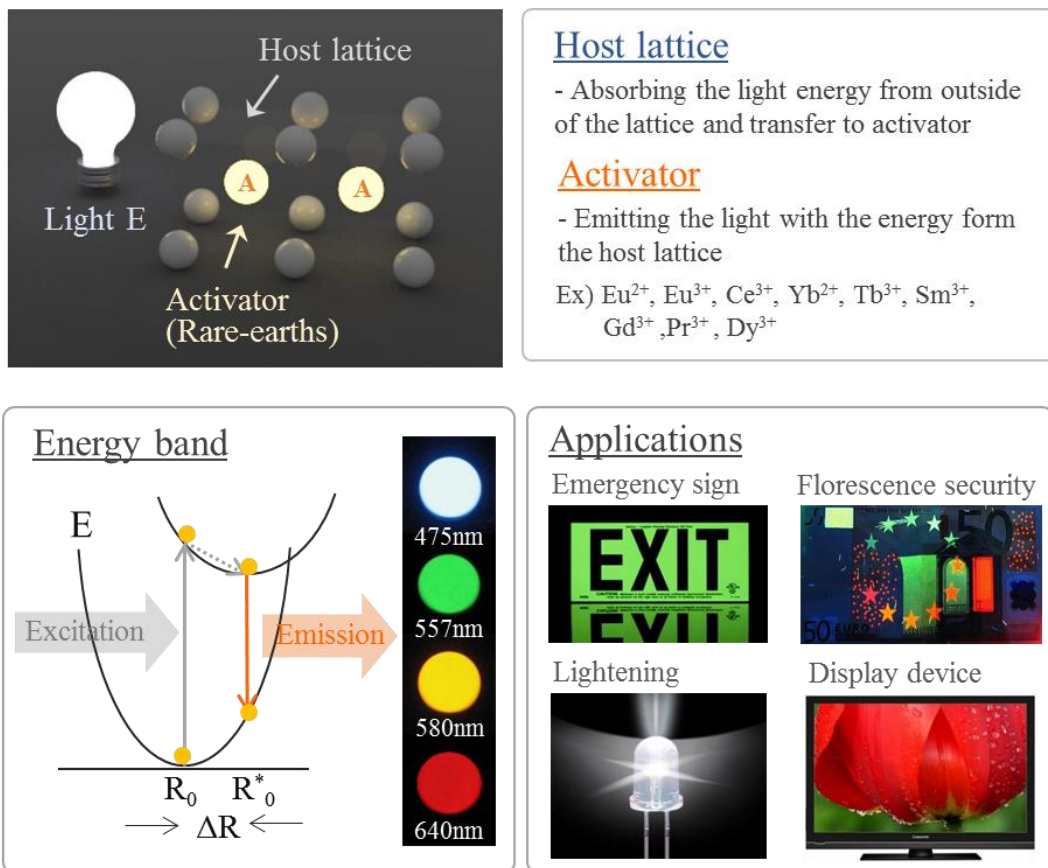
Figure 1.1 Phosphor materials and applications
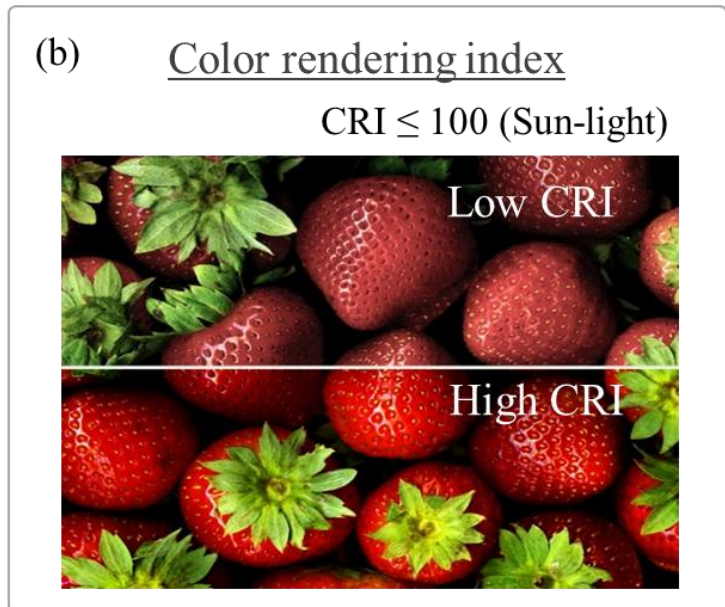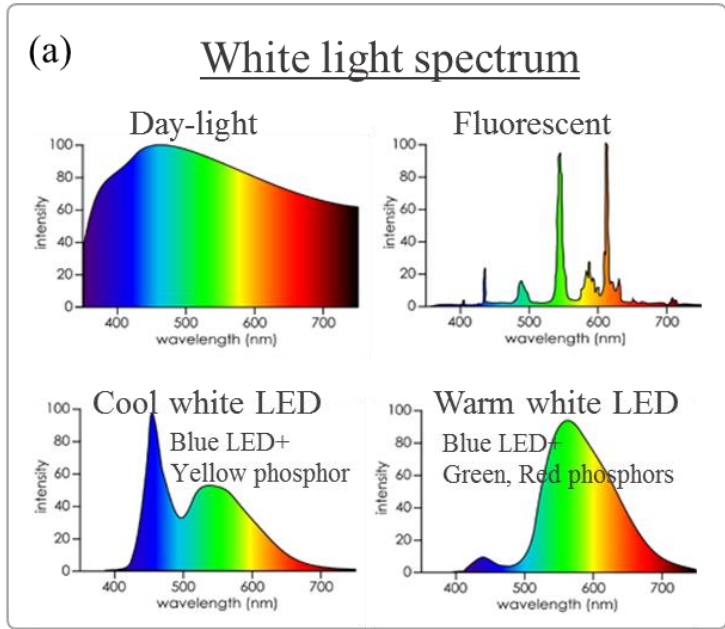
Figure 1.2 White luminescence and color rendering index
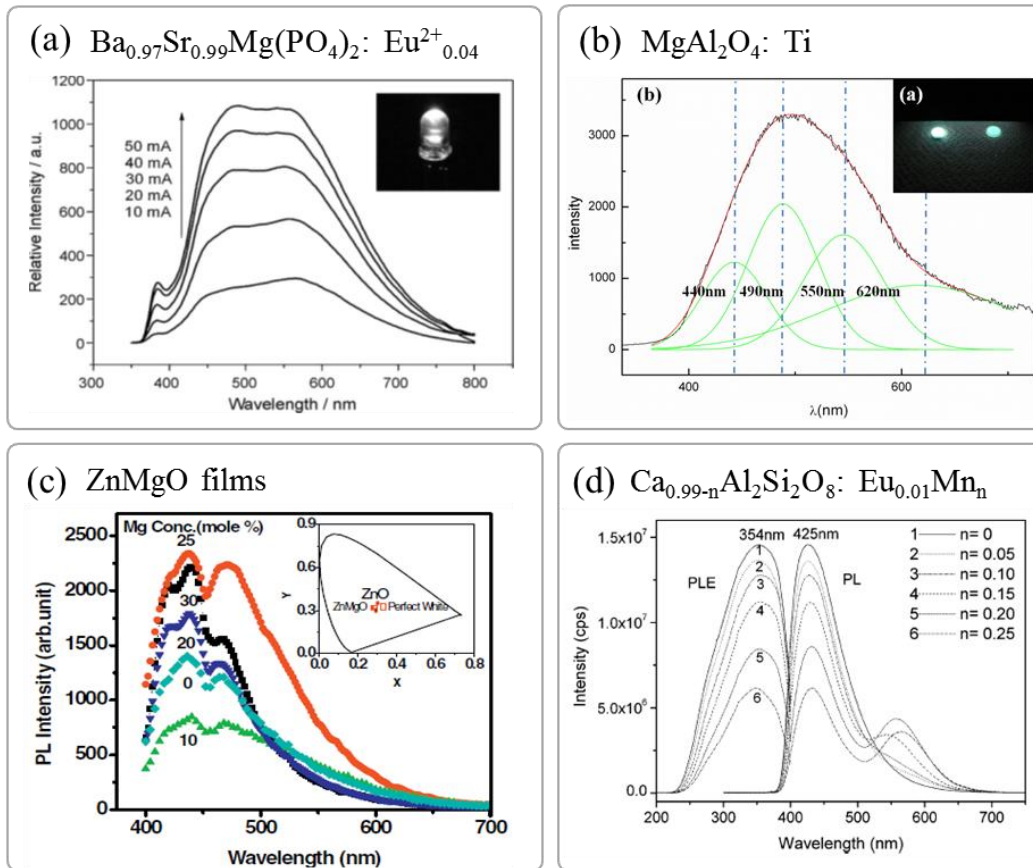
Figure 1.3 white light luminescent phosphors; (a) BaSrMg(PO$_4$)$_2$:Eu phosphor[20], (b) MgAl$_2$O$_4$:Ti [21], (c) ZnMgO nanophosphor film [26], (d) CaAl$_2$Si$_2$O$_8$:Eu, Mn [22]
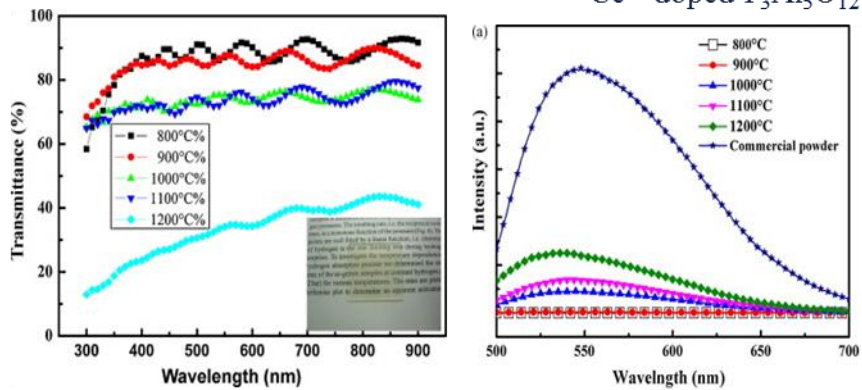
Figure 1.4 Methods for preparing phosphor film (a) radio-frequency magnetron sputtering[23] and (b) Screen printing technique[24]

1.2. Plasma Electrolytic Oxidation

1.2.1 Introductions and applications

Micro-arc oxidation (MAO) which is also called as plasma electrolytic oxidation (PEO) is a new method for surface treatment of metal substrate such as aluminum, magnesium and titanium. This process is based on electrochemical method which applies higher electrical power than anodizing process, so the oxidation of metal substrate is occurred at harsh atmosphere which accompanies discharge phenomenon [27-31]. At the high electrical voltage condition, dielectric breakdown is occurred through the micro-hole of the metal oxide film with the dissolution of metal substrate and oxygen gas evolution, so the ceramic-like thick oxide layer can be obtained with this anodic process. The resulted oxide film is mostly concluded by the metal substrate, electrolyte condition and electrical power condition such as current density frequency and duty ratio.

The surface properties of oxide film such as wear resistance, corrosion resistance, heat resistance, electrical insulation, micro-hardness and adhesion to substrate can be highly improved through the PEO process. This PEO is quiet cheap and simple process, and they produce lower pollution than other surface treatment methods. Therefore, they have much attention in many industrial fields such as aerospace, automobile and portable electricity [32]. In 2012, this process was applied to the smart phone case of HTC Company, and the PEO treated case

9

showed good wear resistance with high strength.

1.2.2 Plasma generation mechanism

In plasma electrolytic oxidation process, a number of electrochemical phenomenon is observed at the electrode in aqueous solution. At the anodic surface, oxygen gas is generated with the oxidation of metal substrate, and the hydrogen gas evolution and cation reduction is occurred on the cathode surface [27]. These electrochemical process at both electrodes conclude current- voltage curves which is shown in the Figure 1.6. A 'type-a' current–voltage curve represents a metal–electrolyte system at the point of gas liberation on either the anode or cathode surface, and 'type-b' represents a system where oxide film formation occurs during oxidation.

At the type-a system, potential and current rise is shown in the early stage with gas generation on the electrode surface. When the current density continues to rise, electrolyte is locally boiled near the electrode, and continuous oxygen or hydrogen gas vapor plasma lead low electrical conductivity. So the electrical channel can be formed through this thin micro region, and they are appeared as sparks on the metal substrate. In the meantime, at the type-b systems, the passive film which is previously formed begins to dissolve due to the corrosion potential of the material. Then, at high voltage, oxidation process is occurred with forming

10

porous oxide film. Over point U5, the film is broken through due to impact or tunneling ionization. At this point, small luminescent sparks are observed to move rapidly across the surface of the oxide film, and larger arc-discharges is getting arise. In the region U6–U7, micro arcs or discharges are generated and the oxide film is gradually fused and alloyed with elements contained in the electrolyte. Above the point U7, the arc micro-discharges transform into powerful, arcs, which may cause destructive effects such as thermal cracking of the film. (This paragraph is a summary of some part in reference [27])

When the coating became thicker and thicker, ions were hard to pass through the film. So, at this point, electric discharge was generated along the micro hole, and plasma enveloped with oxygen gas generation. Under the plasma condition, ceramic-like anodic coating was formed with high temperature reactions, so the porous ceramic layer would be formed. In this process, we had a new idea using this plasma phenomenon. Here is the scheme of the idea in Figure 1.7. When rare-earth materials are added in the electrolyte, the rare earth ions can corporate in the plasma discharge zone. And, high temperature and pressure atmosphere help rare-earth doping in the oxide film. Finally, we can get a rare earth doped oxide film which shows photoluminescence property like phosphor materials. This plasma oxidation process for generation of phosphor film was firstly introduced from our group and this process can be the good synthesis methods for formation of the uniform luminescent film.

Pressure: 102 MPa
Temperature: 2×10^4 K
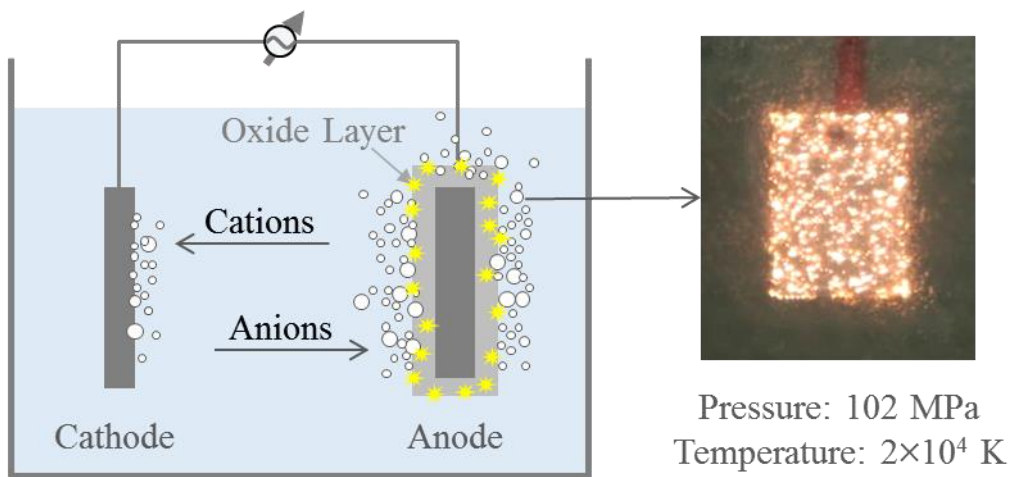
2012 HTC One S.
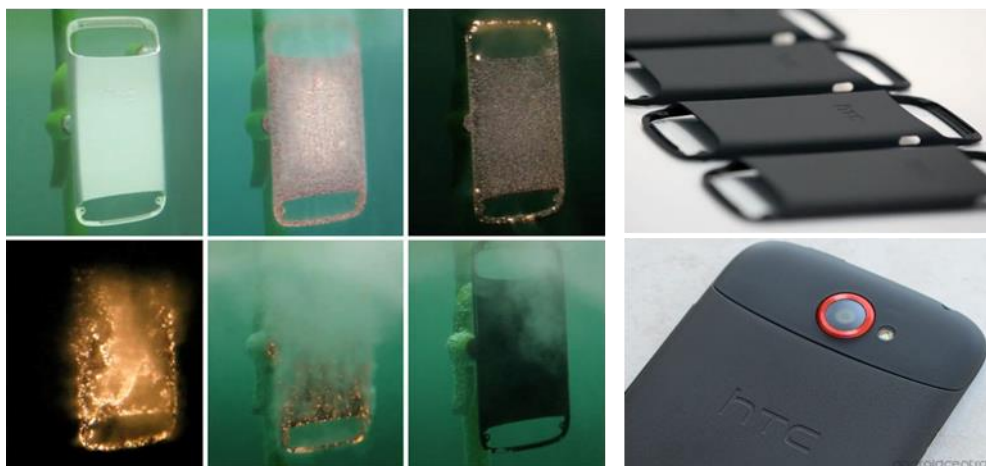
Figure 1.5 Schematic of plasma electrolytic oxidation and applications
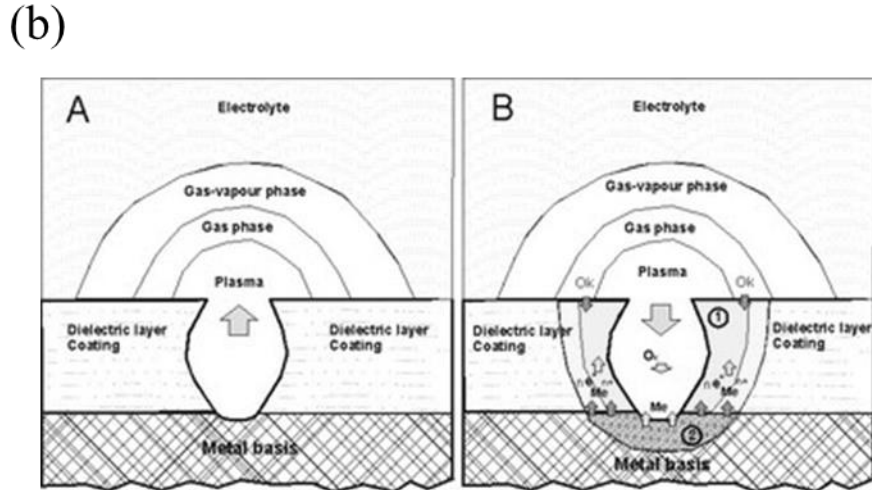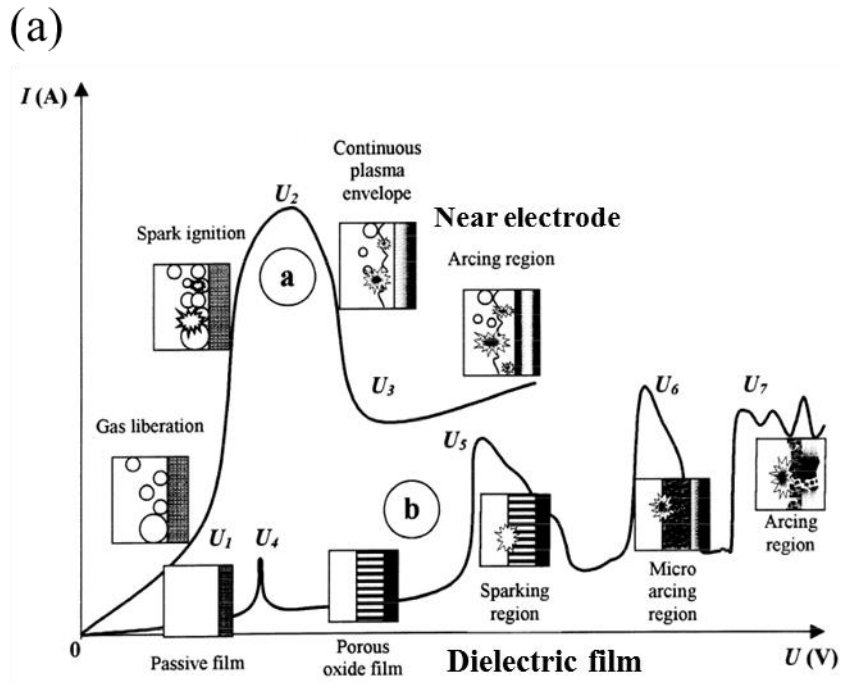
Figure 1.6 Mechanism of plasma generation in PEO process (a) voltage-current

curve[27] and (b) schematic figure of plasma discharge zone
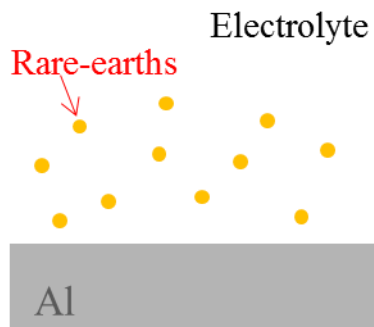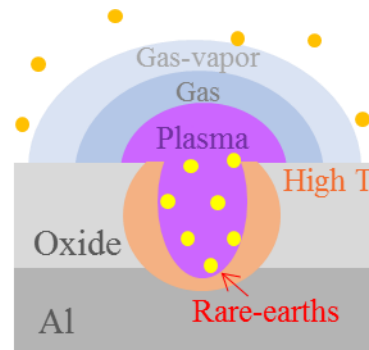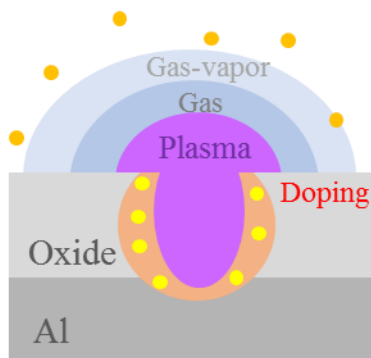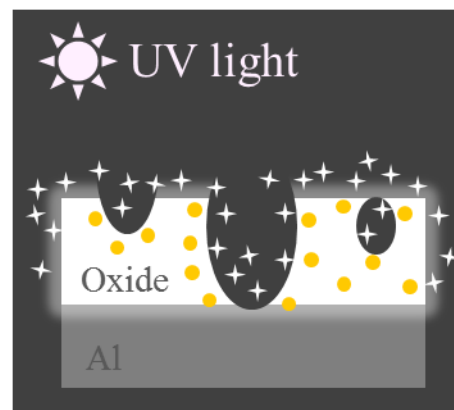
Figure 1.7 Schematic figure of rare-earth doping process in plasma electrolytic oxidation

Chapter 2. Experimental procedure

1.1. 2.1 Luminescent film formation by PEO

Aluminum oxide film

For plasma electrolytic oxidation (PEO) synthesis, commercially available aluminum foil (99.997%, 0.25 mm thick, Puratronic) was prepared and polished with electrochemical polishing methods. The electrolyte was a base aqueous solution containing 1) potassium hydroxide, 2) sodium silicate with potassium hydroxide or 3) sodium aluminate. Europium oxide (Aldrich, Milwaukee, WI) or cerium oxide particles were added in each electrolyte. The detailed electrolyte condition is shown in Table 2.1. A flat stainless-steel plate (50 mm x 100 mm x 1 mm) was used as a counter electrode. PEO was conducted at a constant applied current density of 3 A/dm^2 at 15 ^{o}C up to for 60 min using a DC pulse power supply. A pulse frequency and a duty cycle were fixed at 100 Hz and 60 %, respectively. After the PEO treatment, the specimens were washed with ethyl alcohol and then dried. To fabricate translucent alumina film, the oxidized film was coated with Si resin and annealed at 140 ^{o}C for 2hr. After curing, the aluminum foil was etched in a mixture of saturated copper chloride and hydrochloric acid solution.

15

Magnesium oxide film

The experimental process of preparing magnesium oxide film was the same as that of aluminum oxide film formation. Magnesium AZ31 plate was used for PEO treatment, and potassium hydroxide added sodium silicate electrolyte was used with cerium oxide particle. The current density was 3 A/dm^2, and the frequency and duty cycle were fixed as 100Hz and 6%. The washing process was the same as referred in aluminum oxide condition. In the magnesium oxide film work, magnesium silicate powder was also synthesized by conventional solid state reaction for comparing photoluminescence property with the film. The starting materials were MgO (Magnesium oxide 99+%, ~325mesh, Aldrich, Milwaukee, WI), SiO$_2$ (Silicon dioxide ~325 mesh 99.5%, Aldrich, Milwaukee, WI), CeO$_2$ (Cerium oxide < 25 nm, Aldrich, Milwaukee, WI). For the solid-state reaction synthesis, the stoichiometric mixture of MgO, SiO$_2$, and CeO$_2$ were mixed in absolute ethanol, ball milled for 24 h, and then dried in an oven for 24 h. The dried mixtures were annealed at 1200～1400 ◦C for 3 h under 5% H$_2$/N$_2$ atmosphere to reduce Ce^{4+} to Ce^{3+}.

2.2 Characterization

The phases of as-synthesized films were examined by X-ray diffraction (XRD, D8-Advance, BRUKER MILLER Co.) using Cu Kα radiation (λ = 1.5406 Å). The morphology of the film was observed by field emission scanning electron microscopy (FE-SEM, SU70, Hitachi), and cathodoluminescence property was observed by CL detector (Mono CL4, Gatan) in the FE-SEM. PL spectra were obtained at room temperature using a fluorescence spectrometer (PS-PLEU-X1420, PSI) equipped with a 500 W Xenon lamp at a scanning speed of 60 nm/min. Time-resolved photoluminescence (PL) lifetime measurements were performed via the time-correlated single photon counting (TCSPC) methods using a FluoTime 200 instrument (Picoquant, Germany). A 377nm pulsed diode laser with repetition rate of 250 kHz and 50 kHz was used as an excitation source. Electron Spin Resonance experiments were carried out with JES-TE200 ESR spectrometer operating at X-band micro frequency with 9.21 GHz modulation frequency. The composition of the synthesized film was determined by inductively coupled plasma mass spectroscopy (ICP-MS, Model ELAN 6100, Perkin-Elmer SCIEX). The XPS measurements were performed in a Thermo VG, U.K. XPS (K-alpha) surface analysis system with a monochromated Al x-ray sources (Al Kα line: 1486.6ev). The X-ray power was 12kV and 3mA, and pass

energy was 50eV. An energy step of 0.1 eV was used to acquire the XPS spectra. The TEM specimens were prepared by focused ion beam (FIB, Carl Zeiss Auriga) method, and Cs-corrected FE TEM (JEOL-2100F, Japan) was employed to further investigate the existence of europium ions in gamma alumina film. Scanning transmission electron microscope (STEM) bright field images were collected using a high-angle annular dark-field (HAADF) detector and the chemical composition. The elemental composition was also determined by energy dispersive X-ray spectrometer (EDS) at an acceleration voltage of 20 kV using an ISIS 300 system (Link Analytical, Oxford Instruments), equipped in HR-TEM. For the calculation of crystal structure, first-principles pseudopotential methods based on density functional theory was used. DFT calculations were performed using the Vienna Ab Initio Simulation (VASP) Package with the Perdew–Burke–Ernzerhof (PBE) exchange correlation functional for Al_2O_3 with and without V_0, and GGA+U for europium doped Al_2O_3 with U_{eff}=7eV. For the k-point integration, we use a 4x4x2 mesh for the primitive cell of gamma-Al_2O_3 and only for supercell with V_0 and Eu_{Al}, and the cutoff energy is 600eV.
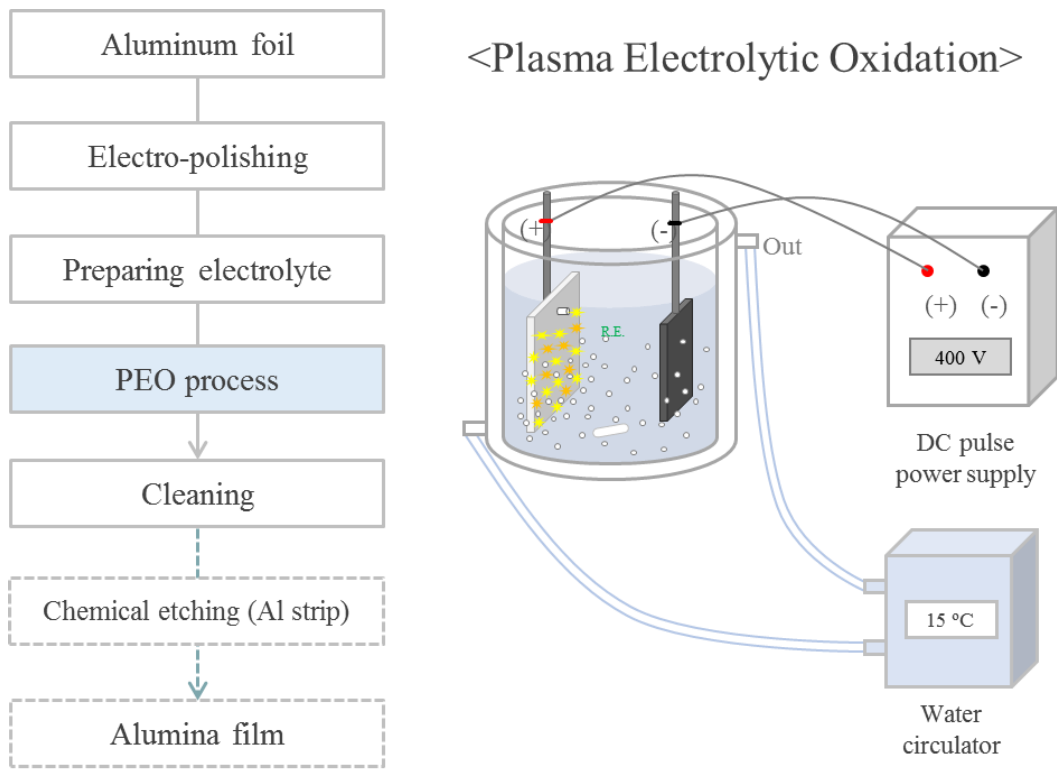
Figure 2.1 Experimental procedure of plasma electrolytic oxidation

Table 2.1 Electrolyte conditions of aluminum and magnesium oxidation in PEO process

Substrate / Electrolyte	Aluminum foil	Magnesium AZ31
KOH (Potassium hydroxide)	1g/l KOH	-
NAO (Sodium aluminate)	15g/l $NaAlO_2$	-
NSO (Sodium silicate)	5g/l Na_2SiO_3 + 3 g/l KOH	10g/l Na_2SiO_3 + 3 g/l KOH
Rare-earths	2g/l Eu_2O_3, 2g/l CeO_2	3g/l CeO_2

Chapter 3. Results and Discussions

3.1 White-light emitting Al$_2$O$_3$:Eu film on aluminum foil

3.1.1. Luminescent oxide film formation

Figure 3.1 (a) shows time-voltage curve at constant applied current density of 3 A/dm2 during PEO. From the other previous reports, the voltage transient was divided into two stages in PEO process [31]. The first stage is corresponded to the conventional anodizing which is a linear voltage increase process accompanied by a gaseous evolution without a sparking. In the second stage corresponding to the plasma anodizing, the intense sparking and vigorous gaseous evolution were observed, and the cell voltage slowly increased to 500 V. The breakdown voltage and ignition time are defined as the voltage and time for the appearance of sparks on the anode surface, and they were approximately 468 V and 31 s, respectively. At this point, white light sparks (inset images in Figure 3.1 (a)) were generated along the edge of the aluminum foil, and sparks were getting larger and moved to the surface as increasing PEO time. The transient curves were not noticeably affected by Eu$_2$O$_3$ addition. As shown in the scheme (Figure 3.1(b)), during spark generation, europium oxide particles might be incorporated in the aluminum oxidation process. At the break down zone, electrical channel was generated along the micro hole with oxygen gas development, and plasma phenomenon was

occurred in this hole with high temperature and pressure atmosphere which could be a driving force for crystallization of the film. When the europium oxide particles existed in that plasma zone, the europium ions might be incorporated and doped in the aluminum oxide film. This phenomenon proceeded continuously with the formation of aluminum oxide film and continued with increasing film thickness.

In order to figure out luminescent film formation at initial stage, cathodoluminescence analysis was performed with morphology observation. Before the sparks generation, only corrosion spots were observed, and they showed no CL property (Figure 3.2 (b), 10sec). After breakdown, spark generated zone was formed with high luminescence performance, and this area was getting broadened and thickened as PEO time increased. As shown in the schematic figure (Figure 3.3 (a)), dissolution and oxidation process of aluminum is occurred at the same time during PEO process. Especially at the spark generated zone, oxidation of aluminum ions were accelerated and annealed at high pressure and temperature atmosphere. The cathodoluminescence spectra showed the luminescence from the sparked area showed intense CL property with broad emission, while the corrosion spot showed very weak and narrow cathodoluminescence spectrum. Thus, from the CL results, it is clearly proved that the luminescence property of oxide film in PEO process results from spark generation mechanism.

As time progressed in PEO process, spark generated oxide layer was randomly covered aluminum foil, and the film thickness was getting thicker. After 45minutes, the thickness of the oxide film was around 6 micron meter (Figure 3.4), and the anodic layer was quiet rough due to the micro pore which was formed by break down generated channel. The breakdown of oxide film in high electrical voltage is randomly and simultaneously generated along the surface of metal, and they moves around the oxide surface. So, the aluminum oxide films were not highly uniform in this process. The x-ray diffraction data of europium doped alumina film prepared by PEO process are shown in the Figure 3.4. After the breakdown voltage, white colored oxide film was formed on the aluminum foil, but the oxide layer was not highly crystallized until 1 min. As increasing PEO time, weak and broad gamma phase of aluminum oxide peaks appeared along with those of aluminum foil, and the XRD intensity of γ-Al$_2$O$_3$ was increased. The diffraction peak related to the europium ion was not observed even at the sample treated for long time.

The photoluminescence property of the europium doped γ-alumina film was shown in the Figure 3.5. The excitation spectrum showed a broad absorption in the UV region (200～400 nm), and the emission spectrum exhibited a broad emission which covered most visible light region from 350 to 650 nm. The highest emission was centered at 408 nm under the excitation of λex=257 nm, and the other emission peak was centered at 495 nm. These two emission centers are

overlapped with large FWHM (~197.6 nm), and it looked as white light in UV lamp (Ex=365 nm). The CIE coordination was (x, y) and this values belongs to bluish white light with 1000K of color temperature. The photoluminescence intensity of the Al_2O_3:Eu film was increased with the oxidation time, and the maximum intensity was shown at the alumina film treated for 45min.

In order to enlargement of application area, additional etching process was performed in the white luminescent aluminum oxide film to develop translucent film (Figure 3.6). At first, as synthesized PEO film was prepared and covered with silicon resin, because the dried resin helped to maintain shape of thin aluminum oxide layer. Then, the silicon resin coated MAO film was immersed in the copper chloride containing hydrochloric acid. After etching process, the translucent aluminum oxide film with intense white luminescence property was finally obtained as shown in the figure (Figure 3.6).
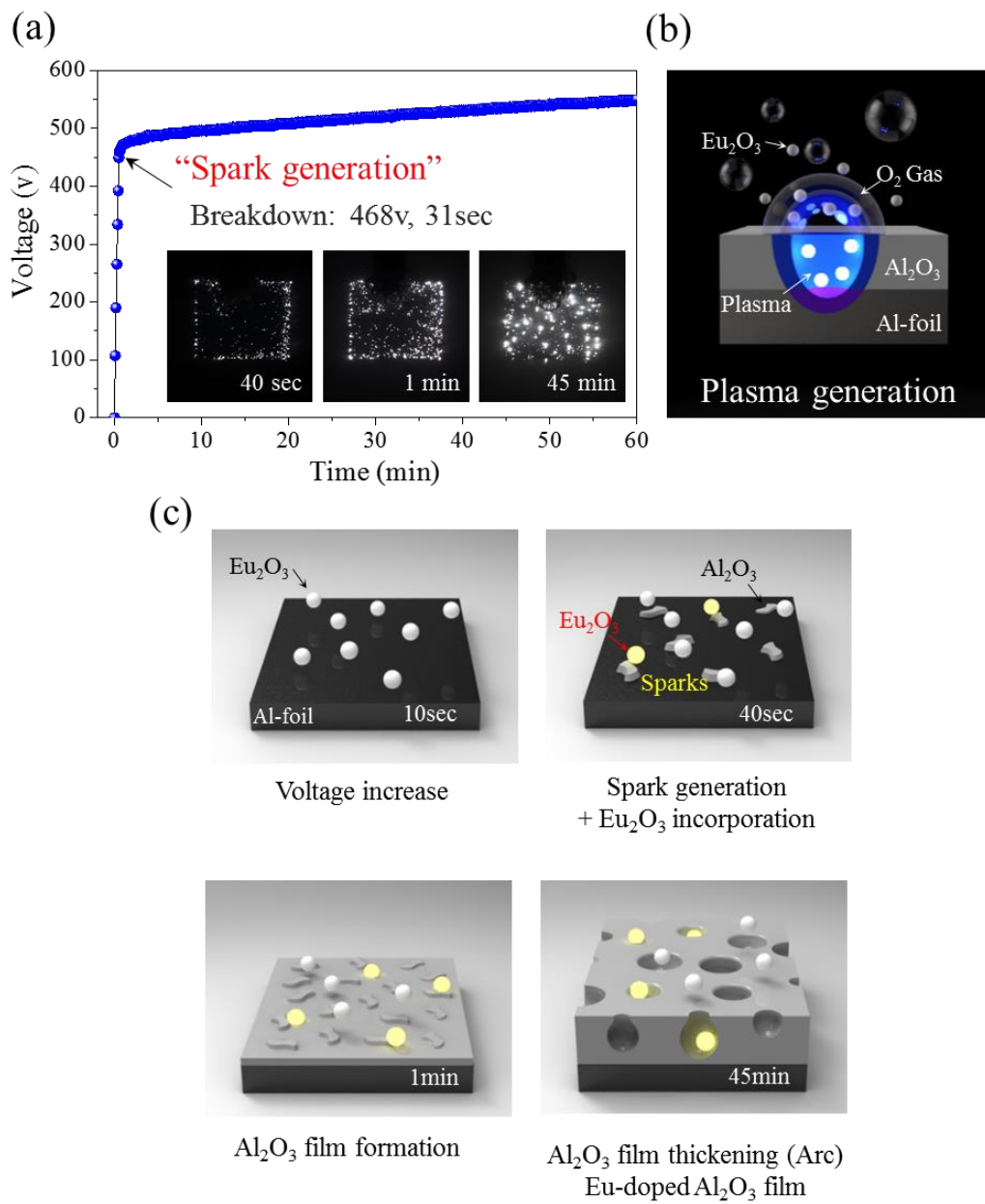
Figure 3.1 (a) Time-voltage curve of PEO process, schematic figure of (b) plasma discharge zone in PEO process and (c) europium cooperation in oxidation process
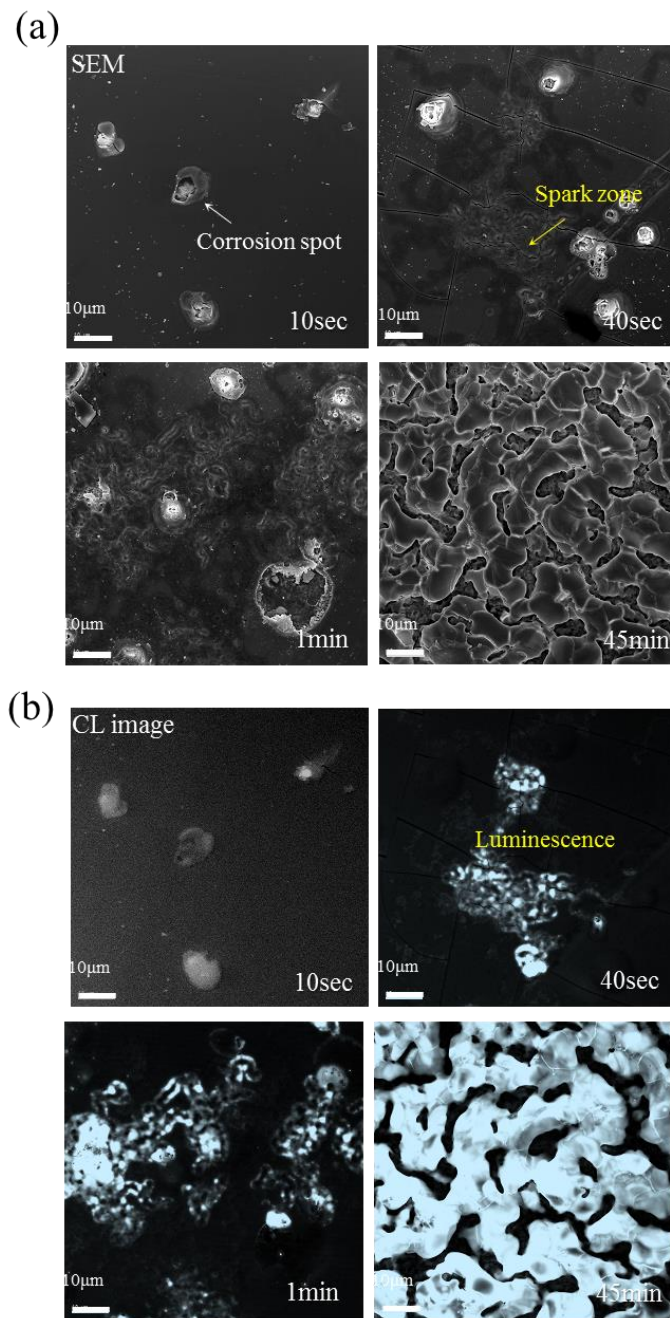
Figure 3.2 (a) SEM images and (b) cathodoluminescence images of aluminum surface in early stage and final stage of PEO process
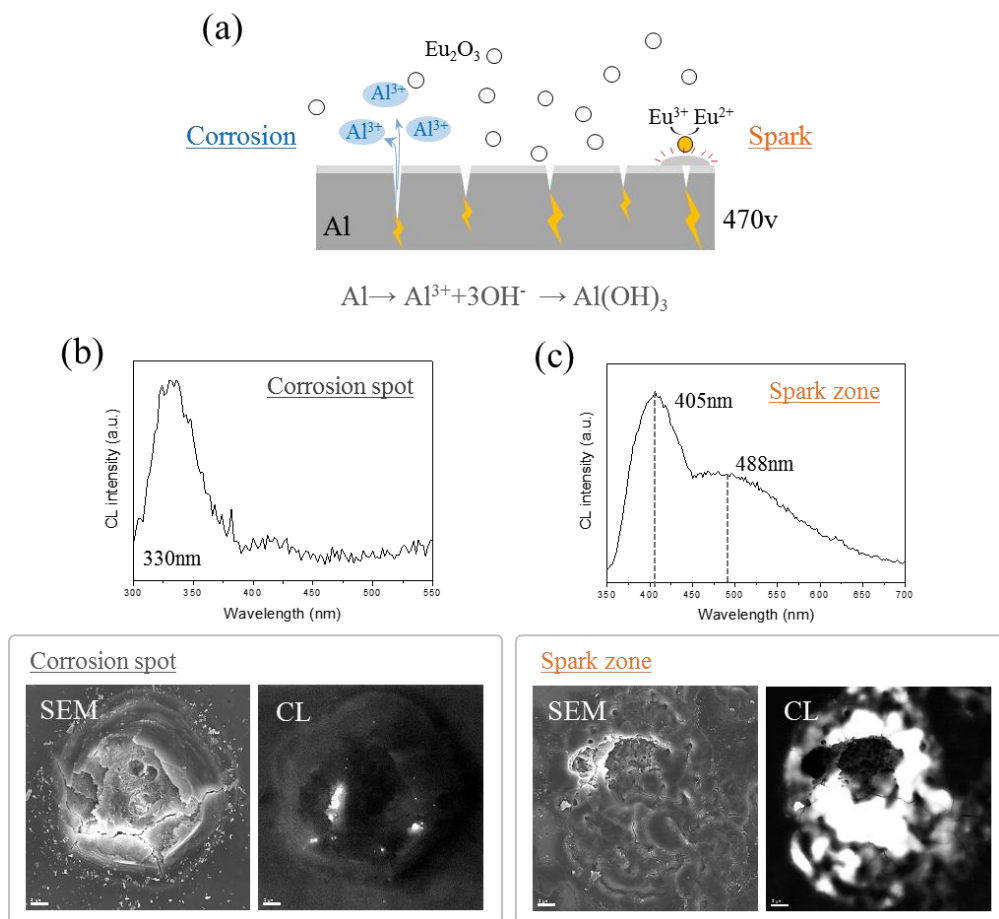
Figure 3.3 (a) Schematic figure of reaction at early plasma generation stage and cathodoluminescence spectra and images of (b) corrosion spot and (c) spark generated zone
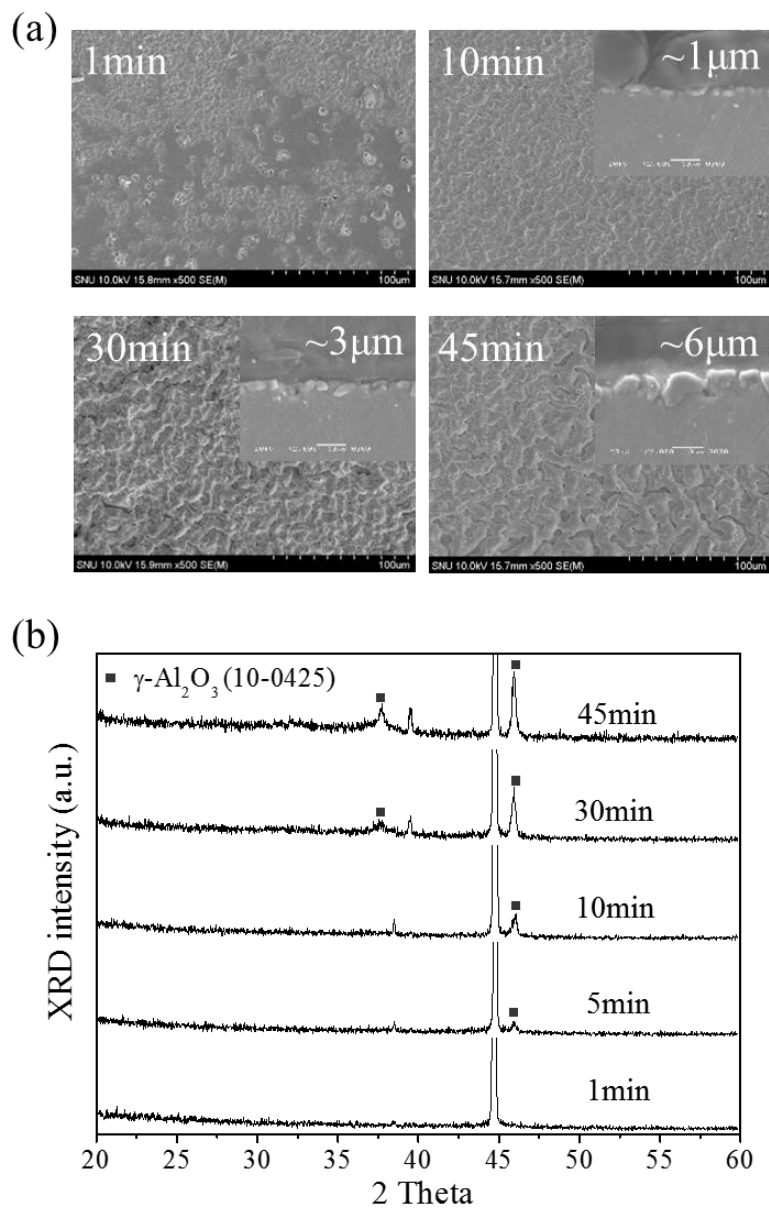
Figure 3.4 (a) FE-SEM images (top & cross view) of aluminum oxide film and
(b) XRD results as increasing plasma oxidation time
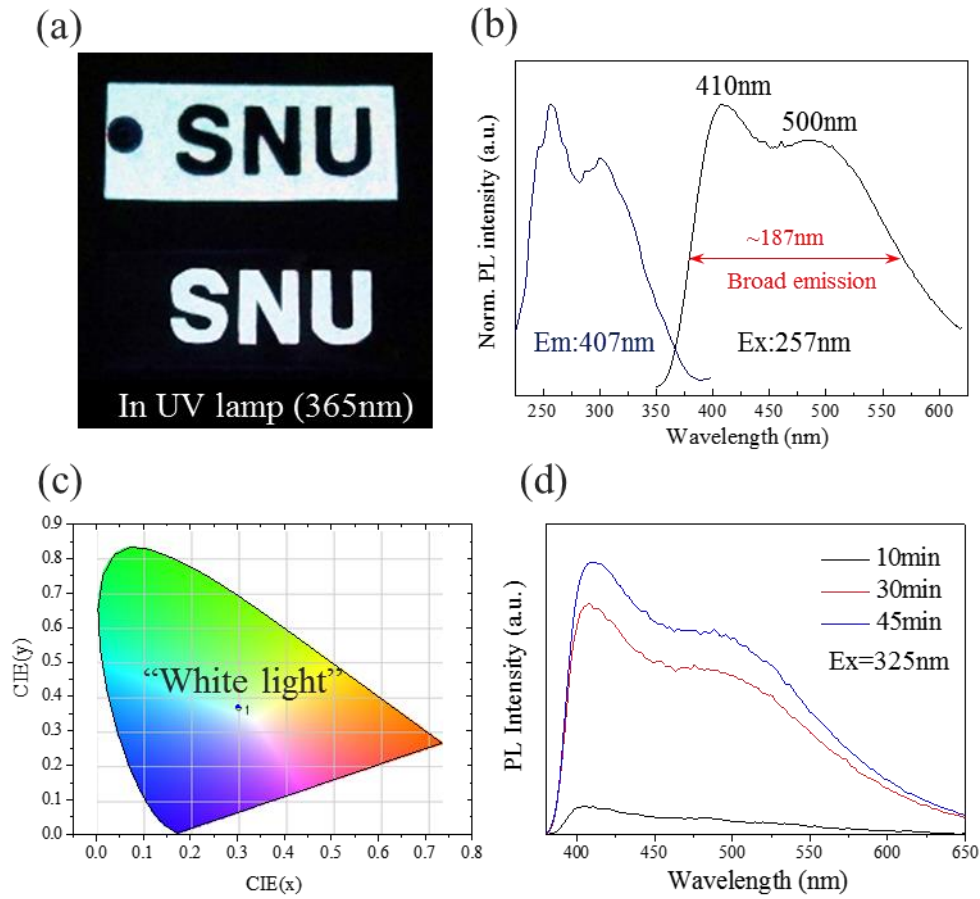
Figure 3.5 Photoluminescence property of europium doped aluminum oxide film; (a) photograph image under UV lamp (ex=365nm), (b) excitation and emission spectra, (c) CIE coordination and (d) emission spectra (ex=325nm) as increasing plasma processing time

(a)

UV(365nm)

"Luminescent film"

(b)

1. Aluminum foil
Al-foil

2. PEO process
Eu_2O_3 Al_2O_3
Al-foil

3. Si-resin coating
Resin
Al-foil

4. Etching
$CuCl_2$ +HCl

5. Translucent film
SNU

6. Luminescent film
Under UV light
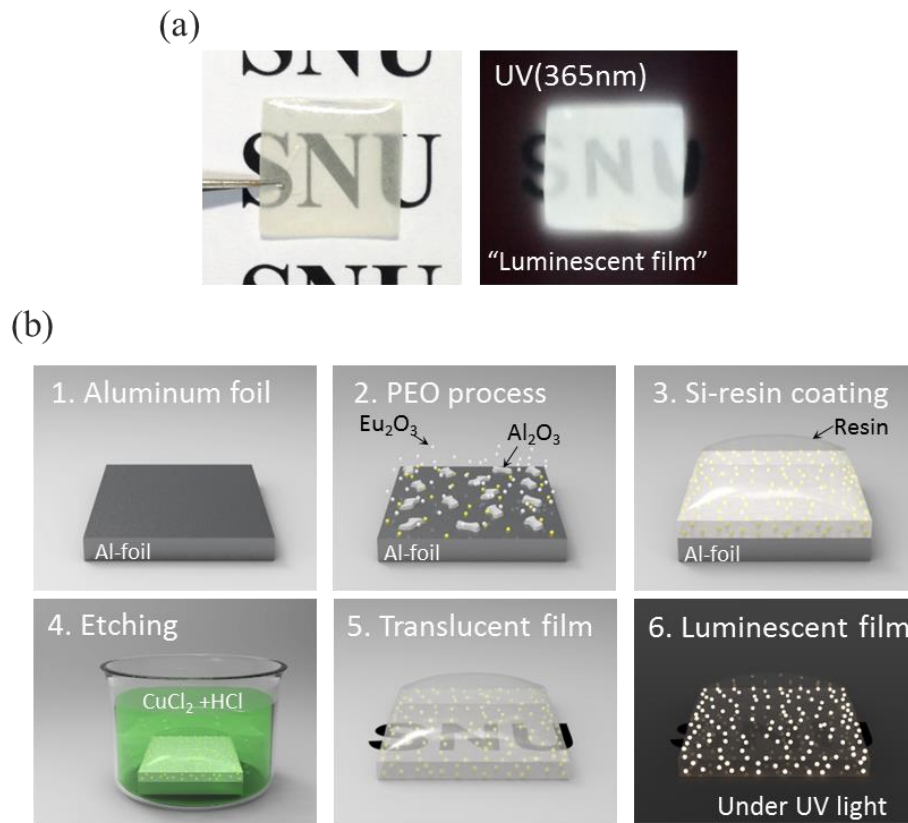
Figure 3.6 Translucent aluminum oxide film; (a) photograph image under sun light and UV lamp, (b) schematic figure of aluminum etching process

3.1.2. Experimental variable effects

In the plasma electrolytic oxidation process, the mechanical or chemical property of the synthesized oxide film is highly affected by elemental composition of electrolyte, because the electrolyte condition (pH or electrolyte conductivity) played decisive role in plasma generation atmosphere [33, 34]. Furthermore, additional ions or elements sometimes changes the crystal structure and composition of the oxide film, so various type of oxide films can be obtained through the electrolyte selection [35, 36].

In this work, sodium silicate and sodium aluminate were conducted as an electrolyte to form an aluminum oxide film in PEO process, and the photoluminescence property was investigated in order to know electrolyte effect on luminescence. As shown in the time-voltage curves in Figure 3.7, the breakdown voltage in sodium silicate and aluminate electrolyte was lower than KOH electrolyte due to their higher electrolyte conductivity. When sodium aluminate was used in electrolyte, alpha phase of aluminum oxide was formed in PEO film, by contrast, only gamma phase of alumina was obtained in KOH and sodium silicate electrolyte.

Morphology of the aluminum oxide film treated in different electrolyte condition was shown in the Figure 3.8. In contrast to KOH electrolyte, when sodium silicate and sodium aluminate electrolyte was used, aluminum oxide films showed porous structure with large size of micro pore, and particle attached like

ununiformed morphology was observed. From the EDS results, the unique morphology was composed of Na, K and Si ions, and these ions in the electrolyte hindered the formation of uniform aluminum oxide film. Especially in case of NSO electrolyte, rough and uniformed oxide layer was covered the smooth surface as shown in the enlarged SEM image, and large amount of silicon was detected in this area. The CL results were also showed that the silicon rich region did not emit cathodoluminescence.

The photoluminescence spectra of europium doped aluminum oxide film treated in various electrolyte condition were shown in Figure 3.9. Each spectrum showed different shape of emission, at the 325nm centered excitation, and the PL intensity of the two emission spectra centered at blue and green region were independently changed in each case. From the overlapped spectra figure, the blue light centered emission spectrum was highly affected by electrolyte composition. When sodium aluminum oxide electrolyte was used, the high energy centered emission was greatly increased whereas sodium silicate electrolyte used aluminum oxide film showed much lower emission intensity at this region. These results indicated that two different factors determining photoluminescence property were existed in this system, and these factors were highly influenced by electrolyte composition.

In order to figure out those factors in different point of view, electrical power condition was changed at the same electrolyte condition. Here, we used the DC

pulse type power source, so the frequency, electrical current density, maximum voltage, and duty cycle could be controlled as experimental variables in electrical power condition [37-40]. Most of those variables caused influence at the characteristics of the resulted film, but the duty cycle effect was the most significant, so it will be only discussed in this chapter.

Duty cycle (or duty factor) in DC pulse power means the percentage of one period in which a signal is on. A period is the time it takes for a signal to complete an on-and-off cycle. As shown in the figure (a), a formula of duty cycle can be expressed as:

$$D = \frac{t_{on}}{T}$$

Where D is the duty cycle, t_{on} is the time the signal is active, and T is the total pulse period of the signal. Thus, a 25% duty cycle means the signal is on 25% of the time but off 75% of the time. The "on time" for a 25% duty cycle could be a fraction of a second, a day, or even a week, depending on the length of the period.

In KOH electrolyte, when the duty cycle was low (6%), only edge side of the aluminum specimen was reacted as shown in the Figure 3.10 (c), and the plasma reaction area was enlarged to the surface as increasing duty cycle (%). The time voltage curve was also affected by duty cycle, and break down voltage and plasma generation voltage was over 520v at the low duty cycle (6%). The normalized photoluminescence spectra with different duty cycle in KOH and NSO electrolyte

were shown in the Figure 3.11(a), (b). In both cases, the green emission centered spectrum was highly increased with increasing duty cycle. As shown in the schematic Figure 3.11 (c), when the DC pulse power is on, plasma development through the micro hole is generated with high gas pressure and temperature which accelerate phase formation and europium doping process. At the period of power off, the heat treated oxide film is cooled down due to low temperature water circulation system, and the vacancy formation is dominantly acted in this period. When the duty cycle is 6%, the plasma generated time is too short to form aluminum oxide layer and to react with europium ions, so the photoluminescence intensity is much lower than high duty cycle condition. As increasing duty cycle, more europium ions can be incorporated to aluminum oxide film, and the vacancy formation can be reduced due to very short cooling time. In that, from the photoluminescence results, the blue emission centered spectrum might be related to the oxygen vacancy, and the green centered emission might be affected by incorporated europium ions in aluminum oxide layer.

Here, in the PEO process, we conducted europium ions to fabricate the photo-luminescent aluminum oxide film. In order to know rare earths effect on the luminescence property, cerium oxide powder was also tried at the same experimental condition. The ionic radius of aluminum, cerium and europium ions are shown in the Figure 3.12. In contrast to the 3+ charge of aluminum ion, the ionic radius of rare earths are much large, so it would be very difficult to

substitute aluminum ion by rare earth ions in theoretical approach. However, through PEO process in extreme circumstance, europium ions could be doped in the aluminum oxide film. In this way, relatively smaller ion of cerium was adopted. The X-ray diffraction patterns of rare-earths free, europium and cerium doped aluminum oxide films prepared in KOH electrolyte were shown in the Figure 3.12. When pure KOH electrolyte was used (R.E. free), alpha phase of aluminum oxide was formed, in contrast to the rare earths containing electrolyte. In case of cerium oxide added condition, gamma phase of aluminum oxide was formed and large amount of cerium oxide peak was observed. In addition, the cathodoluminescence spectra showed very different spectrum shape (Figure 3.12) depending on the doped rare-earths.

When the rare-earth free electrolyte was used, the main luminescence was centered at 310nm and very weak cathodoluminescence was appeared in visible light range from 400 to 500nm, and the emission in red light region was also observed in the CL spectrum. This luminescence can be explained as vacancy center in alpha and gamma alumina phase. In case of cerium doped alumina film, the main luminescence was centered at 380nm, and there were several luminescence centers at 400nm, 450nm, and 670nm. Most luminescence center in visible light region might be due to the vacancy center, but the emission at 380nm could be the luminescence of cerium ion in alumina. From these results, we can guess the luminescence centers by comparing the CL spectra, but finding the exact

factor of luminescence at each wavelength is quiet difficult in this stage. In order to find out the luminescence centers in gamma aluminum oxide crystal system, the simplest case which contained few parameters in experimental process was adopted. In that, KOH electrolyte used Al_2O_3 film was used for further analysis, and detailed explanations were discussed in next section.
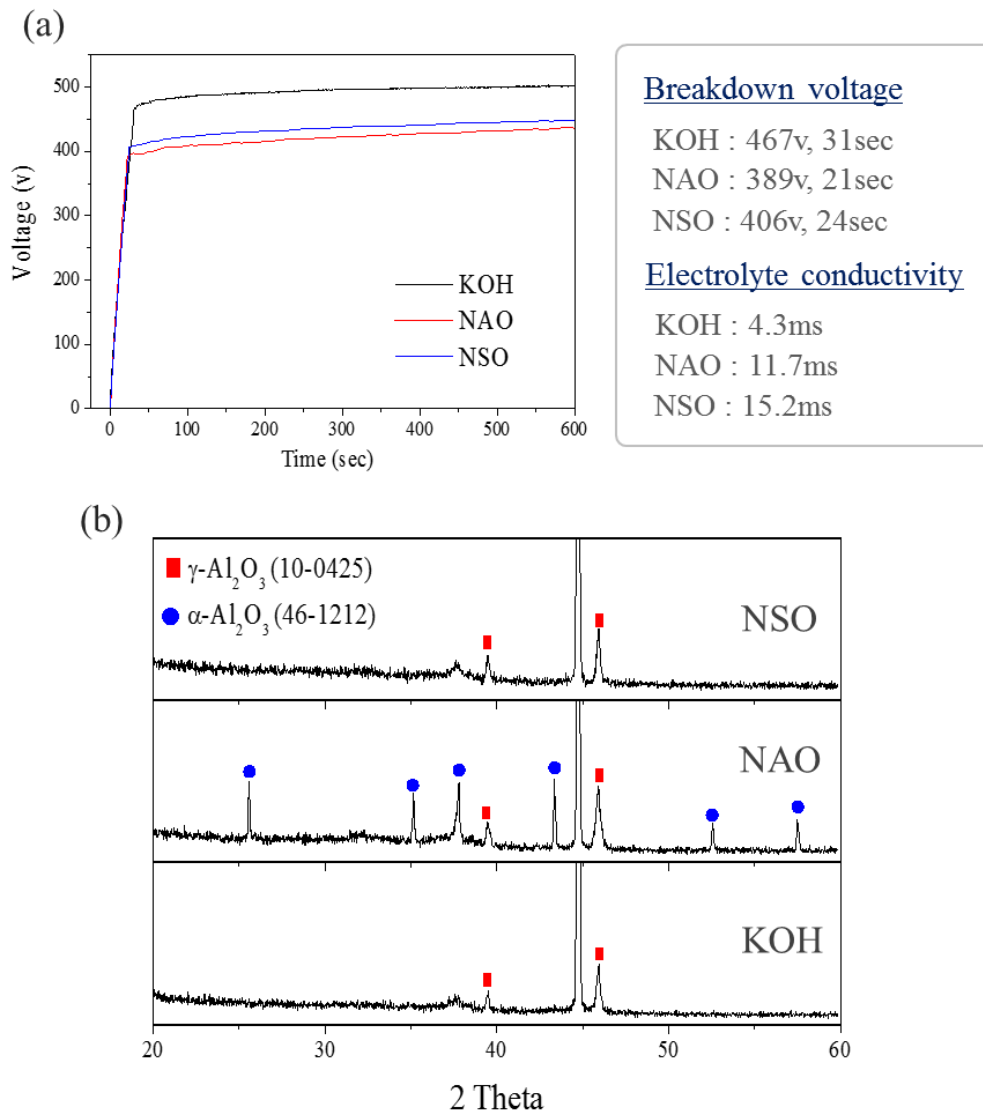
Figure 3.7   Aluminum oxide film prepared in different electrolytes; (a) time-voltage curves and (b) XRD patterns

(a)

1KOH

20µm

SNU 5.0kV 16.1mm x1.00k SE(M)   50.0um

(b)

15NAO

20µm

SNU 10.0kV 15.8mm x1.00k SE(M)   50.0um

(c)

5NSO+3KOH

20µm

SNU 10.0kV 15.7mm x1.00k SE(M)   50.0um

(d)

5NSO+3KOH

5µm

SNU 10.0kV 15.2mm x5.00k SE(M)   10.0um
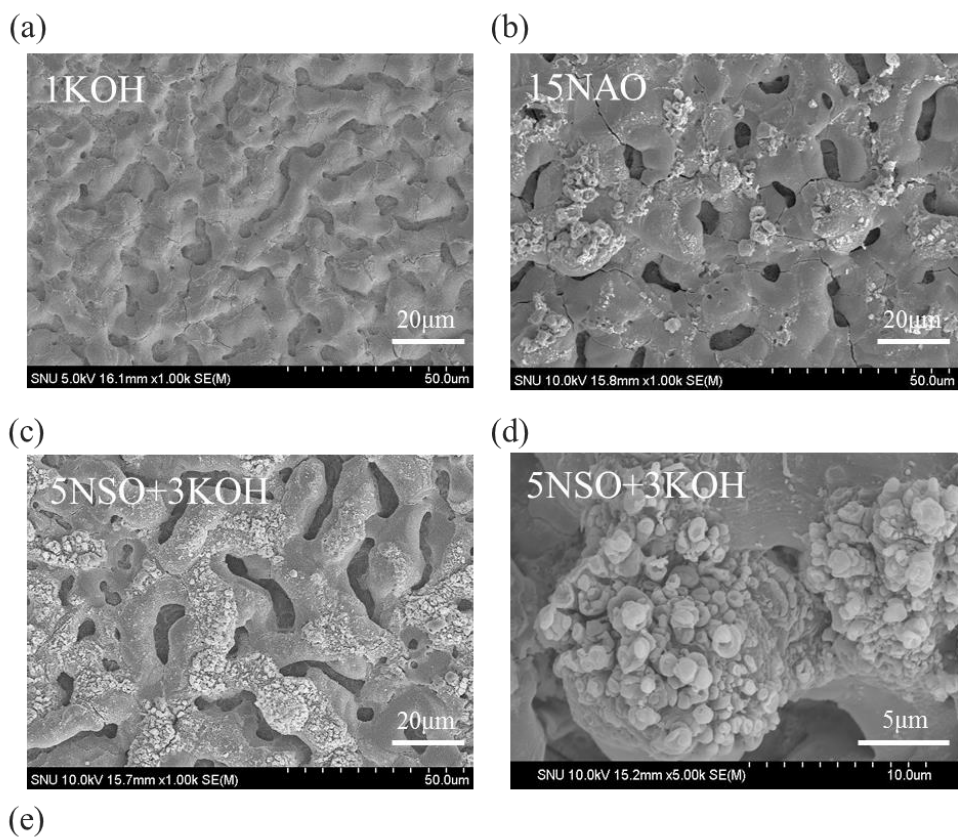
(e)

Element (At. %)	KOH	NAO	NSO	NSO Si-rich
Al K	31.8%	37.6%	21.4%	5.1%
O K	68.0%	60.4%	70.4%	71.0%
Eu L	0.2%	0.7%	0.1%	0.1%
Na K	-	1.3%	0.3%	-
Si K	-	-	7.2%	18.6%
K K	-	-	0.6%	1.9%

Figure 3.8 FE-SEM images of europium doped alumina oxidized in different electrolytes; (a) KOH, (b) $NaAlO_2$, (c) $NaSi_2O_3$ and (d) high magnified image of the sample treated in $NaSi_2O_3$
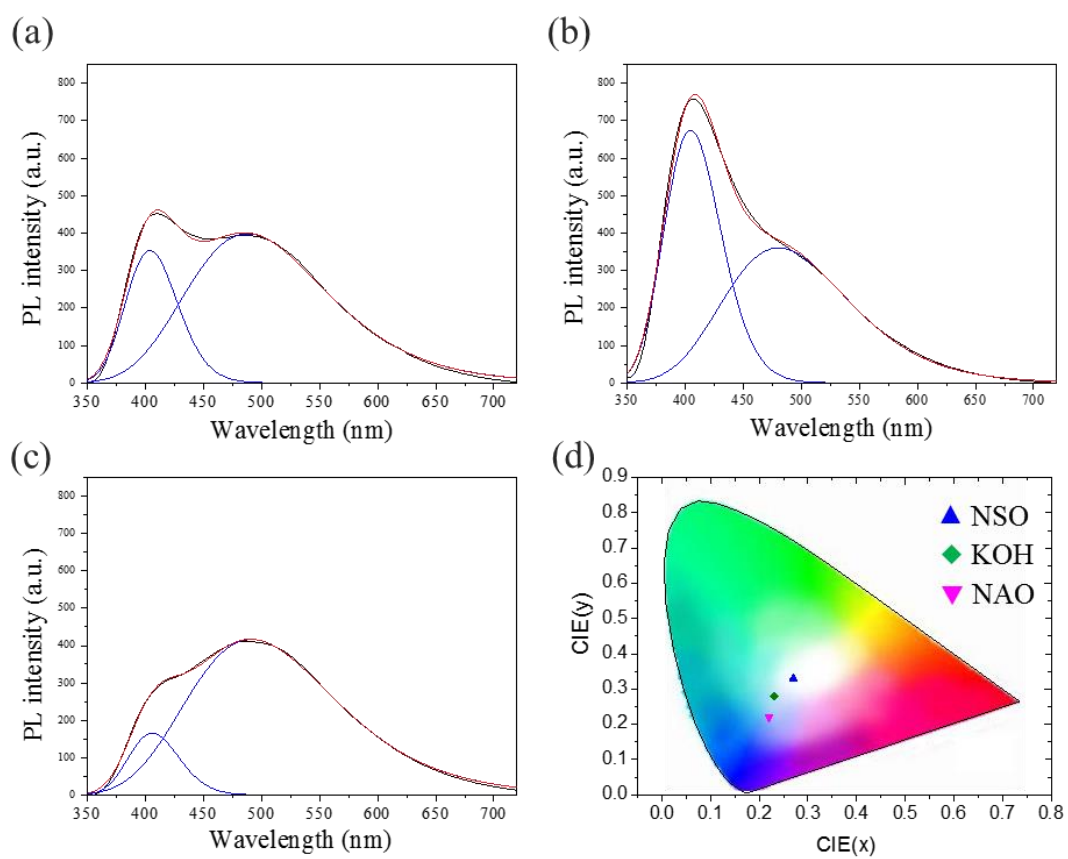
Figure 3.9 Photoluminescence spectrum (ex=325nm) of (a) KOH, (b) NaAlO$_2$,

(c) Na$_2$SiO$_3$ and (d) CIE coordination of each electrolyte condition

Table 3.1 Gaussian fitting results of the emission spectra which is treated in different electrolyte conditions

	1KOH		15NAO		5NSO+3KOH	
	Peak 1	Peak 2	Peak 1	Peak 2	Peak 1	Peak 2
Center(eV)	3.06	2.54	3.06	2.58	3.05	2.52
Wavelength(nm)	405	488	405	480	406	492
FWHM(eV)	0.39	0.73	0.43	0.68	0.38	0.76
Height	353	398	674	360	165	416
Area (%)	32%	67%	54%	45%	16%	83%

(a)

Duty cycle (%) in DC pulse power

$$D = \frac{t_{on}}{T}$$

t_{on} : Pulse width

T : Pulse period

(b)

(c)

PEO Plasma images

Duty 6%   Duty 30%   Duty 60%

(d)

Duty cycle	Breakdown	final
Duty 6%	523v	598v
Duty 30%	454v	519v
Duty 60%	430v	513v
Duty 80%	445v	509v
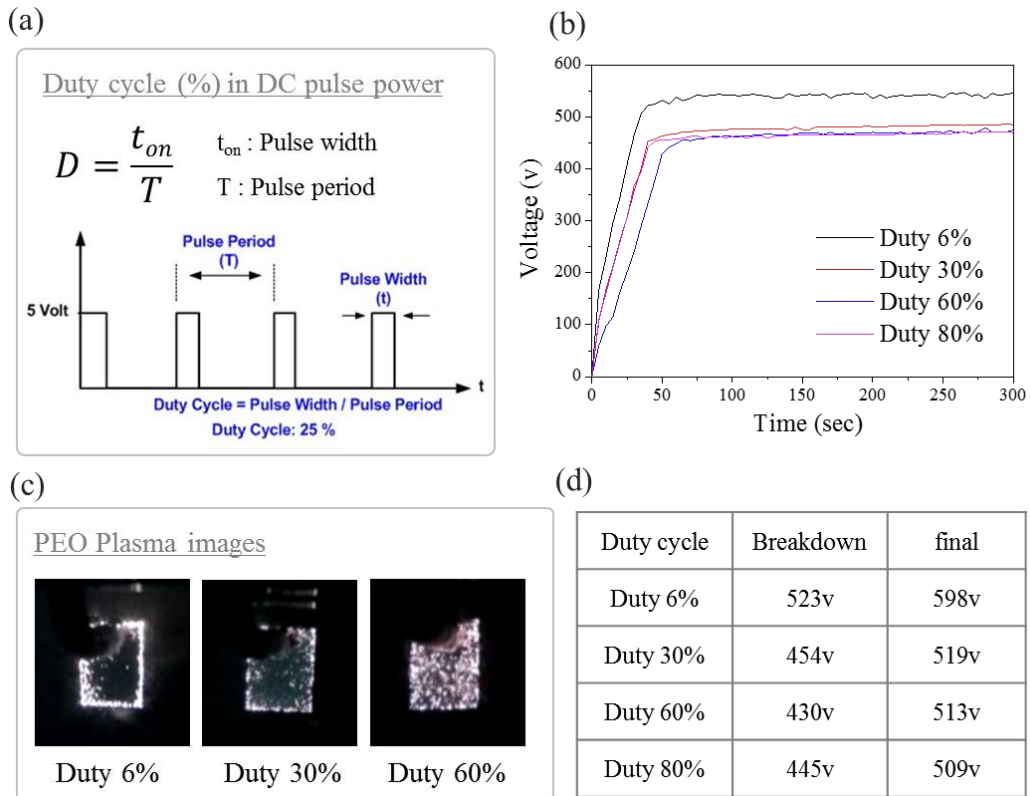
Figure 3.10 (a) Duty cycle in DC pulse power, (b) time-voltage curves as increasing duty cycle, (c) photograph images of plasma generation with duty cycle variation, (d) breakdown voltage and final voltage in different duty cycle
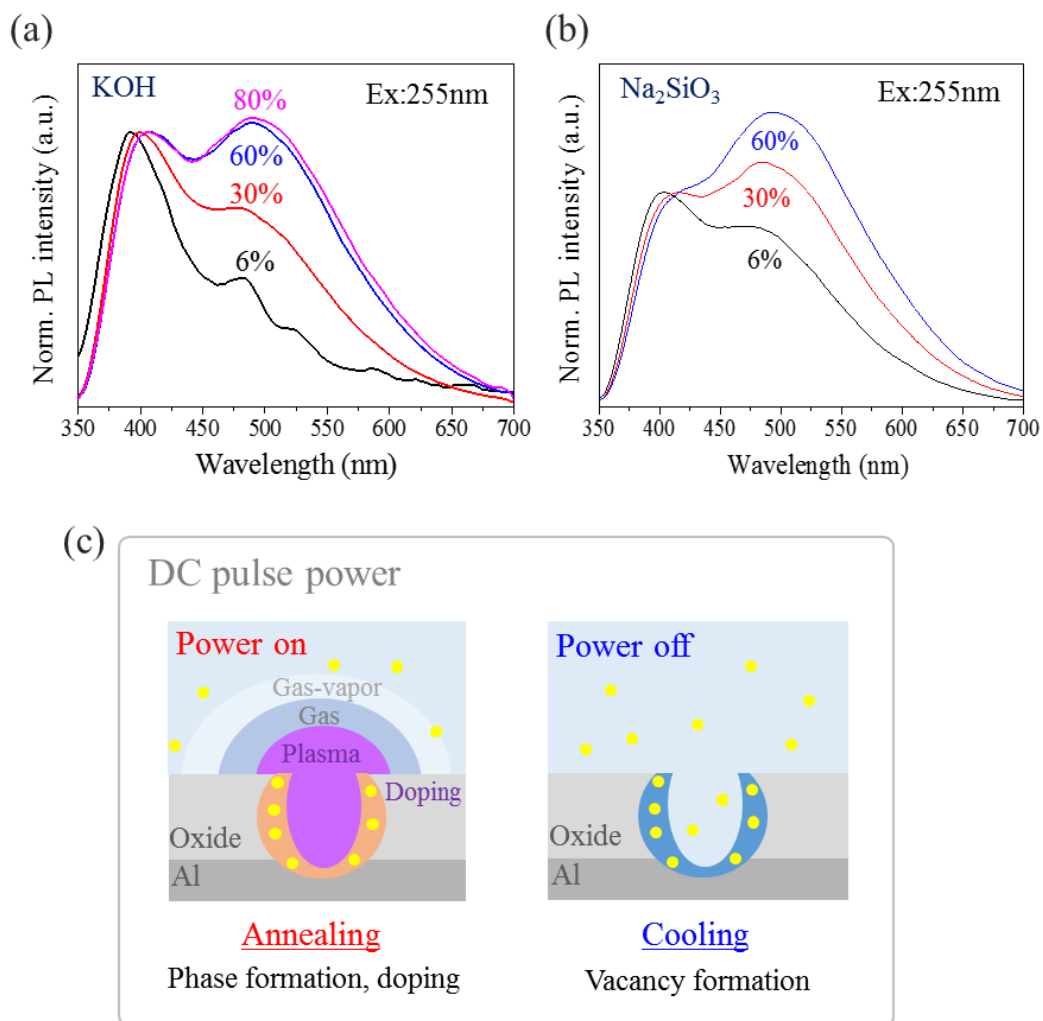
Figure 3.11 Photoluminescence spectral changes as increasing duty cycle; europium doped aluminum oxide prepared in (a) KOH and (b) Na$_2$SiO$_3$ electrolytes, and (c) schematic figures in power on and off conditions
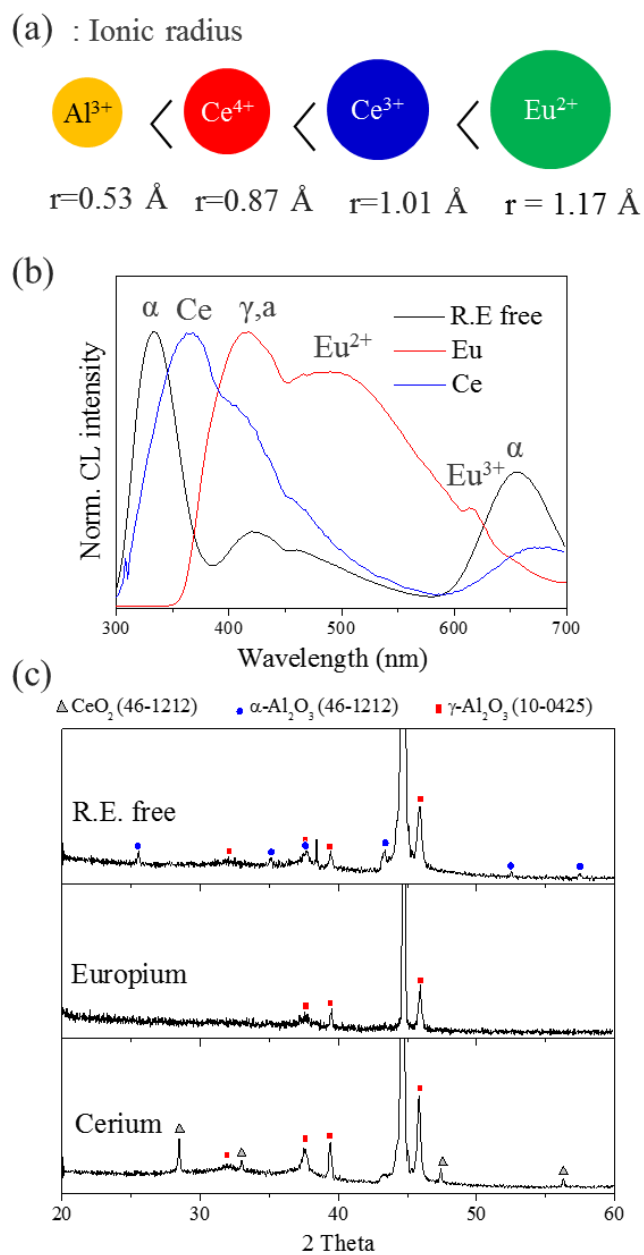
Figure 3.12 (a) Ionic radius of aluminum, cerium, and europium ions (b) cathodoluminescence spectra and (c) XRD patterns of the alumina film treated in electrolytes containing different rare-earths

3.1.3. Oxygen vacancy and europium effects

The photoluminescence property in europium oxide doped aluminum oxide film treated by PEO process can be generated by two main reasons as shown in the Figure 3.13. The first approach is oxygen vacancies in aluminum oxide crystal structure and the second one is europium ions in the alumina crystal. When there are oxygen vacancies in aluminum oxide lattice, three types of vacancies can be existed in the crystal as F (two electrons in vacancy center V_0), F+ (one electrons in oxygen vacancy V_0^+ and F++ (no electrons in vacancy center Vo^{2+}) centers. Among them, while F+ and F centers are quiet stable in crystal, the oxygen vacancy without an electron (F++) is not stable [41-43]. These three type of vacancies can be existed in different aluminum oxide phase of alpha, gamma, and amorphous.

When europium ions are doped in the crystal, the ions can be existed as 2+ or 3+ charge, and the photoluminescence spectral shape is totally different with the charge of ions [44]. In case of Eu^{2+} ion, divalent state has an electron configuration 4f7 because the half-filled f-shell gives more stability. The luminescence of these divalent ion is due to the $4f^n \rightarrow 4f^{n-1}5d$ transition with parity allowance, so they are resulting intense and broad photoluminescence (emission and absorption) spectra. In addition, the absorption and emission bands of divalent europium ions depend on the host lattice, so they are resulting in great

changes in emission color. In general case of trivalent rare-earth ions, electronic configurations of 4f electrons, n, mostly expressed as a general form of $5s^2 5p^6 4f^m$. The 4f electrons that are involved in the optical transitions of trivalent rare-earth ions, however, are well shielded by the outer $5s^2$ and $5p^6$ electrons. Therefore, the energy levels of 4f electrons are not much affected by the ligand ions in the host crystals. As shown in the Figure 3.13(b), the emission of Eu^{3+} is often situated in the red region with sharp spectral lines due to the $5D_0 \rightarrow 7F_J$ transitions, so it is quite easy to find out chemical status of europium ions in Eu-doped aluminum oxide film through photoluminescence spectrum. In order to confirm the quantity and quality of each europium ion, further analyses were performed in detail.

First, to find out vacancy and europium effects, europium oxide free electrolyte was prepared and the PEO process was performed in the same condition. As shown in the Figure 3.14(a), the voltage increase was not highly changed with europium containing condition, and the breakdown phenomenon was generated at the same breakdown voltage at the same time. From the XRD results (b), while only gamma phase of aluminum oxide was formed in europium containing electrolyte, the oxide film prepared in pure KOH electrolyte was composed of gamma and alpha phase of alumina. The pure alumina film showed no photoluminescence at the excitation of 325nm while europium doped film showed intense emission property. However, from the cathodoluminescence analysis, the europium free alumina film showed luminescence which centered at

45

several wavelengths. From the reported papers, oxygen vacancies in alumina could produce photoluminescence in blue emission range. So, in both cases of europium containing film and pure oxide film, the shorter wavelength centered blue emission band could be generated due to the vacancy center of aluminum oxide phase.

Here, in Table 2.1, the reported photoluminescence property and expected center of anodic aluminum oxide is shown. Most of the reported papers, The F+ center (oxygen vacancy with a single electron) can emit a PL peak at about 410 nm (～3.0 eV) in anodic or alpha phase of aluminum oxide, but there has been a controversy for a long time. Some researchers reported a PL peak at 2.9 eV (430 nm) in crystalline alumina yield from F center [45], and Huang et al. presented a PL peak at 455 nm also from the F center of anodic alumina [46]. Some researchers presented that the luminescence from anodic oxide is due to oxalic acid molecule in electrolyte. However, in our research, we did not apply oxalic acid or other organic based elements [47], so it is hard to refer that in this case. From the reported results, the luminescence in blue emission range could be related to oxygen vacancy in aluminum oxide, and this is one of the grounds for vacancy effect in luminescent aluminum oxide film.

In order to confirm the existence of oxygen vacancies in gamma phase of aluminum oxide film, ESR analysis was performed. Electron spin resonance (ESR) which is also called as electron paramagnetic resonance (EPR) analysis is a

powerful technique for studying materials with unpaired electron spin, so the ESR analysis is usually applied to find out oxygen vacancy state (F+) in oxide based ceramic system while F centers (oxygen vacancy with two electrons) in crystalline alumina are not paramagnetic [48-50]. Every electron has a magnetic moment and spin quantum number, and its magnetic moment aligns either parallel or anti parallel directions to the field when they are existed in the external magnetic field. At this point, the separated electron spin having specific energy due to Zeeman Effect, and this energy gap is directly proportional to the magnetic field's strength. The formula is shown here:

$$\Delta E = h\nu = g_e \mu_B B_0$$

Where g_e is the electron's g-factor (g_e for free electron $=2.0023$), μ_B is the Bohr magneton and B_0 is magnetic field.

From the ESR results in Figure 3.15, there was a resonance at the range of 335mT, and this value was calculated as 1.98 of g value which is almost same value of free electron. This resonance was also observed at the pure alumina film which is prepared as the same process without europium ions. This result means that the F+ center which contained single electron at the oxygen vacancy was formed in the PEO treated aluminum oxide film. During PEO process, the oxide layer is randomly formed on aluminum foil in a very short time, then cooled down rapidly. The cycle of annealing and cooling process is quickly repeated, so the resulted oxide film contained many defects like oxygen vacancies. As mentioned

before, in the aluminum oxide system, there are three types of oxygen vacancy which is called as F, F+, F++ based on the number of existed electrons in the vacancy. Here, from the ESR results, we could know the existence of F+ vacancies in aluminum oxide film in both cases of europium containing and europium free alumina film.

In order to confirm the existence of europium ions in PEO film, TEM-EDS and ICP- MS analysis were performed. At first, the EDS mapping result (Figure 3.16) showed europium ions are certainly existed and homogeneously well distributed in the aluminum oxide film. Quantitative results (Table 3.3) showed that the synthesized film was mostly composed of aluminum with very small amount of europium. The weight percentage of europium in the sample was 1.75%, but this result was under the reliable value in EDS analysis. So, the ICP-MS analysis was additionally carried out. As shown in the table, the europium contents was 12×10^6 ppb when aluminum was 557×10^6 ppb in the sample, and the calculated atomic ratio of europium was 0.4% in comparison with aluminum contents.

In case of europium ion, the chemical status can be a key role in photoluminescence property. As mentioned in previous paragraph, 2+ europium ion generate broad band emission due to f-d transition, and 3+ europium emits characteristic red emission from the f-f transition. In order to find out chemical status of europium ions in aluminum oxide film, x-ray photoelectron spectroscopy

was measured in 3d and 4d state of europium. As shown in the Figure 3.17, XPS spectra showed the presence of both europium state of Eu^{3+} and Eu^{2+} [51, 52], and the deconvolution spectra and fitting results (Table 3.5) indicated that the europium ions in PEO treated aluminum oxide layer are mostly existed as trivalent state with small portion of divalent state.

To confirm photoluminescence property of europium ions depending on chemical state, we conducted post annealing process from 600°C to 900°C in air condition. Because melting temperature of aluminum is over 600°C, aluminum substrate was etched after PEO process, and pure Al_2O_3:Eu films were used for post annealing process. From the XRD results (Figure 3.18 (c)), as-synthesized film was gamma alumina, and there was no crystal structural changes even at high temperature. In the CL results Figure 3.18 (a, b), CL intensity of the alumina film was slightly increased at low annealing temperature (~700 °C), but the luminescence intensity was highly decreased over 800 °C. The normalized CL spectra (Figure 3.18) clearly showed that the spectrum centered longer wavelength (500nm) was gradually decreased with increasing temperature. In addition, the red line-emission centered at 617nm was appeared at high annealing temperature which is related to the luminescence of Eu^{3+}, and the CL image (Figure 3.18(d)) showed that the 618nm centered red luminescence was detected not all over the film but in some spot area. From these results, we can suppose that the luminescence quenching in short wavelength ranges (400nm) is due to the

reduction of oxygen vacancy, and the quenching in longer wavelength (500nm) is due to oxidization of europium ion from divalent to trivalent during post annealing process in air atmosphere.

Another approach to confirm vacancy and europium effects on photoluminescence is analysis of photoluminescence decay time (Figure 3.19 Schematic figure of florescence life time. Luminescence is most conveniently defined as the radiation emitted by a molecule, or an atom, after it had absorbed energy to go to an exited state. The main types of luminescence are consist of fluorescence and phosphorescence. Once a molecule arrives at the lowest vibrational level of an exited singlet state, it can do a number of things, one of which is to return to the ground state by photon emission. This process is called fluorescence. The lifetime of an excited singlet state is approximately 10^{-9} to 10^{-7} sec and therefore the decay time of fluorescence is of the same order of magnitude. In case of the phosphorescence, the electrons excited not to singlet state but to triplet state, and singlet-triplet processes are generally less probable than singlet-singlet processes. The life time of a triplet state is much longer than that of an excited singlet state (about 10^{-4} to 10 sec) and therefore loss of excitation energy by collisional transfer is generally enhanced.

The measured lifetimes of luminescent species are generally shorter than the natural lifetimes, because non-radiative processes compete with the radiative decay. Here, the fluorescence decay time is expressed as:

$$\tau_f = \frac{1}{k_{nr} + k_f}$$

Where k_{nr} is decay-time for non-radiative transition and k_f is fluorescence decay term. In order to know the luminescence center of the two spectra overlapped emission spectrum in europium doped alumina film, decay time measurement was performed at different wavelengths (410, 460 and 500nm), and the decay curve was fitted with exponential decay function. The decay curves could be expressed mathematically as:

$$I(t) = \sum_{i=1}^{n} A_i e^{-\frac{t}{\tau_i}}$$

Where τi represents characteristic life time and denotes the time taken to decay from the beginning of the decay to 37% of the original value, Ai is a pre-exponential factor, which includes both instrumental and sample parameters. In a multi-exponential decay, concentration ratio of individual components can be inferred from values of Ai. Each decay curve has been fitted into bi-exponential and the best fit results of the measured decay times are shown in the table. The results indicate that at longer emission wavelengths, the longer decay component predominates.

As shown in the Figure 3.21, decay time was increased with the wavelength, and the average decay time was around 1 micro second at 500nm centered green emission. When europium ions were doped in crystal structure as

divalent state, the decay-time of europium is mostly around few micro second, and few millisecond in case of trivalent europium. Therefore, the emission of green centered spectrum which has 1micro second of decay-time might be the luminescence from europium ions [53, 54]. In case of blue emission, there was a sharp peak in short time range (inset of Figure 3.22), so the decay time analysis was additionally performed with high resolution. As a result, very short time components almost 4ns were calculated, and this result was related to the F+ center from the reported life time results [55-57]. In most cases, the F vacancy center, they show long after glow, and the decay time is almost few ms. However, from the decay time results, long after glow which was the F center component were not detected. Therefore, in this experiment, F+ center was only formed during micro arc oxidation process. In addition, compared with the reported value, we can say that the blue emission in our experimental result is intimately associated with the F+ oxygen vacancy and green emission is from the divalent europium activator.

From the results, considering each luminescence factors, the photoluminescence spectrum was deconvoluted as shown in the Figure 3.23. The emission spectrum of europium doped gamma aluminum oxide was fitted as two different emissions which are centered at 3.06ev and 2.54ev. Each energy level was converted to the wavelength as 405nm and 488nm, and the spectrum portion was calculated as an area (%). The emission spectrum at high energy which is

from F+ center in gamma alumina takes up 32% of the emission, and the lower energy centered spectrum from divalent europium ion in alumina lattice takes up 67%. Both luminescence centers were involved in the emission spectrum, and each luminescence center was highly affected by experimental variables, as we discussed in previous section. In order to find out how these centers can be existed in crystal in atomic scale, further analysis was performed and will be discussed at the next section.

(a) Oxygen vacancy

$\alpha\text{-}Al_2O_3$, $\gamma\text{-}Al_2O_3$, amorphous- Al_2O_3

F center = Vo F^+ center = Vo^+ F^{++} center = Vo^{2+}
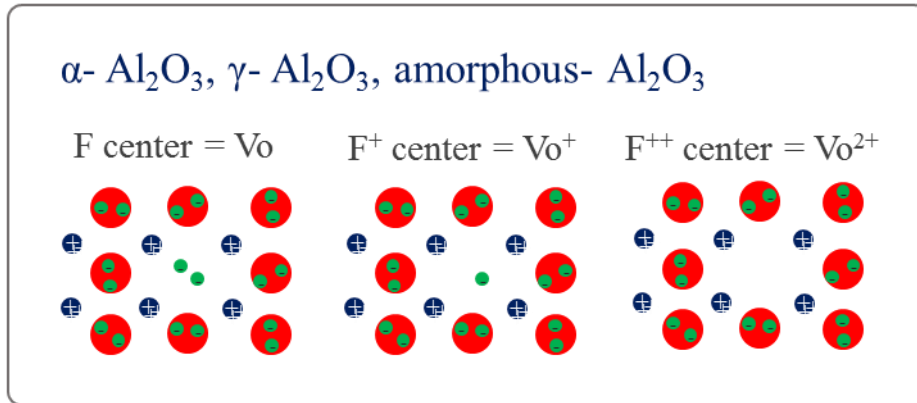
(b) Activator: Europium ions

f-d transition: Eu^{2+}

Eu^{2+} [Xe]$4f^7$ $^8S_{7/2}$ s : 7/2, L : 0

Eu $4f^65d^1$

Eu $4f^7$

Broad emission

f-f transition: Eu^{3+}

Eu^{3+} [Xe]$4f^6$ $^7F_0$ s : 3, L : 3 J : 0~6

D

Eu 4f ^7F_J

Line emission: Red light
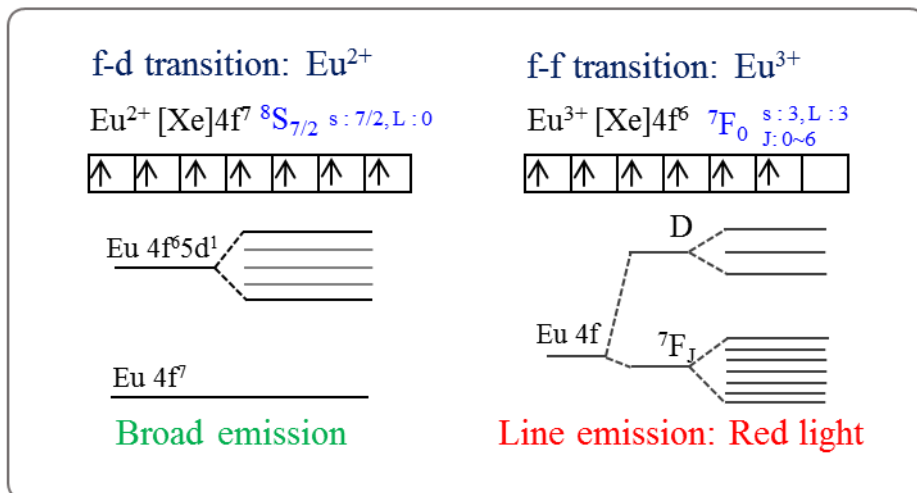
Figure 3.13 (a) Oxygen vacancies in aluminum oxide and (a) energy state of europium ions
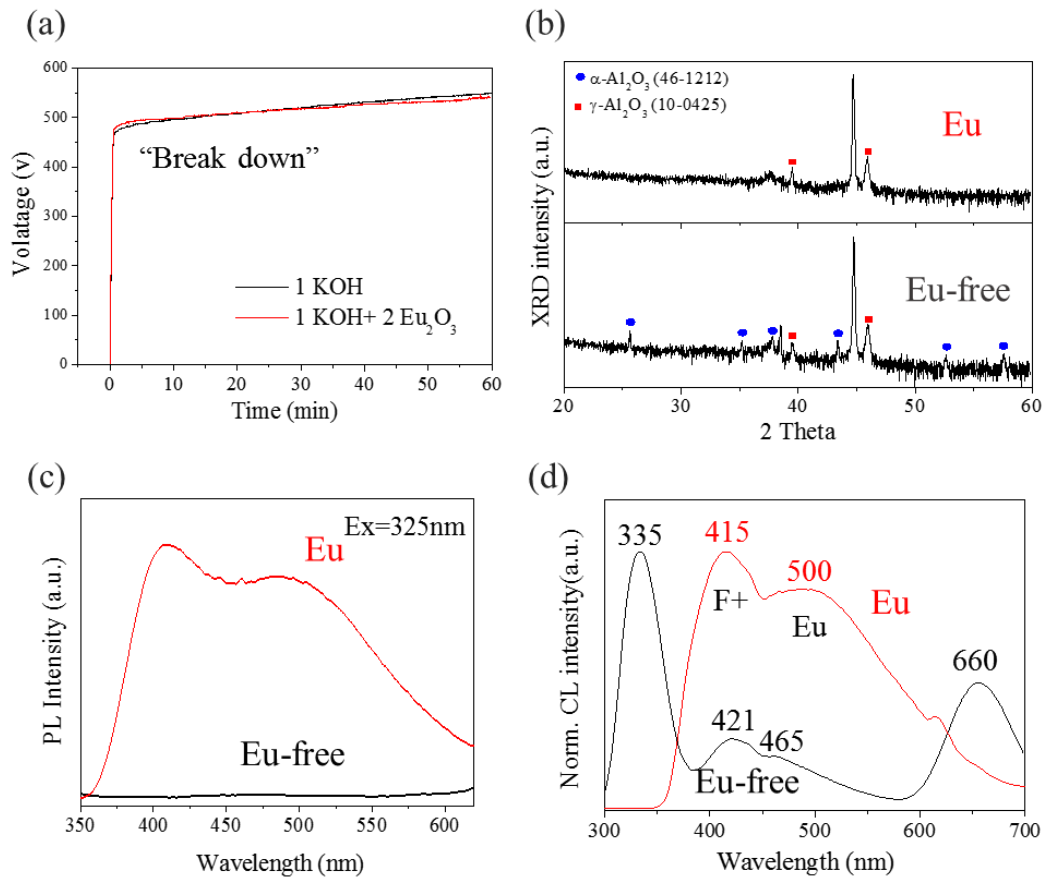
Figure 3.14 (a) Time-voltage curves, (b) XRD patterns, (c) photoluminescence spectra and (d) cathodoluminescence spectra of the plasma treated aluminum oxide films treated with europium oxides and in pure KOH electrolyte condition

Table 3.2 Reported photoluminescence property of anodic aluminum oxide film

#	Excitation (nm)	Emission (nm)	Peak indexing	Ref.
1	300	411,445	F^+=411 , F=445	[58]
2	360, 250	470, 350	Oxalic acid, Per chloric acid	[59]
3	340	430	F^+=430, F=480, F^+=327 (alpha)	[45]
4	360	450	F^+ center	[60]
5	325,350	405,455	F^+=413, F=430 (alpha), F^+=inner, F=surface	[46]
6	315	430, 475, 525	F^+ center	[61]
7	300, 330, 360, 420	425, 430, 543, 500	F^+ center	[62]
8	350	434, 460	F^+=434 inner layer, F=460 surface	[63]
9	365	460, 520	Oxalic acid	[47]
10	345	435	σ- and π-bonds in oxalic acid molecule	[64]

(a)

∴ g value: 1.98

F+
60min-Eu

F+
30min-Eu

F+
10min-Eu

F+
60min-Eu free

ESR intensity (a.u.)

Magnetic field (mT)

(b)

ESR intensity (a.u.)

Magnetic field (mT)
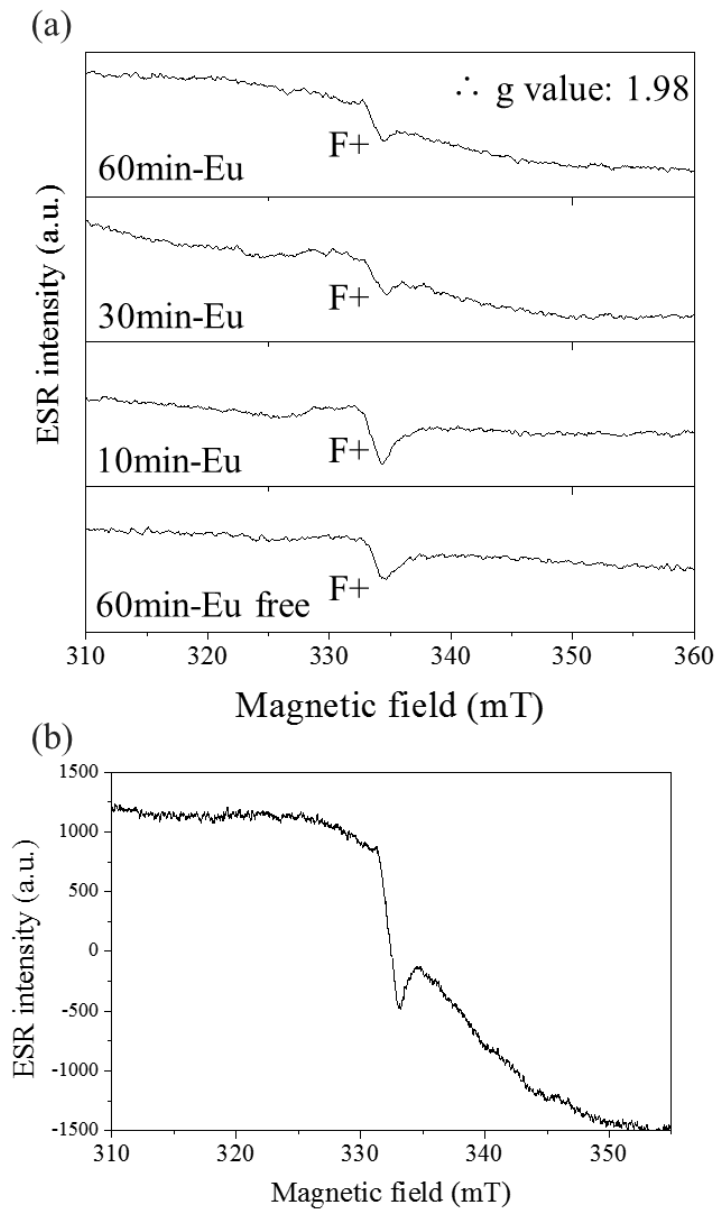
Figure 3.15 (a) Electron spin resonance curves of europium free and europium doped aluminum oxide film with PEO time and (b) high resolution spectrum of Al_2O_3:Eu film treated for 60min
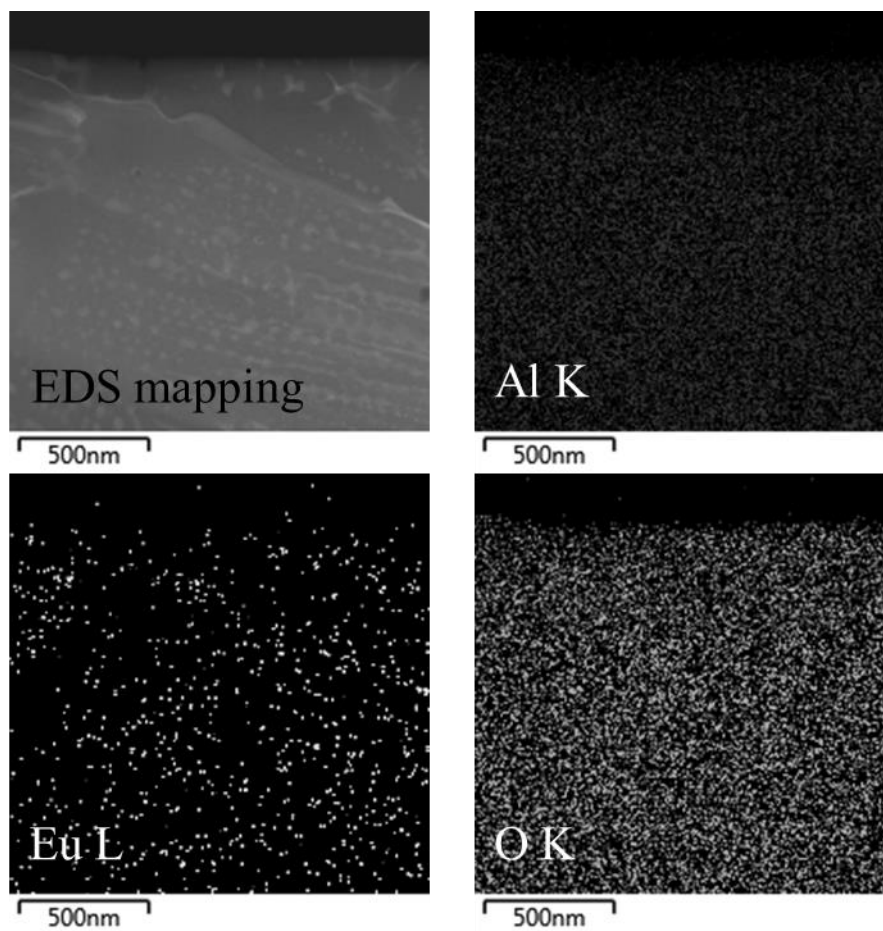
Figure 3.16 EDS mapping results of europium doped gamma aluminum oxide film by STEM

Table 3.3 Energy-dispersive spectroscopy results of europium doped aluminum oxide film

Elements	Al K	O K	Eu L
Weight %	33.3%	37.1%	1.75%
Atomic %	36.5%	24.1%	0.2%

Table 3.4 ICP-MS analysis of Al_2O_3:Eu film and the concentration of elements in samples (ppb=μg/kg)

Elements	Al	Eu
Concentration	577 x 10^6	12 x 10^6
Weight %	97%	3%
Atomic %	99.6%	0.4%
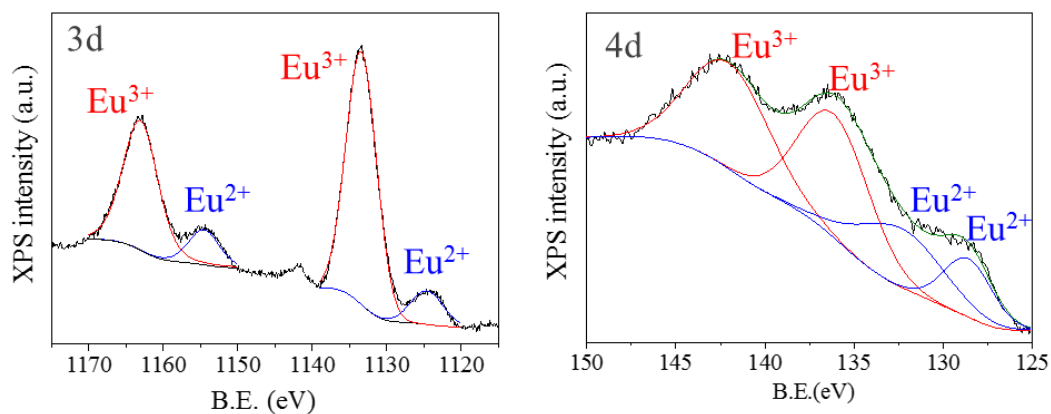
Figure 3.17 X-ray photon spectroscopy curves of europium doped alumina film

Table 3.5 XPS fitting results of europium ion (3d and 4f atomic level) in
aluminum oxide film

Atomic level		Binding energy (eV)	
		Eu^{3+}	Eu^{2+}
3d	3d$_{3/2}$	1163	1154
	3d$_{5/2}$	1133	1124
	Portion	85%	15%
4f	4d$_{3/2}$	142.0	132.4
	4d$_{5/2}$	136.1	128.6
	Portion	67%	33%
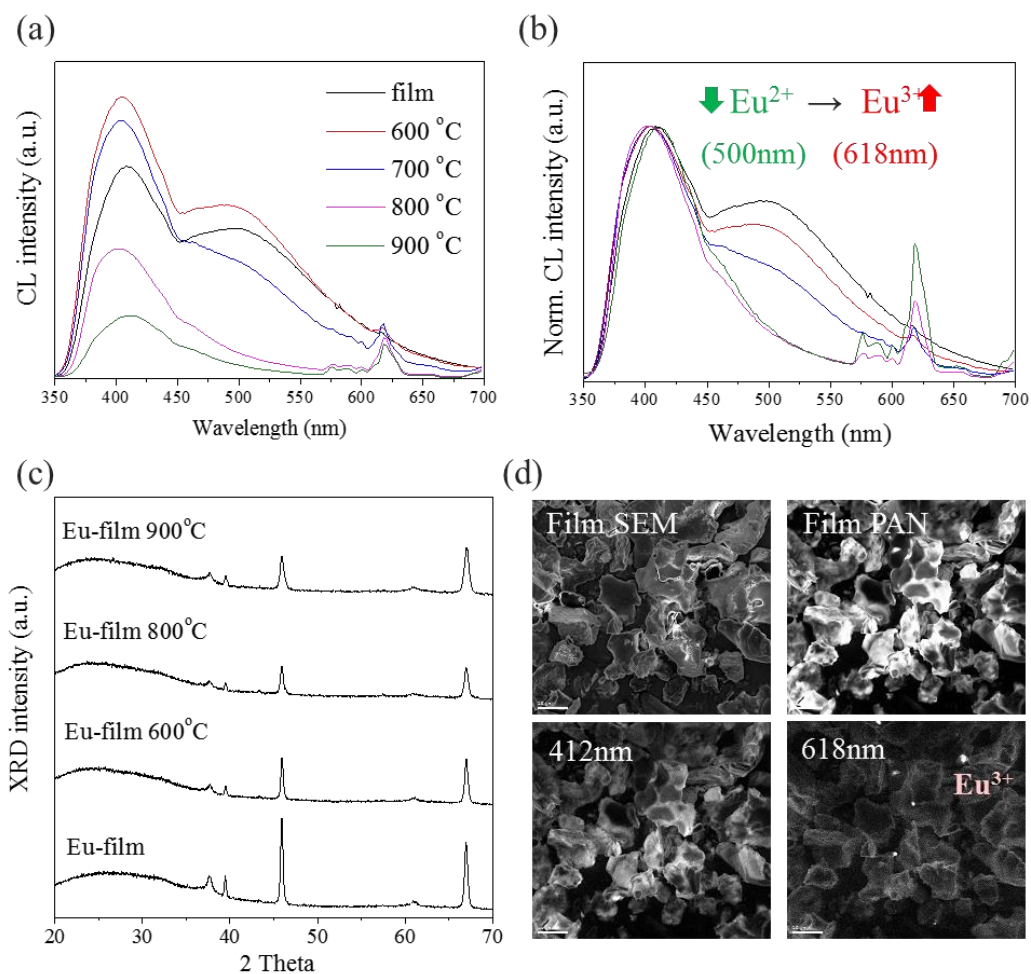
Figure 3.18 Additional heat treated europium doped aluminum oxide film from 600 to 900 °C; (a) cathotoluminescence spectra, (b) normalized cathodoluminescence spectra, (c) x-ray diffraction pattern, (d) SEM and CL images (centered at 412nm and 618nm) of the film annealed at 900 °C

61
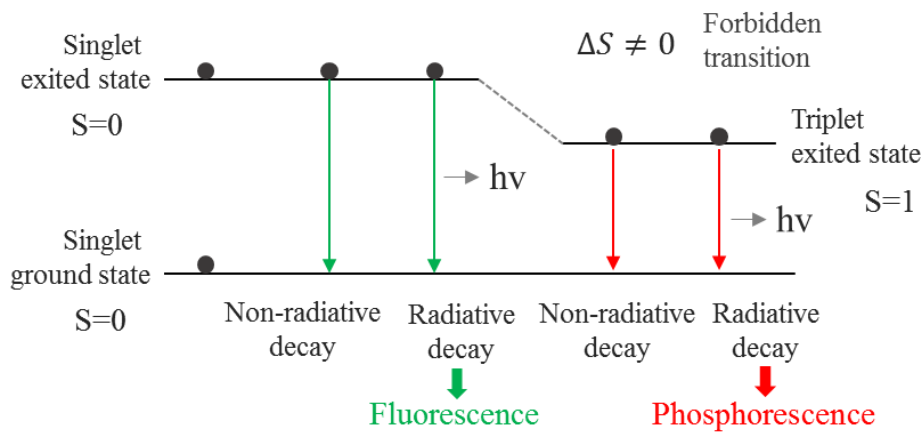
Figure 3.19 Schematic figure of florescence life time
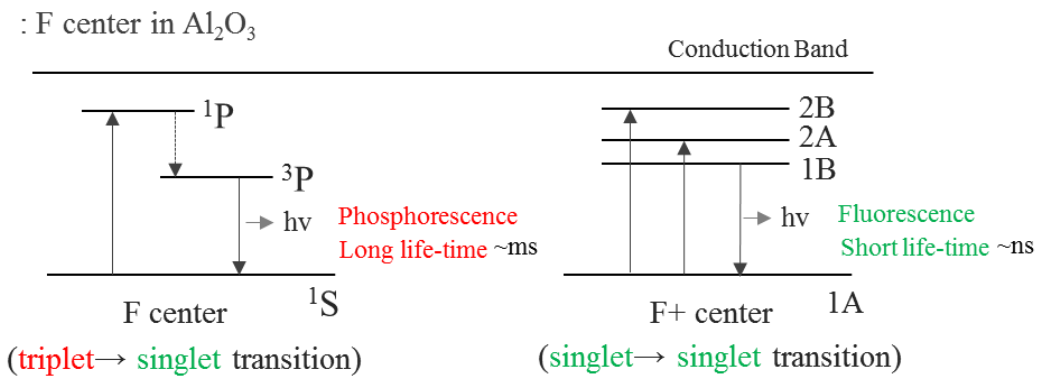
Figure 3.20 Luminescence from vacancy center in aluminum oxide
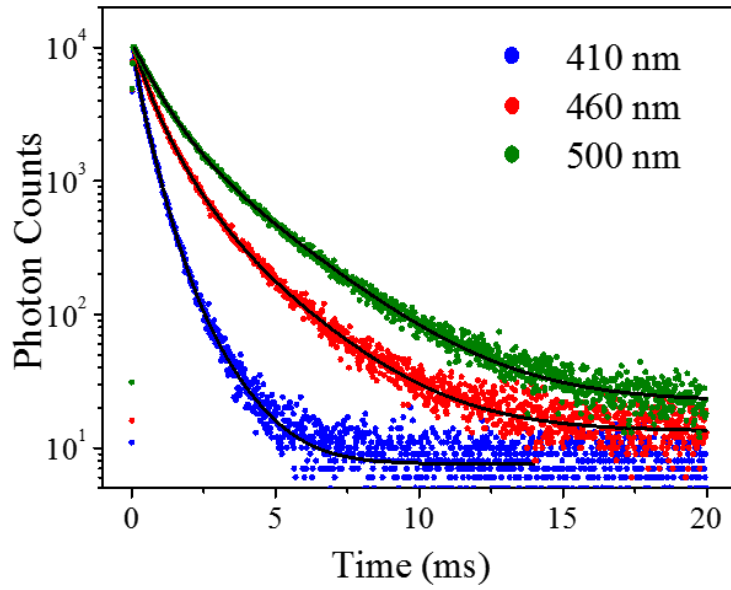
Figure 3.21 Decay time curve of europium doped alumina film at 410, 460 and 500nm centered wavelengths

Table 3.6 Calculated decay time components and average decay time at different wavelength center

	Time 1		Time 2		Time 3		Avg.
	t_1 (µs)	A_1 (%)	t_2 (µs)	A_2 (%)	t_3 (µs)	A_3 (%)	t_{avg} (µs)
410 nm	0.14	31.1	0.45	63.2	1.18	5.7	0.40
460 nm	0.38	36.1	0.87	51.8	2.32	12.1	0.87
500 nm	0.83	70.2	2.56	29.8			1.34
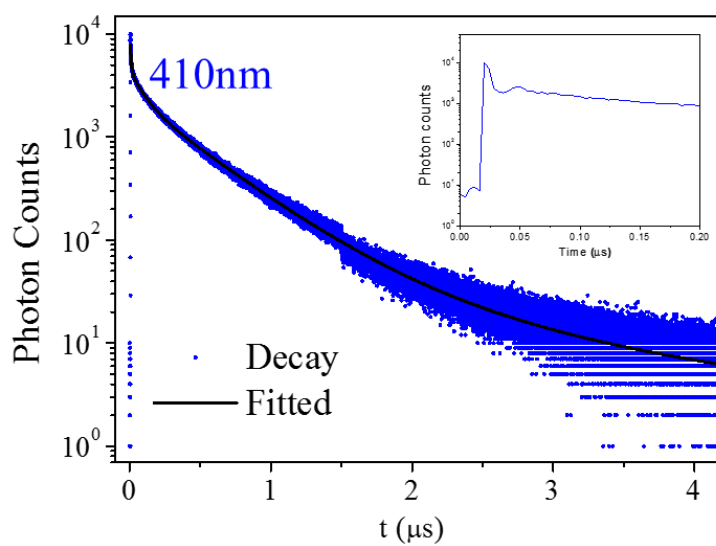
Figure 3.22 High resolution decay curve at wavelength of 410nm

Table 3.7 Fitted decay time components at 410nm measured with high resolution
time-correlated single photon counting (TCSPC) methods

410nm centered	t_1 (µs)	A_1 (%)
Time 1	0.0043	22.6
Time 2	0.093	12.2
Time 3	0.42	57.8
Time 4	1.3	7.4
Average	0.35	
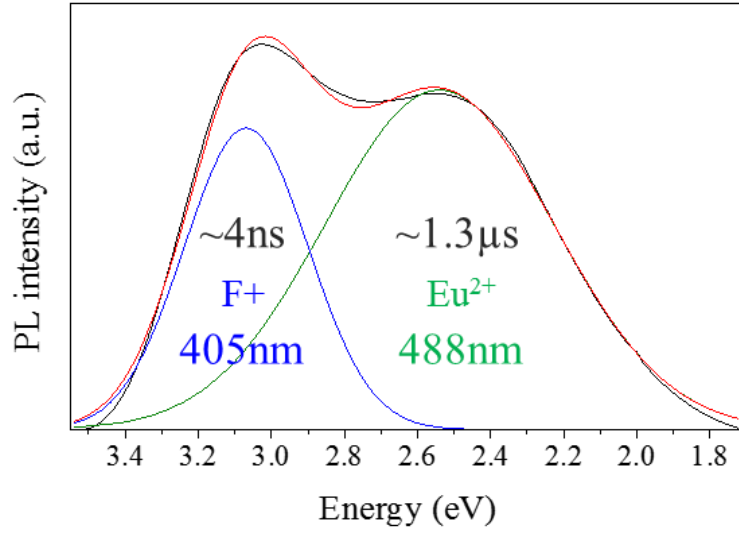
Figure 3.23 Deconvolution of photoluminescence spectrum; europium doped aluminum oxide film prepared by PEO process

Table 3.8 Fitting results of the emission spectrum (Figure 3.23) of Al_2O_3:Eu film

	Peak 1	Peak 2
Center (eV)	3.06	2.54
Wavelength (nm)	405	488
FWHM (eV)	0.39	0.73
Height	353	398
Area (%)	32	67

3.1.4. Crystal structure of europium doped aluminum oxide film

At the previous sections, we concluded that the white luminescence of europium doped aluminum oxide film is highly related to oxygen vacancy F+ center and europium ions. The short wavelength centered emission (405nm) is due to the F+ center and longer wavelength centered emission is from divalent europium ions in gamma aluminum oxide film. In this section, to confirm the europium ions doping mechanism in the aluminum oxide lattice in atomic scale, the rietveld refinement and TEM analysis was performed.

As shown in Figure 3.24, the structure of γ-Al_2O_3 has traditionally been considered as a defective spinel structure [65-67]. The oxygen ions in this crystal lattice are built up by a cubic close-packed stacking, with Al atoms occupying the octahedral and tetrahedral sites. In order to satisfy the γ-Al_2O_3 stoichiometry, some of the lattice positions are not occupied, so called as vacancies. Even though many studies of this crystal system, the precise location of vacancy is still controversial, and the phase transformation of gamma Al_2O_3 is not clearly defined at this stage.

Here, in our experiments, europium oxide is cooperated with the aluminum oxide film during plasma electrolytic oxidation. As shown in the Figure 3.24, the ionic radius of europium ions (six coordinate) are much larger than aluminum ions. While ionic radius of aluminum ion in tetrahedral site is 0.39Å

and octahedral site is 0.53Å. In case of trivalent europium ion, the ionic radius is 0.95 Å, and that of divalent europium ion is much larger (1.17Å). Therefore it is quiet hard to substitute aluminum ions either cases of tetrahedral site and octahedral site. Surprisingly, by plasma electrolytic oxidation, europium ions were quietly doped in aluminum oxide phase.

For the rietveld refinement, the pure europium doped alumina film was obtained by chemical etching of Al foil, and they were finely grounded. X-ray diffraction analysis was precisely performed as 0.01 steps with 1 ^{o}/min scanning rate, and almost single phase of gamma-alumina was obtained (Figure 3.25). The crystal structural information of the synthesized aluminum oxide film was calculated by rietveld method. All the diffraction peaks of gamma alumina were completely indexed based on the cubic structure with a space group of Fd3m, and the calculated lattice parameters were a= 7.9076(8) Å, and it was well agreed with the reported data (a=7.90 in ICDD 18524). In that, even though europium ion was doped in the gamma alumina, there was no large lattice distortion in the crystal structure. In order to figure out europium ion coordination and occupation, rietveld refinement was calculated with europium ions in europium doped aluminum oxide as shown in the Table 3.9. The calculations were performed with the assumption of europium ion substitution at the position of aluminum ion in the spinel structure. The calculated occupancy of each sites showed that the europium ions are favorable to be located at the octahedral sites (Eu3, Eu4) than the

tetrahedral sites (Eu1, Eu2). In the gamma Al_2O_3 spinel structure, average Eu-O bonding length at the octahedral site is 2.07Å, and this is larger value than the 1.64 Å of tetrahedral site. Therefore, in case of europium ion, it is easy to substitute the aluminum at octahedral site than tetrahedral site due to their large ionic radius. To find out europium ion existence in gamma alumina, TEM analysis and electronic structure calculation was performed.

The TEM images (Figure 3.26) showed the oxidized film which contained europium ions in gamma Al_2O_3 crystal. In order to observe accurate information in crystal lattice, in this experiments, Cs corrected STEM was used. As shown in the Figure 3.26, the grain size of MAO film was about few hundred nanometers as width length and the grain was crystalized as a single phase of gamma aluminum oxide with longish shape. In the bright field image and high angle annular dark field image, a lot of spots were aligned along the line which is longitudinal direction of the grain, and this spots were well observed in HAADF image (Figure 3.27) as white spots. In general, in HAADF image, the image contrast indicates the degree of scattering in electron beam, so the brighter spots can be explained as the area containing heavy elements. In our study, atomic number of europium ion is larger than other light materials such as aluminum and oxygen, so we could assume the europium ions were aligned to specific direction in alumina grain and existed in grain boundary.

The Figure 3.27 showed STEM image and EDS results of europium doped

gamma Al_2O_3 grain in high magnification. From the HAADF image, gamma Al_2O_3 grain has two different area which are highly crystalized single gamma Al_2O_3 and europium doped region. The europium doped spots are much brighter than host lattice due to Z-contrast in this HAADF image. Furthermore, the EDS results showed that europium ions were only existed in brighter region and the atomic % of europium was 2% at this point. In high magnified HAADF image (Figure 3.27(d)), the europium doped region showed facet shape with the size of about 30nm, and the facet-like planes were overlapped and aligned along the specific direction. In that, in nano-scale, the europium ions were homogeneously distributed not in whole crystal but in some area like spots.

The boundary layer between europium–rich area and host lattice is shown in the Figure 3.28. In the ADF image, the interface was accurately observed, and we marked each area as grain 1 and grain 2 in order to distinguish europium rich region. From the BF image (Figure 3.28 (a)), FFT patterns of each grain were obtained (Figure 3.28), and the patterns of overall image showed the diffraction pattern of typical gamma Al_2O_3 single crystal at the view of <110> direction. However, the FFT patterns of europium doped area (grain 1) showed forbidden reflection of (002) which is marked as yellow circle in the image, while there was no signal in that reflection in single gamma alumina (grain 2). This result might be due to the europium substituted aluminum oxide lattice, but it is not clearly explained in this stage. Further atomic scale study is needed to figure out

europium doping condition in that crystal system.

As shown in the Figure 3.28 (c), the two diffraction spots were indexed as $1\bar{1}1$ and $1\bar{1}\bar{1}$, and the vertical direction of each diffraction was identified as $(1\bar{1}1)$ and $(1\bar{1}\bar{1})$ plane which is marked in ADF image. So the interface of europium doped facet-like area was identified as (111) plane of gamma Al_2O_3. The schematic figure of [111] atomic projection in gamma aluminum oxide is shown in. In Al_2O_3 cubic crystal, {111} plane is composed of hexagonal shape of oxygen or aluminum atoms. In order to figure out (111) plane in the structure of gamma alumina lattice, the crystal was rotated to the vertical direction of (111) plain in the Figure 3.29 (b), and put the top surface of the gamma aluminum oxide as (111) plane. From the reported crystal structural information, the planar distance of (111) is $4.56\mathring{A}$, and this (111) plane can be the oxygen-oxygen plane, aluminum-aluminum plane (octahedral site) and also aluminum-aluminum (tetrahedral site) plain. As a result, in our experiment, europium ions might substitute aluminum ions in gamma alumina structure, and they were doped along (111) plane with facet-like shape.

In order to figure out electronic structure of europium doped aluminum oxide film, computational methods with pseudopotential methods based on density functional theory was used. The unit cell structure of gamma aluminum oxide for the calculation is shown in the Figure 3.30(a). The γ-Al_2O_3 shows defective spinel structure with the cell parameter of a=5.68, b=5.64, c=13.67,

α=90.5, β=90.0, γ=120.2, and the local environment of aluminum (N_{oct}: N_{tet}= 10:6) and oxygen (O_4:O_3= 12:12) [68, 69] were the same with the rietveld refinement results (ICDD 18524). From the calculated DOS results of perfect gamma alumina crystal, band-gap of direct transition is 3.81eV (Figure 3.30(b)). In the spinel structure of γ Al_2O_3, oxygen ions can be existed in two different sites surrounded with different number of aluminum ion coordination. The vacancy formation energy at Nc=3 is much lower than Nc=4, so the oxygen vacancy at the coordination number=3 is more favorable in this system. In case of aluminum ions, especially at the octahedral sites, each aluminum has the same coordination number of oxygen, but the coordination of the surrounded oxygen ion is different as shown in the Figure 3.30(d). When europium ions are substituted the aluminum ion, the formation energy is low at the position of Al3, so further calculations were performed with the assumption of vacancy centers at Nc=4 oxygen site and europium centers at the coordination of Al3.

The calculated energy levels of oxygen vacancy (F+) or europium 2+ ion contained gamma Al_2O_3 are shown in the Figure 3.31. In case of europium divalent ions in gamma alumina structure, the up spin state of europium 4f state are fully occupied, and 5d orbitals expand in the entire conduction band. The expected energy band structure can be derived as shown in the Figure 3.32. The energy band gap of oxygen vacancy contained alumina was ~3.2eV, and this value indicates blue centered emission. The 4f-5d transition of europium 2+ ion showed

the 2.6 eV which emits green luminescence. As a results, the calculation results were similar with the experimental results, so we could concluded that the white luminescence in europium doped gamma aluminum oxide film is from mixed components of blue emission with vacancy center (F+) and green emission with europium divalent ions.
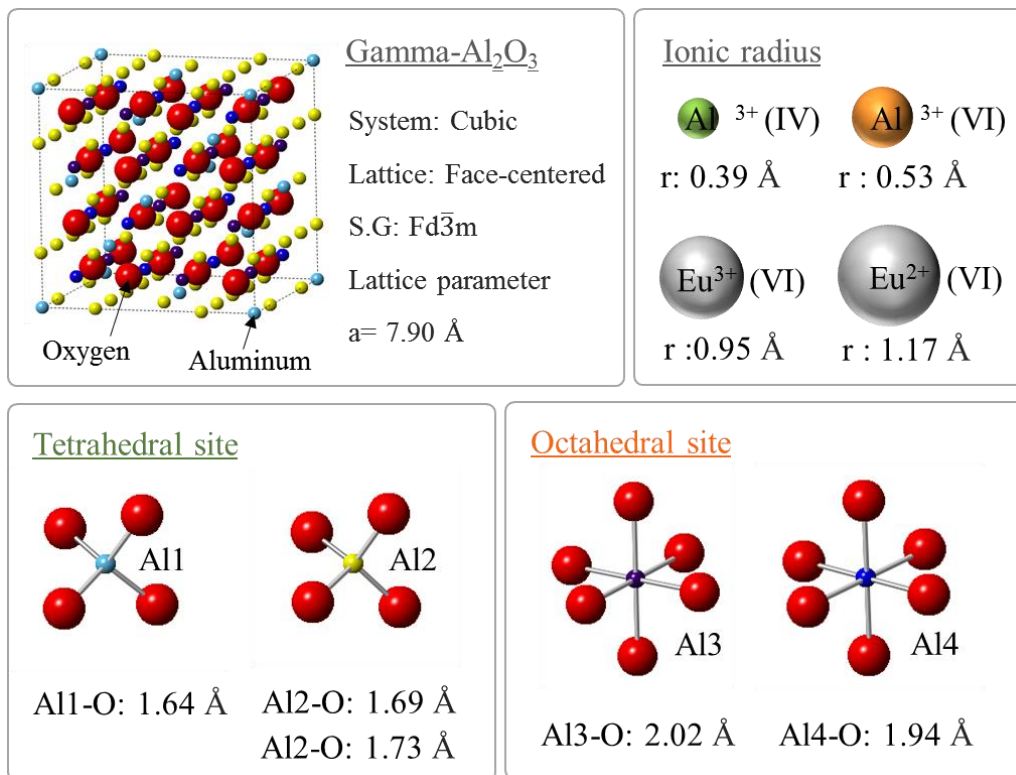
Figure 3.24 Crystal structure of gamma aluminum oxide, ionic radius of aluminum and europium ions and Al-O bonding in tetrahedral and octahedral site in alumina crystal
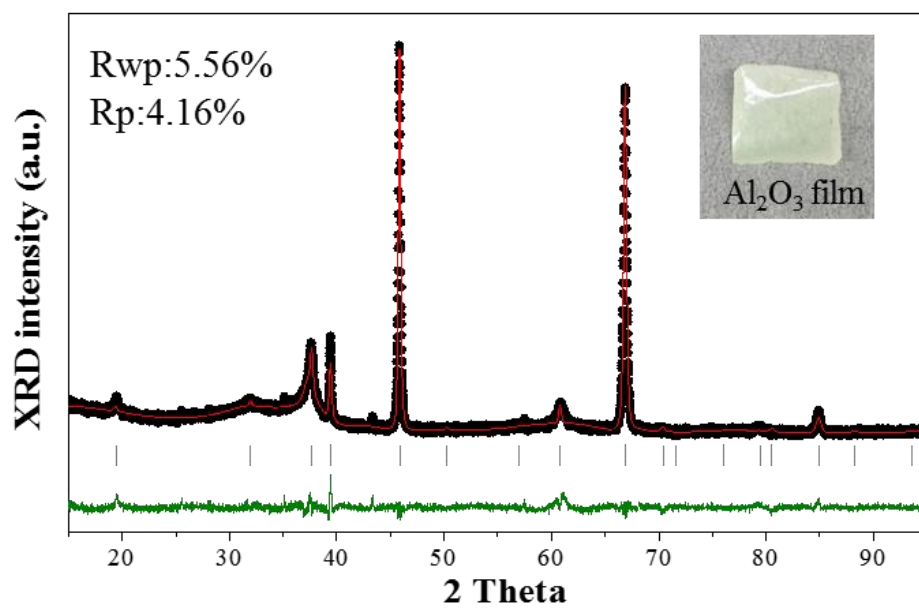
Figure 3.25 X-ray diffraction patterns in precise measure condition and rietveld refinement results of europium doped aluminum oxide film

Table 3.9 Refined crystal structure results of europium doped gamma aluminum oxide film

Elements	x	y	z	Occupancy
O	0.370	0.370	0.370	1.000
Al 1	0.250	0.250	0.250	0.503
Al 2	0.272	0.000	0.000	0.077
Al 3	0.625	0.625	0.625	0.400
Al 4	0.125	0.125	0.125	0.254
Eu 1	0.250	0.250	0.250	0.015
Eu 2	0.273	0.000	0.000	0.004
Eu 3	0.625	0.625	0.625	0.086
Eu 4	0.125	0.125	0.125	0.048
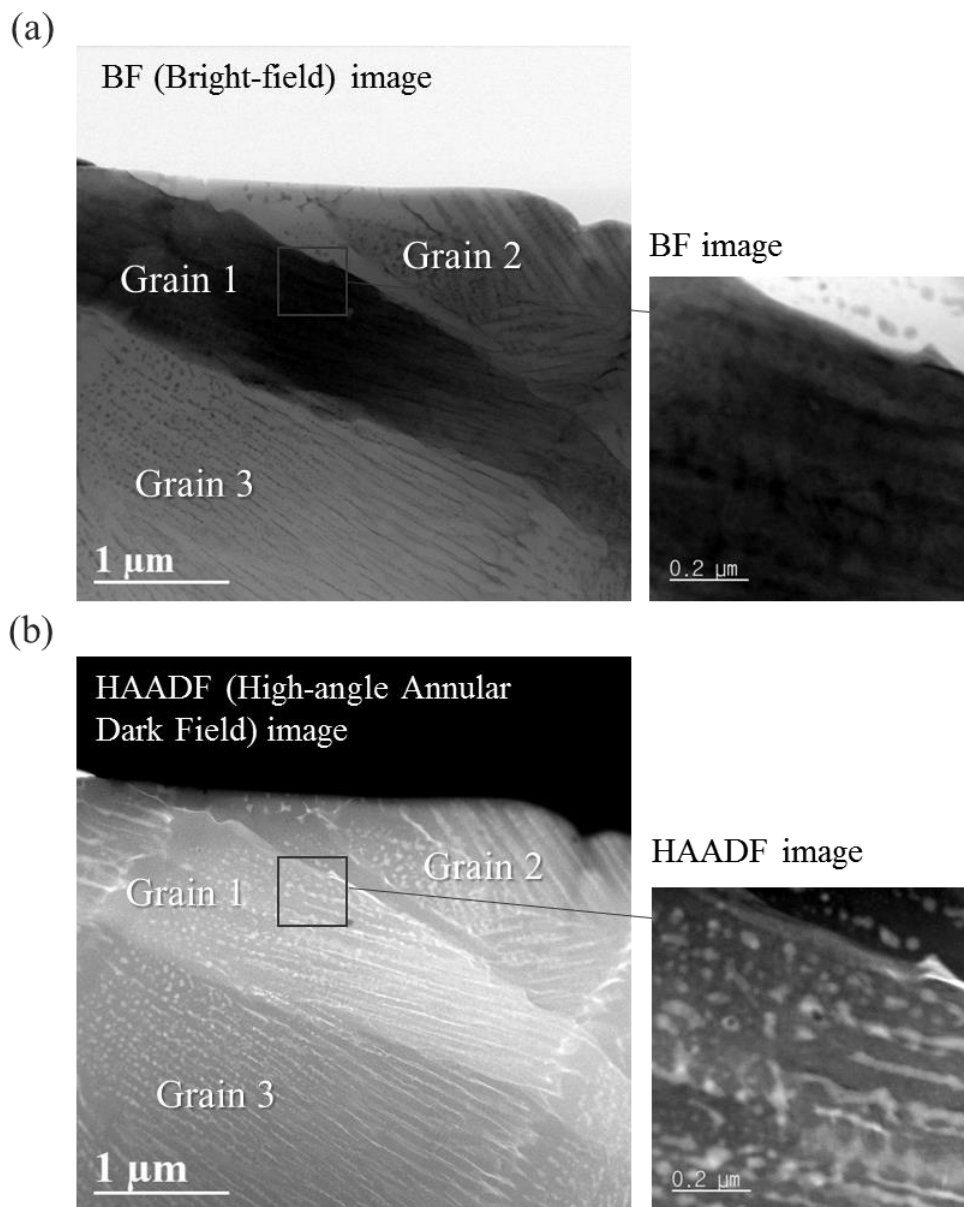
Figure 3.26 STEM images of europium doped aluminum oxide film in low
magnitude (a) bright field image and (b) high angle annular dark field image
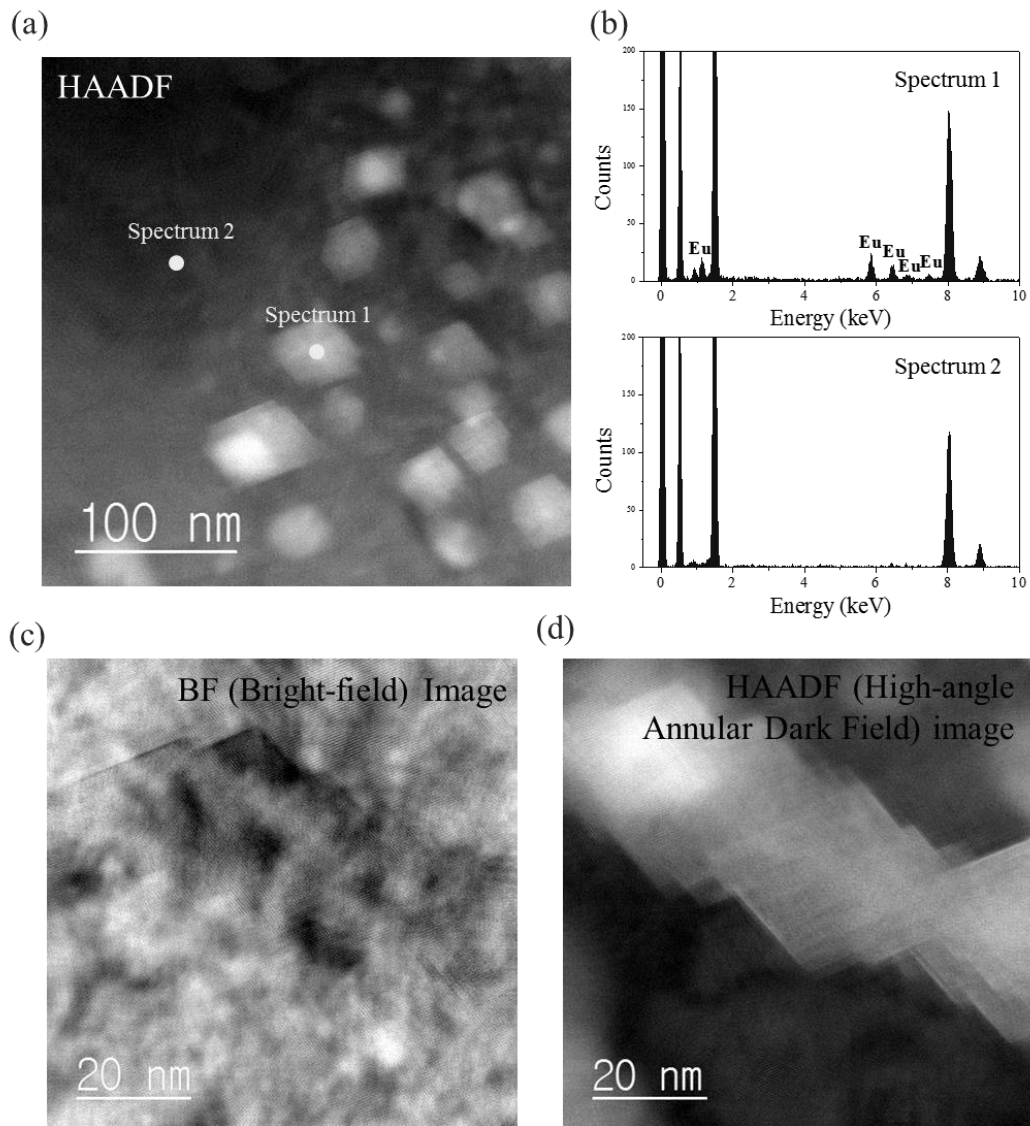
Figure 3.27 (a) High-resolution STEM image of europium containing aluminum oxide film, (b) EDS spectra from different spots, (c) BF image and (d) HAADF image of europium rich area
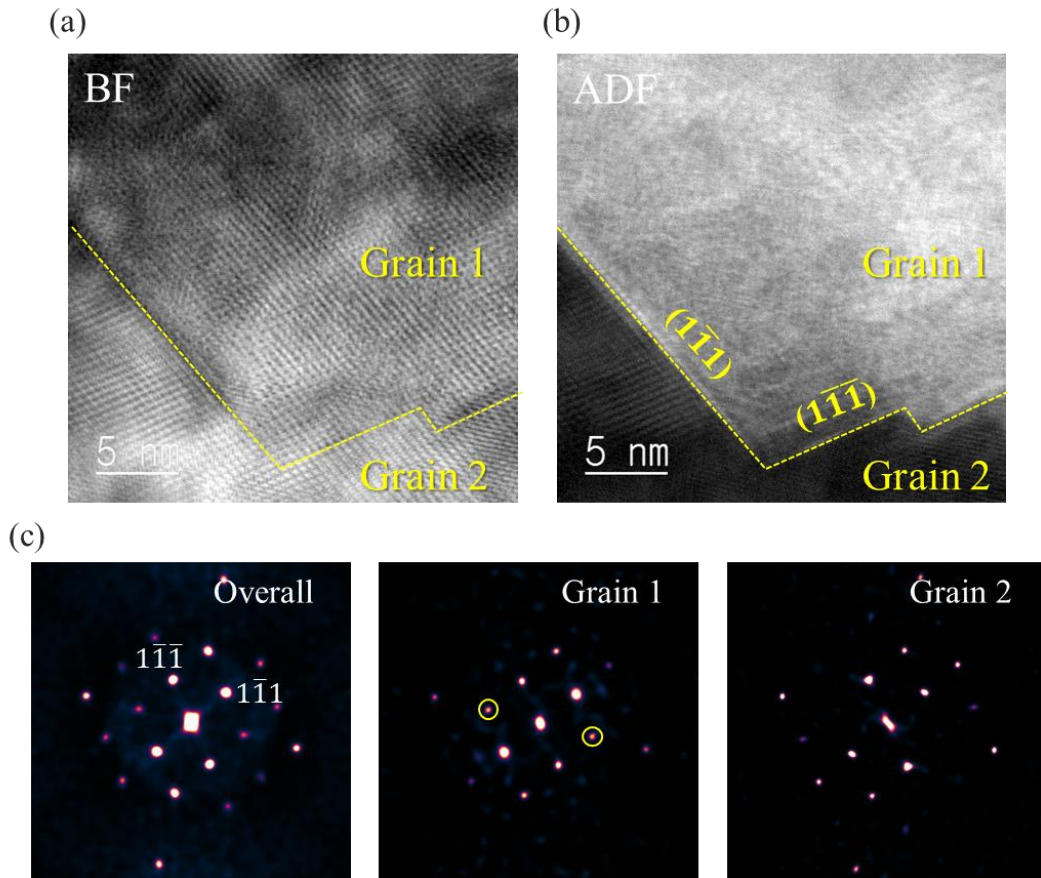
Figure 3.28 (a) BF and (b) ADF images of the interface between pure gamma aluminum oxide and europium-rich area and (c) FFT patterns of overall images and each grain
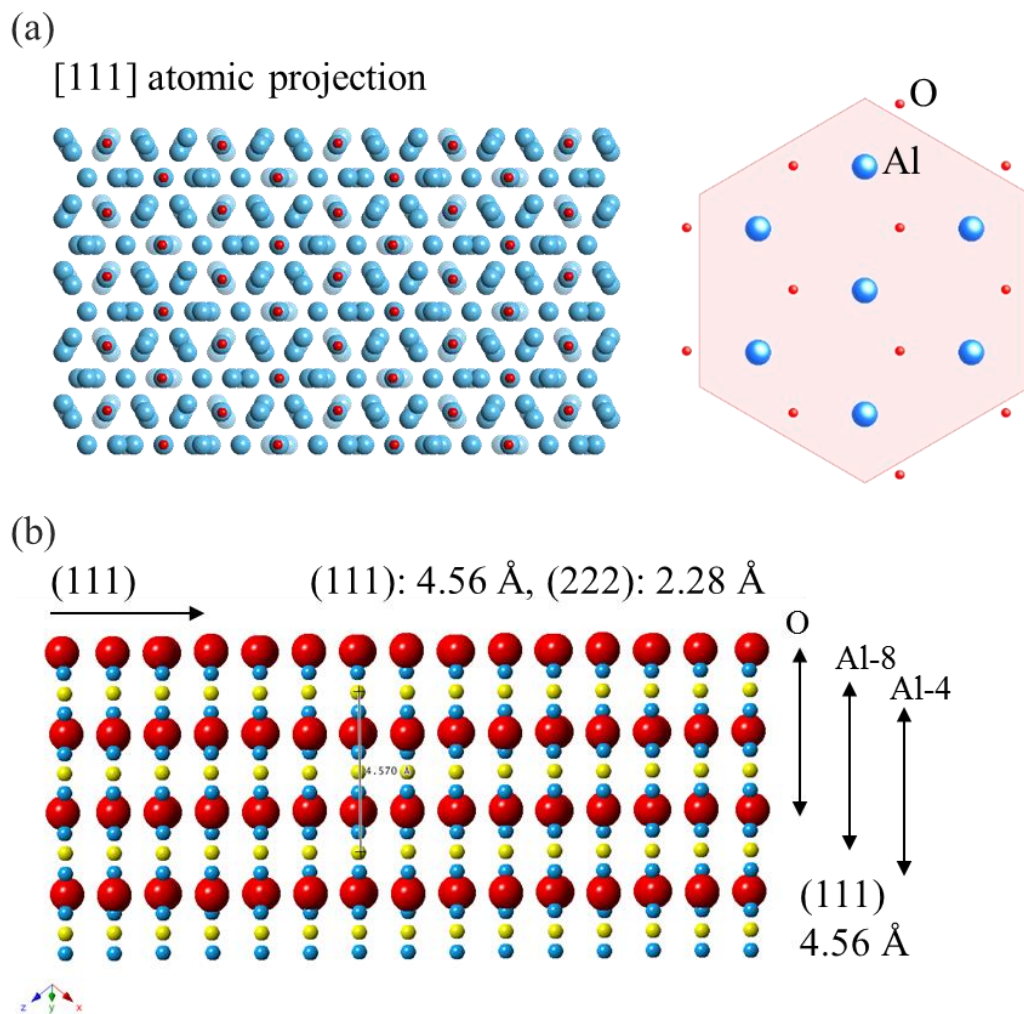
Figure 3.29 (a) Atomic projection of gamma aluminum oxide in [111] and (b)

oxygen and aluminum atomic schematics in (111) plane (top layer)

(a)

(b)

(c)

Oxygen in γ-alumina

Nc=4   Nc=3

*6.59 eV   *6.33 eV

* V₀ formation energy

(d)

Aluminum in γ-alumina

Al3   Al4

*1.73 eV   *1.96 eV

* Eu-Al formation energy
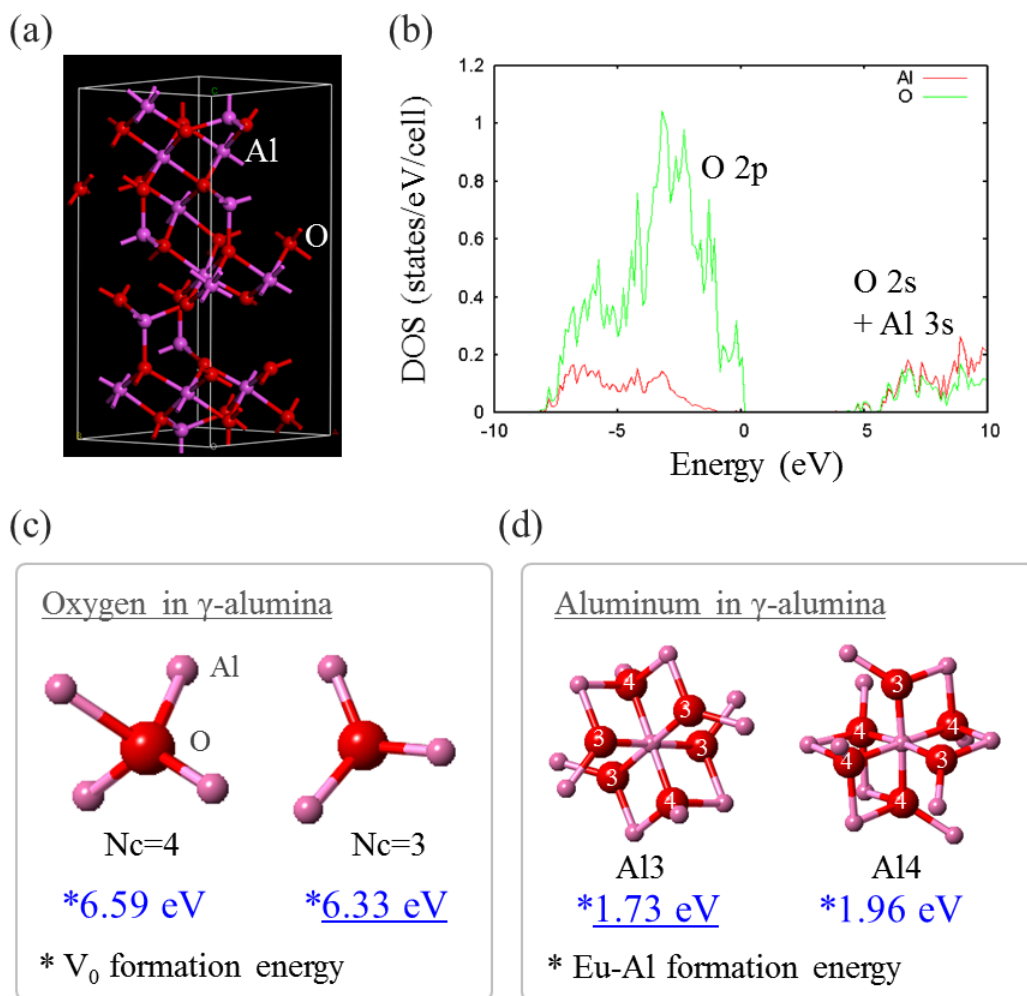
Figure 3.30 (a) Unit cell of χ-Al₂O₃ calculated in this work, (b) partial densities of states onto Al and O atoms, (c) oxygen and (d) aluminum sites in χ-Al₂O₃.
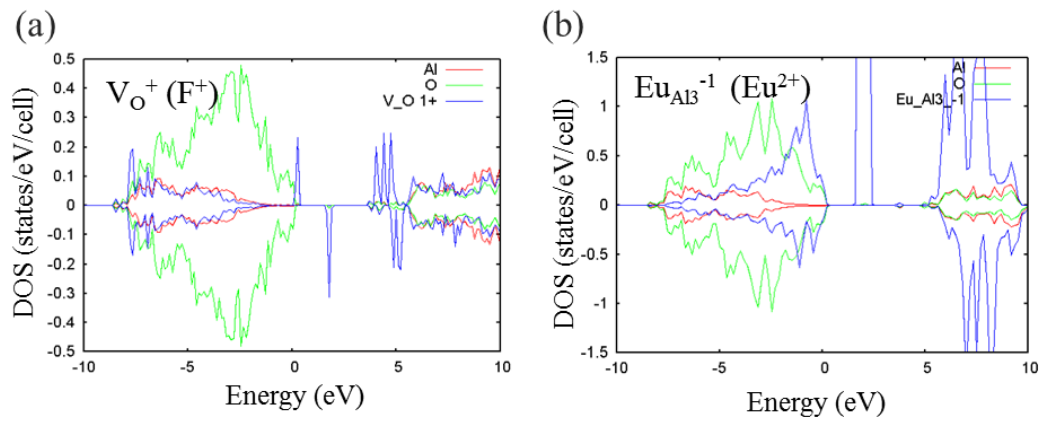
Figure 3.31 Partial densities of states onto (a) Al, O atoms and oxygen vacancy with single electron and (b) Eu^{2+} ion substituting Al^{3+} ion in gamma alumina.
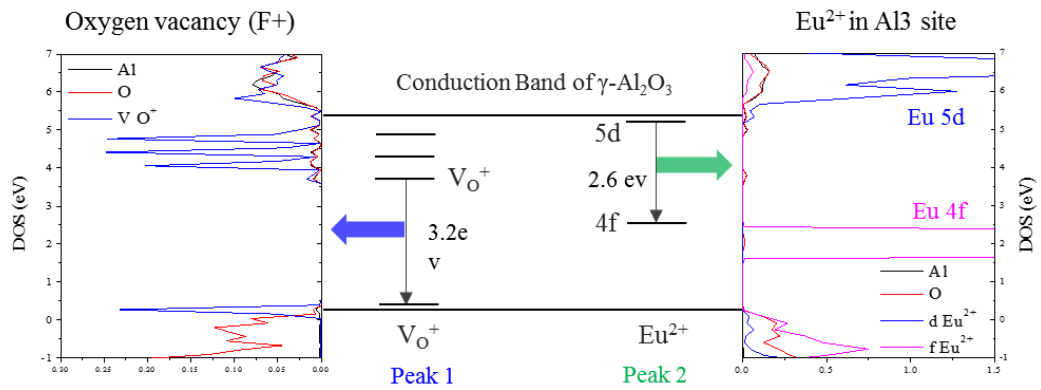
Figure 3.32 Electronic energy band structure of oxygen vacancy and europium divalent ions in χ-Al_2O_3.

3.2. Rare-earths doped magnesium oxide film on Mg foil

3.2.1. Ce-doped magnesium oxide film by PEO process

In this section, photoluminescence property of cerium doped magnesium plate was investigated in different way of comparison with cerium doped Mg_2SiO_4 phosphor powder prepared by conventional solid state reaction. At first, the cerium doped magnesium oxide film was prepared by plasma electrolytic oxidation. Cerium oxide was added as additives in sodium silicate electrolyte. In contrast with europium doping in aluminum substrate, magnesium oxidation is quietly dependent on the electrolyte composition. When silicate base solution was applied in the process, Mg_2SiO_4 (magnesium silicate) film was formed. In case of using sodium aluminate electrolyte [28, 70], $MgAl_2O_4$ spinel structure was generated on magnesium substrate [29, 30]. Therefore, high functional metal oxide layer for appropriate application can be obtained by selection of electrolyte composition.

As shown in the Figure 3.33, the magnesium plate prepared by different electrolyte of sodium silicate and sodium aluminate was composed of magnesium silicate and magnesium aluminate phase. In both cases, cerium oxide peak was also observed. When the PEO treatment was proceeded for 60min, thick oxide layers were covered magnesium plate, and the morphology of magnesium silicate and aluminate surface was shown in the Figure 3.33(b). The FE-SEM image of

MgAl$_2$O$_4$ ceramic film (NAO) showed quiet dense surface with small size of pores with few hundred nanometer. In case of sodium silicate ceramic film (NSO) showed very porous surface and irregular morphology with micron meter size. The magnesium aluminate and silicate matrix is widely used as a host lattice in phosphor material area [71-73], so these ceramics can be adopted to the phosphor film preparations by PEO process. Both cerium oxide doped magnesium silicate and magnesium aluminate films showed photoluminescence property, but in this thesis, the only Mg$_2$SiO$_4$:Ce phosphor film will be discussed in detail. In comparison with phosphor powder, the luminescence property and crystal structural property will be explained. In addition, the difference of photoluminescence in europium doped aluminum oxide film will be mentioned.

Here, the time-voltage curve of magnesium plate in sodium silicate electrolyte is shown in the Figure 3.34 (a). As time goes by, the voltage was highly accelerated and breakdown with spark was generated at 320v. Once the breakdown was occurred, the voltage incensement slowed down and maintained plasma generating voltage. According to plasma processing time, the films were highly thickened with the formation of Mg$_2$SiO$_4$ phase. The Figure 3.34 (b) showed X-ray diffraction patterns of oxidized magnesium film as increasing plasma time. At the early stage (20min) of the oxidation, Mg$_2$SiO$_4$ was formed but the phase was not highly crystallized enough. When the process time was over 90min, the XRD intensity of Mg$_2$SiO$_4$ phase was increased and MgO phase was

also detected. In contrast to the europium doped aluminum oxide film, cerium oxide peak was obviously observed in the film, even though almost same amount of rare earths were used. This might be due to the size of cerium oxide particle and zeta potential of each rare-earths.

The photograph image of cerium doped Mg_2SiO_4 film on magnesium AZ31 was shown in the figure Figure 3.35 (a). Under UV lamp (ex=365nm), the oxidized film generate blue emission. As increasing time, the photoluminescence intensity was highly increased at the excitation of 377nm, but the excitation spectrum centered at 318nm was not changed. The PL spectrum was centered in various luminescence centers, so the spectrum from cerium doped alumina film showed broad band emission. The luminescence spectrum was accurately measured in FE-SEM with cathodoluminescence analysis system. There were three emission centers in the CL spectrum which are 437nm and 461nm centered blue emission with 624nm centered red emission.

In order to find out luminescence centers in Mg_2SiO_4, we could guess several candidate factors for the photoluminescence property in the Ce doped Mg_2SiO_4 film. First, trivalent cerium ion in Mg_2SiO_4 host lattice can be the luminescence center. When cerium ions exist in the lattice as a trivalent state, a single electron in 4f state can generate luminescence, so strong and broad emission was observed in this case. Second, charge transfer of cerium ions can be a candidate of the luminescence center. In case of Ce^{4+} ion, charge transfer in Ce-O bonding is

commonly observed in Mg_2CeO_4 system [74, 75]. The emission center at this charge transfer in $SrCeO_4$ was 485nm, and most emission from charge transfer was in blue emission region. The third assumption is vacancy center in cerium oxide or Mg_2SiO_4 crystal. In case of oxygen vacancy containing cerium-oxide showed 413nm centered blue emission, so the blue emission spectrum of cerium doped magnesium silicate film could be related to the luminescence of vacancy in cerium oxide [76, 77]. In that, a lot of candidates which could be the luminescence source in PEO film were considered in this experiment. Among them, cerium doped Mg_2SiO_4 was the most influential factor, so luminescence property was compared with the synthesized $Mg_2SiO_4:Ce^{3+}$ phosphors in detail in following section.
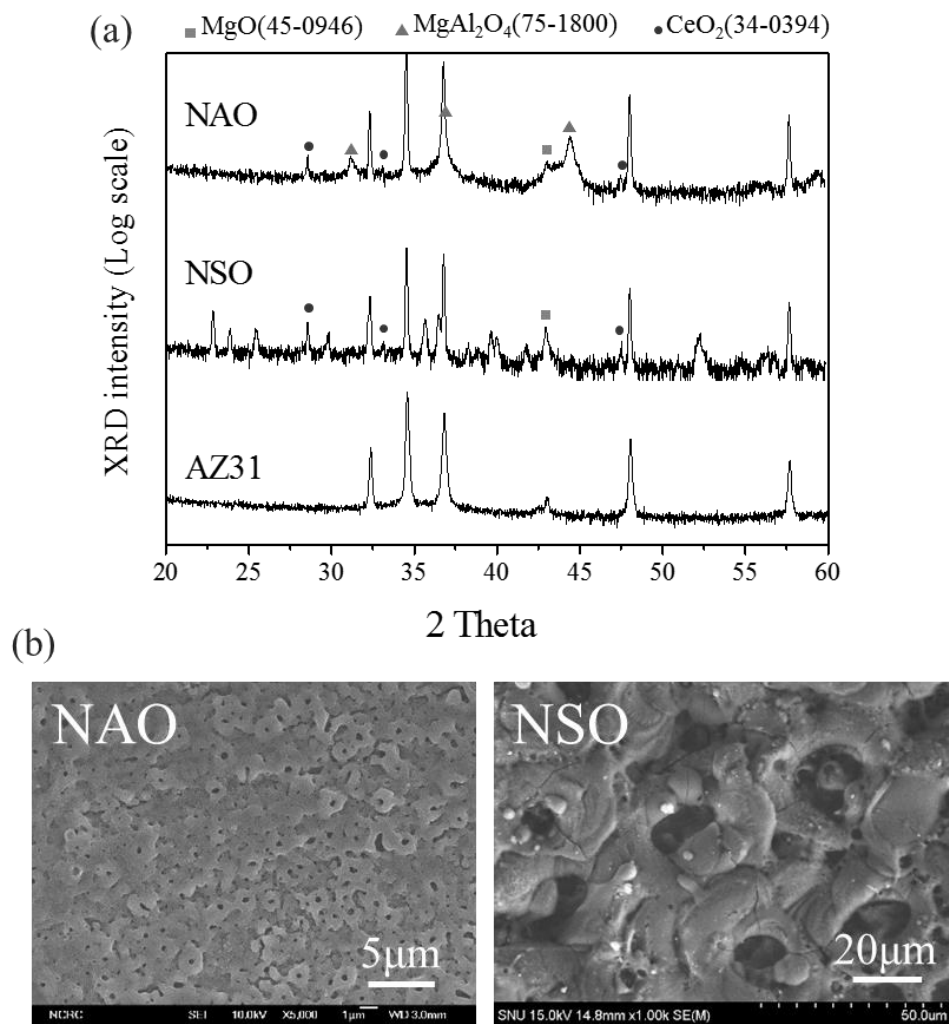
Figure 3.33 Cerium doped Mg_2SiO_4 film and $MgAl_2O_4$ film prepared by plasma electrolytic oxidation using magnesium AZ31 in sodium aluminate and sodium silicate electrolyte.
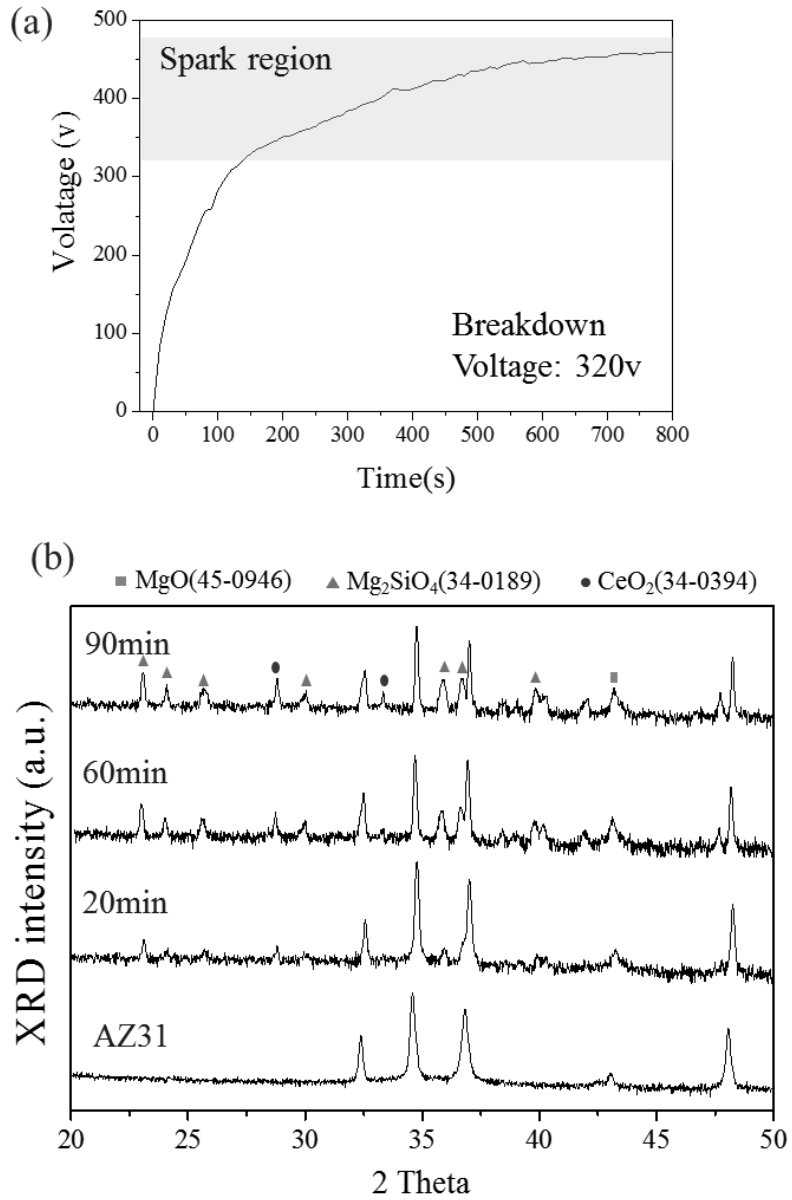
Figure 3.34 (a) Time-voltage curve of plasma electrolytic oxidation process in sodium silicate electrolyte with magnesium AZ31 and X-ray diffraction patterns of the PEO film treated for different oxidation time
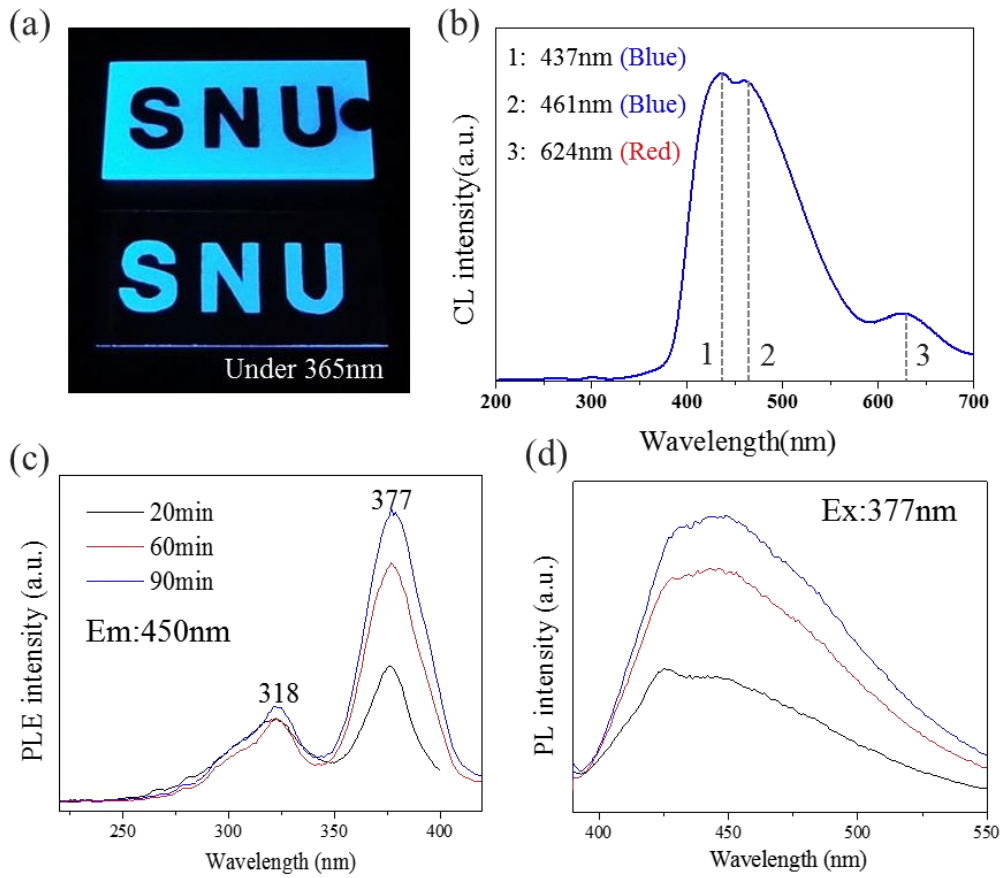
Figure 3.35 Cerium doped Mg_2SiO_4 film by plasma electrolytic oxidation; (a) photograph image under UV excitation, (b) cathodoluminescence spectra and (c) excitation and emission spectra with different plasma processing time

3.2.2. Ce-doped Mg₂SiO₄ phosphor powder

For the comparison of Ce doped Mg_2SiO_4 luminescence between phosphor powder and plasma electrolytic oxidized film, Mg_2SiO_4 phosphor was synthesized by conventional solid-state reaction. The phase analysis of magnesium silicate phosphor annealed with increasing annealing temperature is shown in the Figure 3.36. At 1200 ℃, the Mg_2SiO_4 phase was formed, but the starting materials of MgO and SiO_2 were still existed at this temperature. When the raw starting powders were annealed over 1300℃, the phase of Mg_2SiO_4 was highly increased and crystalized, and at 1400℃ almost single phase of Mg_2SiO_4 was finally obtained. The cerium contents (x) was 0.02 in this material $Mg_{2-x}SiO_4:Ce_x$, but other cerium related phase or cerium oxide was not detected. The photoluminescence spectra of annealed $Mg_{2-x}SiO_4:Ce_x$ were shown in the Figure 3.36 (b), the intensity of excitation and emission spectra were highly increased over 1300℃, and emission spectra was centered at 408nm at the excitation 333nm. The shape of emission spectrum in $Mg_{2-x}SiO_4:Ce_x$ was not ideal Gaussian distribution, so we could guess that two or more luminescence center might be existed in that phosphor material.

In order to find out phase and luminescence spectral changes with cerium oxide contents, the concentration of cerium oxide(x) was varied from 0.005 to 0.1. As increasing cerium concentration, the second phase of cerium silicate was

formed over x=0.05, and the $Ce_2Si_2O_7$ silicate was highly increased at high cerium doping concentration. In this experiment, the Mg_2SiO_4 phosphors were annealed in reducing atmosphere ($5\%H_2/95\%N_2$), so cerium ions are mostly existed in 3+ charges instead of 4+ charged ion. At the six-coordination, ionic radius of Mg^{2+} ion is 0.72 Å, and that of Ce^{3+} ions is 1.01 Å. The size of cerium ion is much larger than magnesium ion, so substitution of magnesium ion by cerium is quiet difficult in high concentration range. For this reason, the second phases relating cerium ion could be easily formed in this system.

In case of photoluminescence property depending on cerium contents, the PL intensity was highly increased with doping concentration, but this luminescence improvement is related to the formation of cerium silicate phosphor. From the reported papers, the $Ce_2Si_2O_7$ is known for strong blue emitting phosphor at the excitation of 308nm [78]. Because of cerium silicate phosphor (centered at 405nm), the luminescence spectrum was increased and blue shifted to 405nm. When cerium ions were doped in the concentration of 0.01, the photoluminescence spectrum was centered at 432nm. In this condition, if cerium ions were mostly doped in Mg_2SiO_4 host lattice, so the luminescence of Mg_2SiO_4:Ce^{3+} might be centered at 430nm. For the accurate structure analysis of cerium doped magnesium silicate, the rietveld refinement of synthesized phosphor was performed. For the precise calculation, the X-ray diffraction analysis was performed as 0.01 steps with 1 °/min scanning rate, and single phase of Mg_2SiO_4

90

was obtained (Figure 3.38). All the patterns were completely indexed based on the orthorhombic structure with a space group of Pmnb, and the calculated lattice parameters were a=4.755, b=10.199, c=5.983. The calculated value was well agreed with the reported data; a=4.75, b=10.19, c=5.98 (ICSD: 18969). The calculations were including cerium ions in magnesium silicate crystal at each magnesium site (Mg1, Mg2), but the calculated magnesium atoms were slightly out of the site.

The XPS results (Figure 3.39) showed that cerium ions in 3d state, and the calculated binding energy of cerium ion was u_0=884.5, u_1=880.7, u'_0=902.9 and u'_1=898.9. In case of trivalent cerium ions, the binding energy in 3d was almost the same as the reported value [79]. As results, we can say that the cerium ions in magnesium silicate powder were mostly existed in 3+ charge valance. The trivalent cerium ion has single electron in 4f state, so the electron spin resonance can be detected for that single electron. In order to know the chemical state of cerium ion, ESR analysis was also performed in both cerium doped Mg_2SiO_4 phosphor powder and film. As shown in the Figure 3.39(b), both $Mg_2SiO_4:Ce^{3+}$ showed the resonance at the g=1.8538, and this value was near at the value of free electron (g=2.0). So we can say that the cerium ions are existed in Mg_2SiO_4 crystal structure as trivalent chemical state.

Here, in order to know the distribution of cerium ions, EDS and cathodoluminescence analysis was performed. In the Figure 3.40(a), the

$Mg_2SiO_4:Ce^{3+}$ powder showed unique surface which looked like as some particles was attached or secondary phases were formed on the powder. In cathodoluminescence image, the unique surfaces only showed cathodoluminescence property as shown in the Figure 3.40 (b). The EDS mapping results showed that a lot of cerium ions were existed in the selected area. From the quantitative analysis, the cerium-rich luminescent area contained 16.8 at% while there is only 2.6% of magnesium ions were in that spot. In that, the luminescence in magnesium silicate phosphor was due to the cerium and silicon rich phase. From the results that the atomic ratio of silicon and cerium was the same, the luminescent region might be dominantly composed of $Ce_2Si_2O_7$ phase. So, it could be say that the luminescence property of Mg_2SiO_4 phosphor is not form the cerium doping process, but from the secondary phase formation of $Ce_2Si_2O_7$. In this stage, we can guess that the photoluminescence of Mg_2SiO_4:Ce film is due to the cerium doping mechanism during PEO process, or due to the presence of cerium related secondary crystal which emits luminescence in the Mg_2SiO_4 crystal. For the precise analysis, atomic scale study is needed.
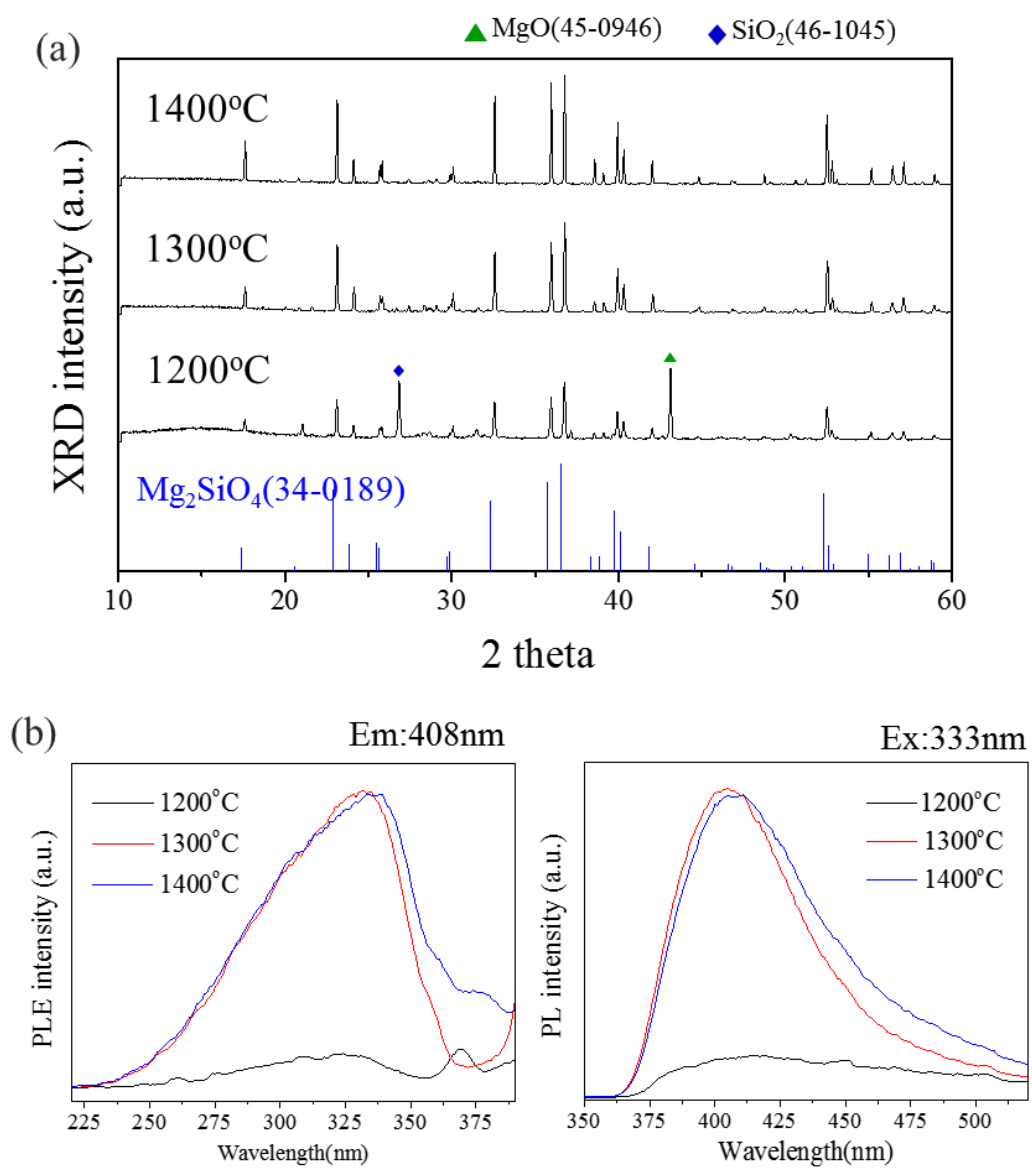
Figure 3.36 Cerium doped Mg₂SiO₄ phosphors annealed at 1200-1400°C for 3 hours; (a) XRD patterns, (b) excitation and emission spectra
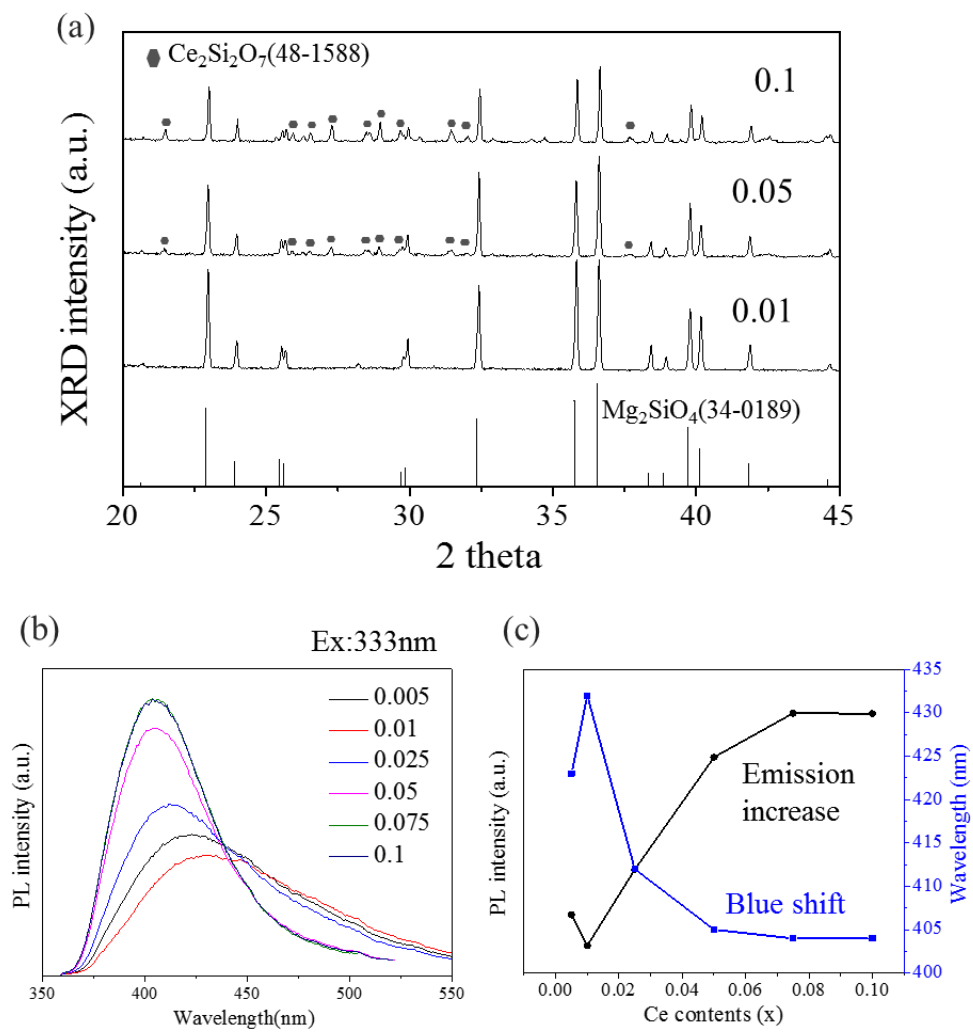
Figure 3.37 Mg$_2$SiO$_4$:Ce phosphors with increasing cerium contents; (a) XRD patterns, (b) photoluminescence spectra (ex=333nm) and (c) PL intensity and wavelengths
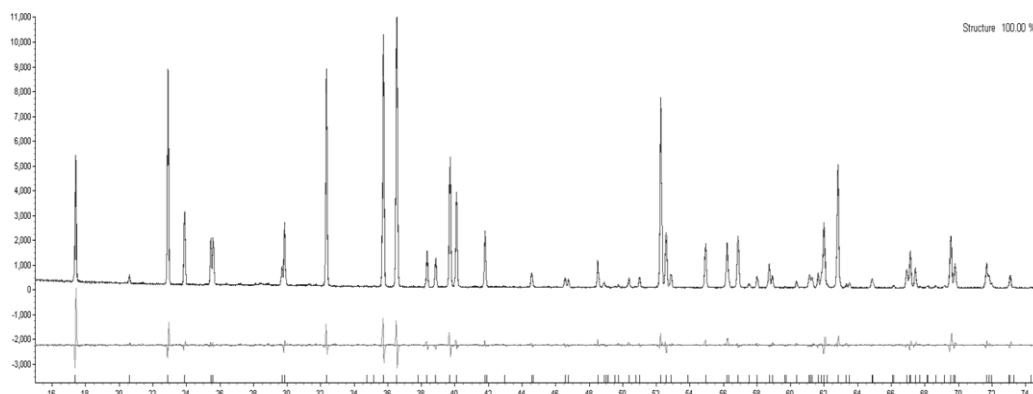
Figure 3.38 Rietveld refinement fitting results of $Mg_{1.97}SiO_4$:$Ce_{0.02}$ phosphor

Table 3.10 Crystal structure of magnesium silicate (Mg_2SiO_4)

Atom	#	OX	SITE	X	Y	Z	SOF
Mg	1	2	4a	0	0	0	1
Mg	2	2	4c	0.9915(1)	0.2774(1)	0.25	1
Si	1	4	4c	0.4265(1)	0.0940(1)	0.25	1
O	1	-2	4c	0.7658(1)	0.0917(1)	0.25	1
O	2	-2	4c	0.2218(1)	0.4471(1)	0.25	1
O	3	-2	8d	0.2774(1)	0.1631(1)	0.0331(1)	1

Table 3.11 Calculated crystal structure (rietveld refinement)

SITE	X	Y	Z	Occ
Mg1	0.02789	0.00027	-0.03228	0.241
Mg2	0.9953	0.27723	0.26538	0.5551
Si	0.4249	0.09431	0.25	1.208
O1	0.75989	0.09131	0.25	1.116
O2	0.22256	0.44933	0.25	1.02
O3	0.29472	0.16317	0	0.4521
Ce1	-0.06095	-0.00366	-0.46147	0.07751
Ce2	1.27066	0.16473	0.44151	0.1001
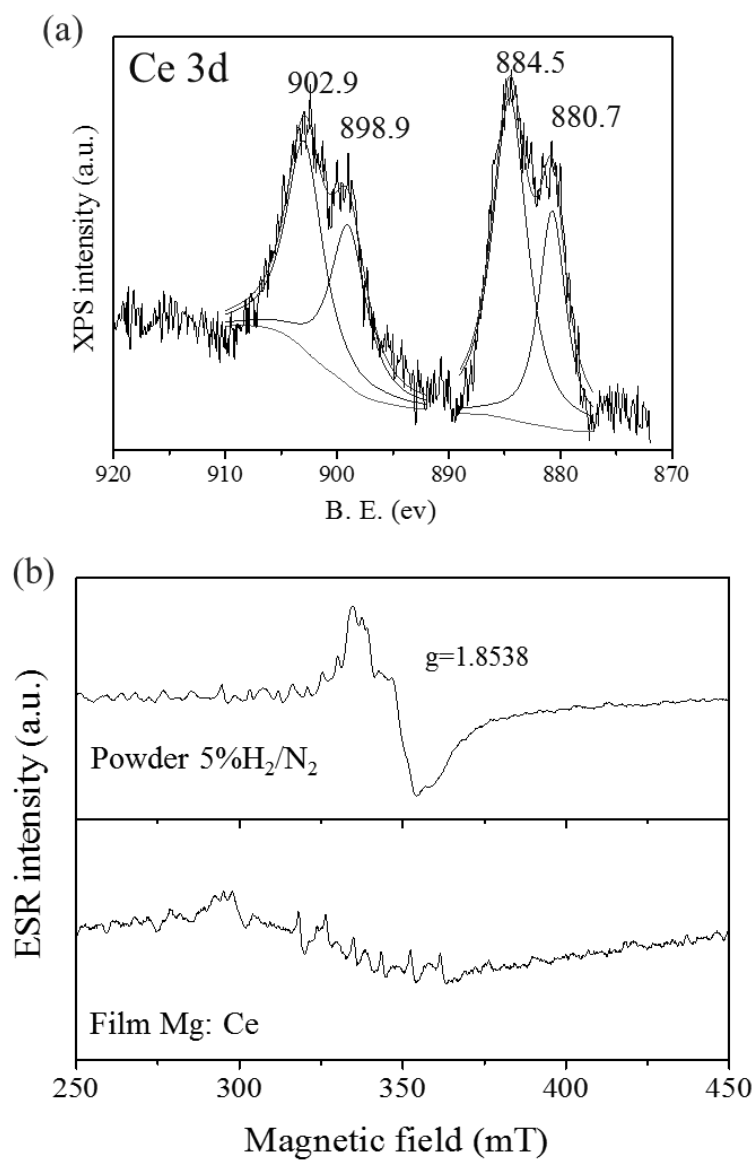
Figure 3.39 (a) XPS analysis of cerium doped Mg_2SiO_4 phosphor powder and (b) electron spin resonance of cerium doped Mg_2SiO_4 powder and MAO film
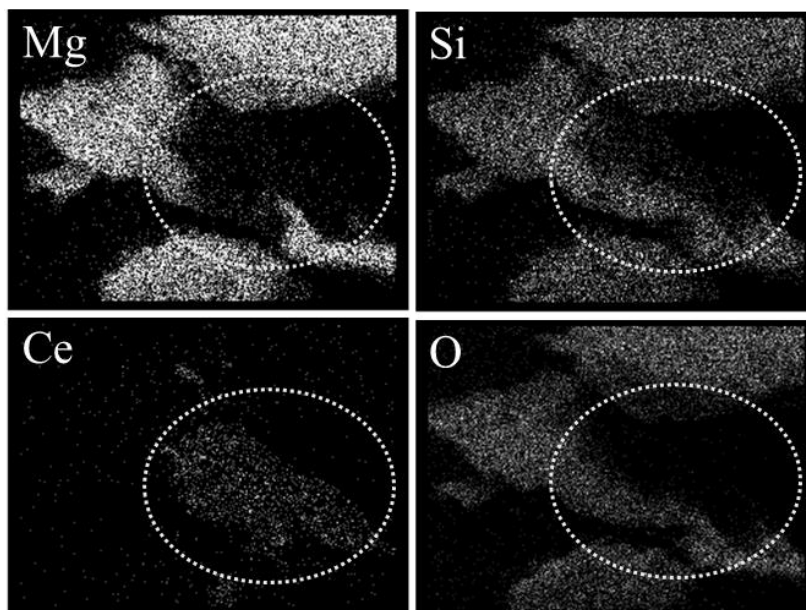
Figure 3.40 Cerium doped Mg_2SiO_4 phosphors; (a) FE-SEM image, (b) cathodoluminescence image (PAN mode) and (c) EDS images of Mg, Si, Ce O

Chapter 4. Conclusion

In this work, luminescent rare-earths doped metal oxide films were firstly introduced and successfully obtained by plasma electrolytic oxidation. The resulted oxide film showed intense and wide emission spectrum at the excitation of ultra-violet region.
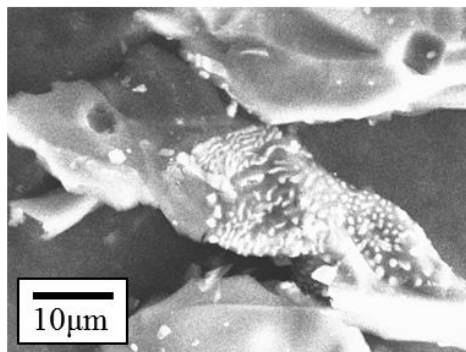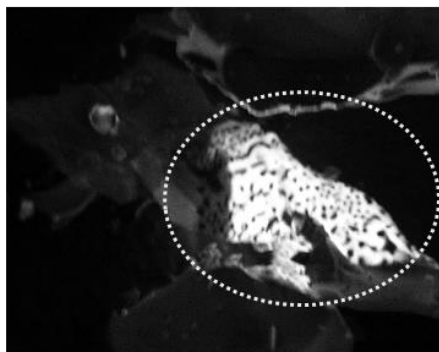
When europium oxide was added in the electrolyte at the plasma electrolytic oxidation process of aluminum foil, white light emitting aluminum oxide was formed. The oxide film was identified as gamma phase of aluminum oxide, and the film composition and characteristics were highly affected by experimental variables. At the early stage of PEO process, aluminum oxide layer with white luminescence was formed at the spark generated region, and the films were highly thickened with plasma processing time. In order to know the luminescence centers in alumina structure, various analysis were performed in the first section. From the ESR results, the oxygen vacancy in gamma alumina was identified, and europium existence as both divalent and trivalent state was also confirmed by EDS, ICP and XPS. The decay-time signal of the europium doped film revealed that the luminescence at short wavelength is from vacancy center (F+) in aluminum oxide, film and the longer wavelength is from europium 2+ center. The rietveld refinement calculations indicated that the europium ions were mostly

existed at the octahedral sites in defective spinel structure of gamma alumina. From the TEM results, the europium ions in the gamma phase of aluminum oxide lattice were confirmed, and they were existed locally in specific area with facet like shape. In addition, in the gamma alumina crystal, europium ions were doped along the (111) plane with the specific orientation. These europium ions, from the DFT calculation, emit green light luminescence due to the f-d transition when they are existed as a divalent state, and the existence of F+ type vacancy center showed blue emission in gamma aluminum oxide system.

At the second section, cerium doped magnesium silicate film was obtained through the PEO process, and they showed blue emission (440nm) under UV excitation. The cerium doped Mg_2SiO_4 phosphor was prepared for comparing luminescence property between phosphor and film. They showed blue emission, and the emission spectrum was shifted to shorter wavelength as increasing cerium oxide contents. This phenomenon might be due to the formation of cerium silicate which emits blue luminescence centered at 408nm. In that, from the synthesis of phosphor ceramic, quiet large size of cerium ions were difficult to substitute magnesium ion, but that could be realized though the PEO process.

In conclusion, rare-earths doped metal oxide film prepared by PEO process showed luminescence property, and the luminescence was from both rare-earth doping effects and vacancy centers in metal oxide crystal system which is formed in high temperature and pressure atmosphere of plasma assisting process.

References

[1] W.M. Yen, H. Yamamoto, Phosphor handbook, CRC press2006.

[2] G. Blasse, B. Grabmaier, B. Grabmaier, Luminescent materials, Springer-Verlag Berlin1994.

[3] A. Kitai, Luminescent materials and applications, John Wiley & Sons2008.

[4] T.L. Barry, Journal of The Electrochemical Society, 115 (1968), pp. 1181-1184.

[5] J.K. Park, M. Lim, C.H. Kim, H.D. Park, J.T. Park, S.Y. Choi, Applied Physics Letters, 82 (2003), pp. 683-685.

[6] R.-J. Xie, N. Hirosaki, T. Suehiro, F.-F. Xu, M. Mitomo, Chemistry of materials, 18 (2006), pp. 5578-5583.

[7] X. Piao, K.-i. Machida, T. Horikawa, H. Hanzawa, Y. Shimomura, N. Kijima, Chemistry of Materials, 19 (2007), pp. 4592-4599.

[8] Y.Q. Li, A. Delsing, G. De With, H. Hintzen, Chemistry of materials, 17 (2005), pp. 3242-3248.

[9] S.-W. Choi, Y.J. Kim, S.-H. Hong, Optical Materials, 33 (2011), pp. 1700-1703.

[10] Y. Hu, W. Zhuang, H. Ye, S. Zhang, Y. Fang, X. Huang, Journal of luminescence, 111 (2005), pp. 139-145.

[11] Y. Sato, N. Takahashi, S. Sato, Japanese journal of applied physics, 35 (1996), p. L838.

[12] S. Ye, F. Xiao, Y. Pan, Y. Ma, Q. Zhang, Materials Science and Engineering: R: Reports, 71 (2010), pp. 1-34.

[13] Y.C. Kang, I.W. Lenggoro, S.B. Park, K. Okuyama, Appl Phys A, 72 (2001), pp. 103-105.

[14] M. Pang, J. Lin, J. Fu, R. Xing, C. Luo, Y. Han, Optical Materials, 23 (2003), pp. 547-558.

[15] C.-C. Yang, C.-M. Lin, Y.-J. Chen, Y.-T. Wu, S.-R. Chuang, R.-S. Liu, S.-F. Hu, Applied physics letters, 90 (2007), pp. 123503-123503-123503.

[16] K. Bando, K. Sakano, Y. Noguchi, Y. Shimizu, Journal of Light & Visual Environment, 22 (1998), pp. 2-5.

[17] J.-K. Sheu, S.-J. Chang, C. Kuo, Y.-K. Su, L. Wu, Y. Lin, W. Lai, J. Tsai, G.-C. Chi, R. Wu, Photonics Technology Letters, IEEE, 15 (2003), pp. 18-20.

[18] R.A. Hajjar, 72.5 L: Late-News Paper: Introducing Scalable, Freeform, Immersive, High-Definition Laser Phosphor Displays, SID Symposium Digest of Technical Papers, Wiley Online Library2012, pp. 985-988.

[19] A.G. Shapiro, J. Pokorny, V.C. Smith, JOSA A, 13 (1996), pp. 2319-2328.

[20] Z.-C. Wu, J. Liu, W.-G. Hou, J. Xu, M.-L. Gong, Journal of Alloys and Compounds, 498 (2010), pp. 139-142.

[21] J.H. Lim, B.N. Kim, Y. Kim, S. Kang, R.J. Xie, I.S. Chong, K. Morita, H. Yoshida, K. Hiraga, Applied Physics Letters, 102 (2013), p. 031104.

[22] W.-J. Yang, L. Luo, T.-M. Chen, N.-S. Wang, Chemistry of materials, 17 (2005), pp. 3883-3888.

[23] W.-H. Chao, R.-J. Wu, T.-B. Wu, Journal of Alloys and Compounds, 506 (2010), pp. 98-102.

[24] K.Y. Jung, Y.C. Kang, Materials letters, 58 (2004), pp. 2161-2165.

[25] Z. Kang, Y. Liu, B. Wagner, R. Gilstrap, M. Liu, C. Summers, Journal of

luminescence, 121 (2006), pp. 595-600.

[26] S. Chawla, K. Jayanthi, H. Chander, physica status solidi (a), 205 (2008), pp. 271-274.

[27] A. Yerokhin, X. Nie, A. Leyland, A. Matthews, S. Dowey, Surface and Coatings Technology, 122 (1999), pp. 73-93.

[28] H. Guo, M. An, H. Huo, S. Xu, L. Wu, Applied surface science, 252 (2006), pp. 7911-7916.

[29] S.P. Sah, Y. Aoki, H. Habazaki, Materials transactions, 51 (2010), pp. 94-102.

[30] Y. Ma, X. Nie, D.O. Northwood, H. Hu, Thin Solid Films, 494 (2006), pp. 296-301.

[31] M. Boinet, S. Verdier, S. Maximovitch, F. Dalard, Surface and Coatings Technology, 199 (2005), pp. 141-149.

[32] F. Walsh, C. Low, R. Wood, K. Stevens, J. Archer, A. Poeton, A. Ryder, Transactions of the IMF, 87 (2009), pp. 122-135.

[33] L. Snizhko, A. Yerokhin, A. Pilkington, N. Gurevina, D. Misnyankin, A.

Leyland, A. Matthews, Electrochimica Acta, 49 (2004), pp. 2085-2095.

[34] A. Yerokhin, X. Nie, A. Leyland, A. Matthews, Surface and Coatings Technology, 130 (2000), pp. 195-206.

[35] H. Duan, C. Yan, F. Wang, Electrochimica Acta, 52 (2007), pp. 3785-3793.

[36] J. Liang, P.B. Srinivasan, C. Blawert, M. Störmer, W. Dietzel, Electrochimica Acta, 54 (2009), pp. 3842-3850.

[37] R.F. Zhang, D.Y. Shan, R.S. Chen, E.H. Han, Materials Chemistry and Physics, 107 (2008), pp. 356-363.

[38] G.-H. Lv, H. Chen, W.-C. Gu, L. Li, E.-W. Niu, X.-H. Zhang, S.-Z. Yang, Journal of Materials Processing Technology, 208 (2008), pp. 9-13.

[39] Y. Tang, X. Zhao, K. Jiang, J. Chen, Y. Zuo, Surface and Coatings Technology, 205 (2010), pp. 1789-1792.

[40] V. Dehnavi, B.L. Luan, D.W. Shoesmith, X.Y. Liu, S. Rohani, Surface and Coatings Technology, 226 (2013), pp. 100-107.

[41] B.D. Evans, M. Stapelbroek, Physical Review B, 18 (1978), p. 7089.

[42] T. Perevalov, V. Gritsenko, Electronic structure of oxygen vacancy and

poly-vacancy in α-and γ-Al 2 O 3, Microelectronics Proceedings (MIEL), 2010

27th International Conference on, IEEE2010, pp. 123-126.

[43] V.A. Pustovarov, V.S. Aliev, T.V. Perevalov, V.A. Gritsenko, A.P. Eliseev, J.

Exp. Theor. Phys., 111 (2010), pp. 989-995.

[44] M. Peng, G. Hong, Journal of Luminescence, 127 (2007), pp. 735-740.

[45] S. Stojadinovic, R. Vasilic, Z. Nedic, B. Kasalica, I. Belca, L. Zekovic, Thin

Solid Films, 519 (2011), pp. 3516-3521.

[46] G.S. Huang, X.L. Wu, Y.F. Mei, X.F. Shao, G.G. Siu, Journal of Applied

Physics, 93 (2003), pp. 582-585.

[47] S. Tajima, N. Baba, K. Shimizu, I. Mizuki, Active and Passive Electronic

Components, 3 (1976), pp. 91-95.

[48] Y. Li, G. Li, G. Meng, L. Zhang, F. Phillipp, Journal of Physics: Condensed

Matter, 13 (2001), p. 2691.

[49] Y. Chen, J.L. Kolopus, W.A. Sibley, Physical Review, 186 (1969), pp. 865-

870.

[50] S.Y. La, R.H. Bartram, R.T. Cox, Journal of Physics and Chemistry of

Solids, 34 (1973), pp. 1079-1086.

[51] R. Vercaemst, D. Poelman, L. Fiermans, R. Van Meirhaeghe, W. Laflere, F. Cardon, Journal of electron spectroscopy and related phenomena, 74 (1995), pp. 45-56.

[52] J. Qi, T. Matsumoto, M. Tanaka, Y. Masumoto, Journal of Physics D: Applied Physics, 33 (2000), p. 2074.

[53] S.H.M. Poort, A. Meyerink, G. Blasse, Journal of Physics and Chemistry of Solids, 58 (1997), pp. 1451-1456.

[54] S.H. Sohn, J.H. Lee, S.M. Lee, Journal of Luminescence, 129 (2009), pp. 478-481.

[55] Y.V. Zorenko, A. Voloshinovskiĭ, I. Konstankevych, Optics and spectroscopy, 96 (2004), pp. 532-537.

[56] M. Itou, A. Fujiwara, T. Uchino, The Journal of Physical Chemistry C, 113 (2009), pp. 20949-20957.

[57] A. Surdo, V. Pustovarov, V. Kortov, A. Kishka, E. Zinin, Nuclear Instruments and Methods in Physics Research Section A: Accelerators,

Spectrometers, Detectors and Associated Equipment, 543 (2005), pp. 234-238.

[58] D. Fang, L. Li, W. Xu, Y. Wang, M. Jiang, X. Guo, X. Liu, G. Cao, G. Li, G. Li, N. Wang, Z. Luo, Materials Science and Engineering: B, 179 (2014), pp. 71-76.

[59] G. Tao, M. Guo-Wen, Z. Li-De, Chinese physics letters, 20 (2003), p. 713.

[60] Y. Du, W.L. Cai, C.M. Mo, J. Chen, L.D. Zhang, X.G. Zhu, Applied Physics Letters, 74 (1999), pp. 2951-2953.

[61] G.G. Khan, A.K. Singh, K. Mandal, Journal of Luminescence, 134 (2013), pp. 772-777.

[62] X. Wu, S. Xiong, J. Guo, L. Wang, C. Hua, Y. Hou, P.K. Chu, The Journal of Physical Chemistry C, 116 (2012), pp. 2356-2362.

[63] Y.-F. Liu, Y.-F. Tu, S.-Y. Huang, J.-P. Sang, X.-W. Zou, Journal of materials science, 44 (2009), pp. 3370-3375.

[64] I. Vrublevsky, A. Jagminas, S. Hemeltjen, W. Goedel, Applied Surface Science, 254 (2008), pp. 7326-7330.

[65] G. Paglia, C.E. Buckley, A.L. Rohl, B.A. Hunter, R.D. Hart, J.V. Hanna, L.T.

Byrne, Physical Review B, 68 (2003), p. 144110.

[66] R.-S. Zhou, R.L. Snyder, Acta Crystallographica Section B: Structural Science, 47 (1991), pp. 617-630.

[67] G. Gutiérrez, A. Taga, B. Johansson, Physical Review B, 65 (2001), p. 012101.

[68] G. Gutiérrez, A. Taga, B. Johansson, Physical Review B, 65 (2001), p. 012101.

[69] C.-K. Lee, E. Cho, H.-S. Lee, K.S. Seol, S. Han, Physical Review B, 76 (2007), p. 245110.

[70] H. Luo, Q. Cai, B. Wei, B. Yu, D. Li, J. He, Z. Liu, Journal of Alloys and Compounds, 464 (2008), pp. 537-543.

[71] L. Lin, M. Yin, C. Shi, W. Zhang, Journal of Alloys and Compounds, 455 (2008), pp. 327-330.

[72] H. Yang, J. Shi, M. Gong, K. Cheah, Journal of luminescence, 118 (2006), pp. 257-264.

[73] X.Y. Chen, C. Ma, Z.J. Zhang, X.X. Li, Microporous and Mesoporous

Materials, 123 (2009), pp. 202-208.

[74] L. Li, S. Zhou, S. Zhang, Chemical Physics Letters, 453 (2008), pp. 283-289.

[75] E. Danielson, M. Devenney, D.M. Giaquinta, J.H. Golden, R.C. Haushalter, E.W. McFarland, D.M. Poojary, C.M. Reaves, W.H. Weinberg, X. Di Wu, Science, 279 (1998), pp. 837-839.

[76] F. Ying-Cui, Z. Zhuang-Jian, S. Jie, L. Ming, Chinese Physics Letters, 23 (2006), p. 1919.

[77] A.H. Morshed, M.E. Moussa, S.M. Bedair, R. Leonard, S.X. Liu, N. El-Masry, Applied Physics Letters, 70 (1997), pp. 1647-1649.

[78] L. Kępiński, D. Hreniak, W. Stręk, Journal of alloys and compounds, 341 (2002), pp. 203-207.

[79] F. Larachi, J. Pierre, A. Adnot, A. Bernis, Applied Surface Science, 195 (2002), pp. 236-250.

국문 초록

본 연구에서는 플라즈마 전기화학법을 응용하여 형광 금속 산화막을 개발하였고, 형광특성 및 다양한 분석을 통해 발광 메커니즘을 규명하는 연구를 수행하였다.

전기화학적 표면 코팅 기술은 경량 금속 및 합금의 부식 방지를 위한 표면처리 기법으로 많이 사용되어왔다. 그 중에서도 고전류 고전압의 전력을 인가하여 플라즈마를 동반하는 표면처리 기법으로 Plasma Electrolytic Oxidation (PEO)법이 많은 관심을 받고 있는데, 이 방법은 기존의 화성 도금 처리에서 사용되는 크롬 및 중금속 등의 유해물질을 사용하지 않는다는 점에서 친환경적이며 세라믹형태의 산화막을 형성하기 때문에 내마모 및 내부식성이 매우 우수하다는 장점을 가지고 있다. 특히, PEO법은 산화 막이 형성될 때 plasma 및 spark가 수반되는 특수한 환경이 조성되는데, 본 연구에서는 이러한 plasma 현상을 응용하여 희토류 금속원소를 추가하여 처음으로 PEO법을 통해 형광특성을 나타내는 신개념의 형광 금속 산화막을 형성하고, 이때 형성 되는 형광 금속 산화 막의 형광 특성 분석 및 발광 요소에 대한 연구를 진행하였다. 공정 조건 및 금속 기판의

변화에 따라 산화막의 조성 및 특성이 변화하였으며 이에 따른 형광 특성 또한 다양하게 변화하는 것을 확인 하였다.

첫번째 장에서는 유로퓸이 도핑된 산화 알루미늄 옥사이드를 형성하고 이에 따른 형광 특성분석을 진행한 결과에 대해 기술하였다. 플라즈마 전해 산화법을 통해 형성된 산화막은 UV에서 여기 하였을 때 백색의 형광을 나타내었으며, 이때 형성된 산화막은 감마 알루미나임을 확인 하였다. 초기 반응을 확인함으로써, 전해산화공정에서 스파크 또는 플라즈마가 형성되는 표면에서 형광특성이 나타나는 것을 알 수 있었으며, 이는 알루미늄 표면에서 플라즈마가 형성되는 순간 산화막의 형성과 동시에 유로퓸 이온이 도핑 되면서 나타나는 것으로 판단 하였다. 실험조건을 변화하며 산화막을 형성하였을 때, 발광 스펙트럼의 변화가 나타남을 통해 형광특성에 영향을 미치는 요인을 파악 해 볼 수 있었으며, 이후 여러 방향의 추가적인 실험 및 심도 있는 분석을 진행함으로써 유로퓸이 도핑된 감마 알루미나에서의 백색 발광의 형광인자를 탐색 하였다.

두번째 장에서는, 마그네슘 기판을 사용하여 세륨이 도핑된 청색 발광의 형광막을 형성하고, 이를 형광체 합성을 통해 발광인자를 확인한 연구에 대해 기술 하였다. XRD 및 PL 분석을 통해 세륨을

첨가한 마그네슘 산화막은 자외선 영역에서 청색발광특성을 보이며, 상은 마그네슘 실리케이트임을 확인 하였다. 이렇게 형성된 형광막의 발광 인자를 확인하기 위해, 마그네슘 실리케이트에 세륨을 도핑하여 고상법을 통해 형광체를 합성하였다. 이후 형광특성분석 및 상분석을 통하여 마그네슘실리케이트의 형광특성과 비교하여 분석 하였다.

본 연구는 참신한 아이디어를 바탕으로 새로운 공정을 적용하여 형광막을 개발하였다는 점, 단 한번의 공정으로 백색 형광을 내는 산화막을 형성하였다는 점, 여러 금속 기판에 응용가능하며, 더 나아가 형광막의 분리공정을 통해 반투명 형광막의 제조가 가능하다는 점에서 다양한 응용분야에 적용 가능하며, 또한 준안정상인 감마 알루미나에 유로퓸을 성공적으로 도핑하여 새로운 관점에서 형광 메커니즘을 규명할 수 있다는 점에서도 큰 의의를 가진다고 할 수 있다.